The Dissertation Committee for Robert Matavosian

certifies that this is the approved version of the following dissertation:

COMPLEX PROBLEMS ARISING IN THE COLLISION PROBABILITY THEORY FOR NEUTRON TRANSPORT

Committee:

_____

Erich A. Schneider, Supervisor

_____

Sheldon Landsberger

_____

Steven R. Biegalski

_____

Robert D. Moser

_____

James J. Thompson

COMPLEX PROBLEMS ARISING IN THE COLLISION PROBABILITY THEORY FOR NEUTRON TRANSPORT

by

Robert Matavosian, B.S.; M.S.; M.E.

Dissertation

Presented to the Faculty of the Graduate School of

the University of Texas at Austin

in Partial Fulfillment

of the Requirements

for the Degree of

Doctor of Philosophy

The University of Texas at Austin

December 2007

DEDICATIONS

I would like to dedicate this work to my wife, Ginger Atwood, for all her understanding and support during my studies at The University of Texas at Austin. She made it possible for me to dedicate a substantial amount of time to complete this dissertation while working full time. She stepped up and filled the gaps for all those things in life and work that I did not have enough time to complete. I will be indebted to her forever.

ACKNOWLEDGEMENTS

I would like to thank my supervisor, Dr. Erich A. Schneider, for his assistance and support for the preparation of this dissertation. He provided me with ideas on dissertation topics and supported me with formulating the dissertation proposal and its successful presentation. In addition, I would like to thank each of my committee members, Drs. Landsberger, Biegalski, Moser and Thompson for their support and review of this dissertation. I would like to especially thank Dr. Landsberger for his efforts to reintroduce me to academia and facilitate my admission to the University.

COMPLEX PROBLEMS ARISING IN THE

COLLISION PROBABILITY THEORY

FOR NEUTRON TRANSPORT

Publication No. _____

Robert Matavosian, Ph.D.

The University of Texas at Austin, 2007

Supervisor: Erich A. Schneider

Several comprehensive but time consuming neutronic codes are available for performing nuclear reactor and fuel cycle evaluations. In addition, simple models utilizing collision probability theory are used to perform similar tasks with reasonable accuracy. However, the current collision probability theory treats the heterogeneous reactor configurations with a two region unit cell model. This model does not address several important reactor parameters including spatial self-shielding effects and simultaneous use of different reactor fuels within a reactor core.

This dissertation studies the fidelity of expanding the collision probability theory to address the stated shortcomings through analyzing two problems.

Problem 1 analyzes the effects of self-shielding. The cylindrical fuel region is divided into several sub-regions and an overall equivalent escape probability from the entire fuel region is developed based on the identified neutron transmission and escape probabilities within each fuel sub-region. The multiplication factor and radioisotopic inventory results based on modified V:BUDS (Visualize: Burnup, Depletion, Spectrum) code are in good agreement with benchmark scenarios for a reactor unit cell. The accurate multiplication factor calculation allows more accurate studies on the maximum fuel burnup and radionuclide inventories of interest in nuclear non-proliferation studies.

Problem 2 analyzes the effects of simultaneous use of different fuels within a fuel lattice where the zero neutron leakage assumption across the unit cell boundaries is not valid. The developed methodology expands capabilities of the collision probability theory to a supercell model that allows existence of two different fuels. The radioisotopic inventory results for different fuels obtained from the modified V:BUDS code are in excellent agreement with the benchmark problems. These accurate results may be used in general fuel cycle and transmutation studies within power reactors.

TABLE OF CONTENTS

List of Figures

List of Tables

1. Introduction

The purpose of this dissertation is to expand the applications of the collision probability theory in the reactor performance and safety analysis and fuel cycle evaluations. This expansion can result in increased accuracy and utility of the collision probability theory in the treatment of heterogeneous cores and hence provide a faster and much simpler alternative when compared to much more complicated neutronic computer codes in addressing the feasibility and effectiveness of fuel cycle strategies.

The past few years have seen a clear resurgence of public opinion and interest in use of nuclear energy to meet future energy demands. This resurgence has been echoed by the Administration through its National Energy Policy where it calls for an increase in the diversity of the nation's sources of traditional and alternative fuels. As part of this policy, the Administration calls for the safe expansion of nuclear energy by streamlining the licensing of nuclear power plants and establishing a national repository for nuclear waste [1]. Some of the specific points of this policy are the development of the advanced fuel cycles and next generation technologies for nuclear energy. The policies of the United States to develop and deploy fuel conditioning methods that reduces waste streams and enhances proliferation resistance are specifically noted.

In addition, while there has not been a major power plant construction in the United States since 1990's, the increase power demand over the past two decades has outstripped

the added capacity and the price of petroleum and natural gas has dramatically increased the unit cost of electricity derived from these natural resources. For example, while the residential sector electric energy consumption has increased from 2.5 quadrillion BTU in 1980 to 4.5 quadrillion BTU in 2006, the average retail price of this electricity generated from fossil fuel has increased from 5.5 ¢/kwh in 1980 to 10.5 ¢/kwh in 2006 [40].

In lieu of these developments, some electric utility companies have expressed interest in developing, licensing and operating the next generation of the power reactors. As part of the decision making process for the selection of the reactor type and the fuel cycle, several parameters and variables are being considered by utilities and government. Reactor safety, economics, disposal of the spent nuclear fuel and nonproliferation concerns constitute four of these major parameters.

As part of the reactor safety considerations, determination of neutron flux within the reactor core plays an important role in regards to improving the overall reactor thermal efficiency by flattening the neutron flux in the fuel axial and radial direction and hence increasing the reactor thermal output for a given maximum fuel temperature and increasing the reactor safety by decreasing the temperature peaking within the reactor fuel.

In regards to the fuel cycle considerations, several alternatives are required to be considered which includes economic as well as non-proliferation considerations.

The economic considerations are based on minimization of the volume, decay power and radiotoxicity of the spent fuel or ancillary waste, the fuel reprocessing costs for the chosen fuel cycle, and the storage costs of the final spent nuclear fuel which is correlated to its volume.

Reactors and fuel cycles are protected by intrinsic and extrinsic safeguards. The intrinsic aspects with which this study is concerned relate to the quantity and isotopic content of the spent fuel that is to be reprocessed or stored within a temporary storage facility such as the power plant spent fuel pool storage system or a permanent geological repository system. In addition to affecting the proliferation-relevant characteristics of nuclear fuel and waste, the isotopic vector directly impacts the storage capacities of short and long term storage facilities via the heat generation capabilities of the actinides and fission products.

All of these metrics depend strongly on the neutron flux spectrum and distribution characteristic of the reactors within a fuel cycle system. Therefore, determination of the flux as well as the isotopic contents of the fuel during its burnup process becomes a vitally important task for fuel cycle analysis.

There are several elaborate and comprehensive neutronic codes that can satisfy the above stated objectives. However, these codes are laborious and very time consuming. In recent years, efforts have been initiated to develop simple code models that can satisfy the

required technical challenges in determining the needed reactor and fuel cycle study parameters and be implemented on a PC platform with a few seconds run time.

These simple models utilize collision probability theory that yields reasonably accurate results at the fraction of the computational times that is required by the more elaborate computational approaches.

In the collision probability theory, the reactor core is assumed to consist of identical unit cells where each cell consists of a fuel region in the center and moderator/coolant region surrounding the fuel region. The neutron transport equation in the unit cell is then solved by decoupling the spatial and energy effects in the transport equation and then writing equations for the flux for each of the fuel and moderator/coolant regions of the unit cell. The result is a set of algebraic equations that are coupled through region-to-region transmission and escape probabilities.

The current collision probability theory used to analyze heterogeneous reactor cell unit treats each of the fuel and moderator regions as single lump with uniform properties and fluxes within each lump. It also assumes that the unit cells are uniform throughout the core with a single type of fuel material. This work attempts to improve the current theory by treating the fuel region of the unit cell as a multi-region area and investigate whether the developed methodology enhances the results of the current lumped two region unit cell analyses in regards to multiplication factors and isotope inventory calculations versus

postulated burnup periods. The current work also attempts to develop a methodology to investigate similar types of analyses based on existence of two types of different fuel materials within the reactor core unit cells. This developed methodology will allow the usage of the collision probability theory to study the disposition of excess reactor or weapon grade plutonium within a commercial power reactor. The current methodologies on treatment of heterogeneous reactor cores are limited and do not allow high fidelity treatment of two different fuel types within the reactor core.

At the present time, the modeling of unit cell is rather coarse in a sense that the neutron fluxes are taken to be constants in each of the unit cell fuel and moderator/coolant regions. This modeling neglects the effect of fuel self shielding and hence neglects the neutron flux gradient in the fuel region. Therefore, it increases the inaccuracy of the predicted results in regards to actinide and fission products in the spent fuel and hence increases the uncertainty in the fuel cycle and reactor safety selection and design process.

In addition, the current model is a situation where the reactor consists of a lattice of identical unit cells. This approach can treat heterogeneous lattices where the composition of the fuel varies from pin to pin, say only through decoupled calculations for each fuel type. In cases where large regions of fuel, at the level of assemblies or larger, remain homogeneous this treatment retains a good deal of validity. However, there are many circumstances when this approach would yield unsatisfactory results. For example, there are proposals from the Department of Energy to use excess weapon grade plutonium as a

fuel in the civilian power reactors. In collaboration with Canadian and Russian agencies, prototypes of manufactured fuel using excess weapon grade plutonium have been designed and produced. Use of these mixed oxide fuel (MOX) within the power reactors satisfies two goals. First, it provides a high heat value fuel source and secondly, burns up excess actinides to a point where the material is not attractive from nuclear proliferation perspective. As part of implementation of the above strategy, Department of Energy started construction of the mixed oxide (MOX) fuel fabrication facility at Savannah River Site in November of 2005 and consequently, the United States Nuclear Regulatory Commission (NRC) amended the license for the Catawba Nuclear Station to irradiate four MOX fuel assemblies [41]. Duke Power is now seeking NRC approval to burn MOX fuel assemblies in its four units at McGuire and Catawba Nuclear Stations. The above practice is more established in Europe where 37 reactors are operating with part MOX loading and some additional reactors are licensed to do so when need arises [42].

The current heterogeneous treatment of the reactor core using collision probabilities do not account for the fact that a different fuel type may be present in the core. Furthermore, the MOX fuel design in the example given above calls for heterogeneity to exist at the fuel assembly level, so that the neutronic coupling between uranium oxide and plutonium oxide bearing pins will be considerable.

Therefore, there is a need to expand the current modeling of the reactor core using collision probability theory in solving for fluxes within a unit cell. This expansion will

provide allowance to account for the non-uniformity of the neutron flux in the fuel region and use of MOX or other fuel in the reactor core in addition to standard enriched uranium oxide (UOX) fuel.

2. Review of Current Literature

An accurate understanding of neutron transport processes is necessary in several fields of study; however full neutron transport solution of time dependent problems encountered in these fields can be computationally expensive. Hence, considerable effort has been dedicated to developing approximate solution techniques that are computationally much faster and at the same time are accurate enough for intended applications. The focus of this dissertation is on generalizing the collision probability theory for solving the neutron transport equations in several configurations with applications in studies of next generation of power reactors, nuclear reactor safety analysis, advanced fuel cycle initiatives, and use in transmuting extremely long lived radioactive isotopes for addressing the nuclear non-proliferation issues and more economical storage capabilities.

Several textbooks and journal articles provide an overview of many of these approximation methodologies [2], [3], [4], [5], [13], [38] and [39]. Reference [32] provides a review of numerical methods for solving the integro-differential, integral, and surface-integral forms of the neutron transport equation. Reviewed methodologies in Reference [32] include the discrete ordinates finite difference method, the method of characteristics, finite element approximations, the collision probability method, and the nodal methods. Also, a comprehensive review of these methodologies is provided in References [10] and is updated and summarized in this section.

The energy dependence of the flux is usually treated by one of the two methods. In the multi-group formulation, the energy spectrum is discretized into tens or hundreds of groups. The neutron flux, nuclear cross sections and group to group transfer functions are averaged over each group in a manner that aims to preserve the correct interaction rate within that group. The energy dependent equation of neutron conservation is then written as a set of coupled algebraic equations in energy. Typically the control absorber concentration is iterated upon, or the multiplication factor k_{eff} is treated as an eigen value.

The continuous method aims to avoid complications that arise in calculations involving discontinuous functions such as the scattering kernel. The aim is to formulate approximate differential equations for a smooth, slowly varying function such as the slowing-down density q. The slowing-down density is the number of neutrons per cm^3/sec at which neutrons slow down past a given energy E. This is accomplished by a Taylor series expansion of the collision density, which appears in the integrand of q. Truncation of the series allows the integral equation to be transformed to a set of coupled first order differential equations.

Since the spatial dependence of the flux exhibits higher order dimensionality, methods for its treatment are necessarily more involved. In this section, common approximations to the spatially dependent neutron transport equation and their computational implementation are summarized. [10]

The collision probability method approximates the integral transport equation by dividing space into a set of homogeneous regions or cells and then computing the probability that a neutron in one region will contribute to the flux in another region. This contribution is modeled by formulating region-to-region transmission and escape probabilities. This method is exact provided that the correct probabilities are obtained. However, they are obtained beforehand as a function of geometry and collision probability via a simplified transport calculation employing one of several other methodologies. While this method requires a considerable amount of work for initial problem setup, subsequent computational effort is low. In this scheme, the spatial variation of flux in a region of interest is unimportant and hence each region is represented by equivalent homogenized cross sections $\overline{\Sigma}$ and average fluxes $\overline{\phi}$ that preserves interaction rates within macroscopic homogenized region. This condition over a heterogeneous region with volume V is satisfied by $\overline{\Sigma}\overline{\phi} = \int_V dV\Sigma(r)\phi(r)$.

Nodal methods are often used when the spatial dependence of the flux in full three dimensions is of interest. This method can be a good substitute for numerical solution of diffusion equations in three dimensions which can be computationally time consuming and prohibitive for parametric studies. In this methodology, the reactor core is subdivided to relatively large regions or node cells in which the material composition and flux are assumed to be uniform. Then attempts are made to determine the coupling coefficients characterizing node cell to node cell leakage and then determining the node cell fluxes.

The flux for each node n is developed as $\phi_n = \sum_{n'=1}^{N} K_{nn'} S_{n'}$ where $S_{n'}$ is the neutron source strength in node n', $K_{nn'}$ is the nodal coupling coefficient and N represents the total number of node cells. The nodal coupling coefficients are typically obtained in empirical fashion. Proper selection of nodal coupling coefficients will generate extremely useful three dimensional flux distributions. Selection of the coupling coefficients is very problem sensitive and requires adjustments to obtain good agreements against more detailed calculations or power distribution measurements. Nodal methods are computationally very fast and have found acceptance for use in three dimensional reactor simulations [3, 5].

The position dependence of the flux is heavily dependent upon the angular dependence of the scattering transfer function, which is itself generally a strong function of position. Discrete ordinates method addresses and discretizes this angular dependence of the transport equation. In the discrete ordinates approximation, the transport equation is evaluated at only a few discrete directions or ordinates. Thus the full transport equation may be reproduced, with appropriate weighting, by quadrature. The scattering and fission kernels are formulated in terms of the laboratory frame cosine of the neutron scattering angle, μ, expanded in Legendre polynomials (the P_N method), and represented as discrete functions of the ordinates. The ordinates themselves are often chosen to the roots of the highest order Legendre polynomial in the expansion. Spatial discretization schemes incorporate algorithms for sweeping in the direction of neutron motion, necessitating

several ‘passes’ through each location. Often, the inner iterative solution for $\phi(x_i, \mu_j)$ is accelerated by using a low-order deterministic calculation, perhaps via diffusion theory (the P_1 method), to generate an initial guess for ϕ. High order discrete ordinates calculations are also used as trial functions to formulate a lower-order approximation to ϕ for use with the nodal approach.

The discrete ordinates method in more than one spatial dimension has a well known defect named as ‘the ray effect’. Due to the discrete nature of the angular approximation, neutrons do not reach regions where they otherwise would, sometimes producing large spatial oscillations in the scalar flux ϕ [5, 19]. However, some methods have been developed to eliminate these ray effects by introducing extra terms in the discrete ordinates equation [20]. These extra terms are designed to ensure that the discrete ordinates equations will produce the same angular moments as the P_N equations.

At a fundamental level, neutron transport through matter is an essentially stochastic process. The total cross section is a probability and not a certainty that a neutron will have a collision while traversing a certain spatial distance. If neutron has a collision, the cross section for various processes such as scattering, radiative capture, fission, and so on are then just probabilities. Hence the neutron flux is actually the mean or expectation value of the neutron distribution function. So, the Monte Carlo method directly simulates neutron process as a stochastic process [5]. In this methodology, neutron histories are directly simulated from birth, usually through isotropic emission from fission. The

fission source is generated by sampling a Bayesian statistical distribution in the energy, positional and directional variables; the prior distribution is obtained from guess work, iteration or experience. A neutron is followed through the slowing down process, until it is absorbed or escapes. Treatment is as exact as the geometric and physical inputs allow, either point-wise or group-wise cross sections may be used. A large number of histories are generated to reduce variance to within specified tolerances. Variance reduction may be accelerated by the attachment of weights to individual neutron histories. This is often carried out on the basis of an adjoint or importance function obtained beforehand by deterministic means [10].

Now we will briefly discuss some of the more widely used software packages that are used to perform reactor physics analysis including neutron flux and fuel burnup determinations. This task is performed to evaluate the relevance of these packages to modeling of reactor core and fuel burnup analysis as related to the topic of this dissertation.

SCALE (Standardized Computer Analysis for Licensing Evaluation) computer software system developed at Oak Ridge National Laboratory (ORNL) is a widely used computational tool used to investigate issues related to criticality safety and burnup credit analysis [22]. The latest version of the code package, SCALE 5, has the capability to treat multiple unit cells. Each unit cell specification contains the cell type (infinite homogeneous medium, multi-region, or lattice cell), cell geometry type, and appropriate

material and geometry data. Any number of unit cells may be specified, but each material may appear in only one unit cell. SCALE code package has several modules and these modules are used for different applications. We will discuss some of the modules that have relevance to the topic of this dissertation.

The SCALE package contains KENO V.a and KENO-VI Monte Carlo criticality safety modules. These modules provide SCALE 5 with criticality search capabilities that allow each unit cell to be explicitly identified with either a unit or a material that is being modified. A search case may alter the material densities, the pitch of the cells in a lattice, or simple geometry boundaries. Since multiple unit cells are allowed, a criticality search may be performed on lattices containing more than one fuel pin type. As the geometry or material is modified, the unit cell is similarly modified, thus ensuring that the cross sections for the material are appropriately processed. Cell-weighted materials can be included in the searches, updating the geometry, material, and cross sections as the search progresses.

CENTRM (Continuous Energy Transport Module) of SCALE package is a one-dimensional (1-D) discrete ordinates code that uses a point-wise continuous energy cross-section library to produce a set of point-wise continuous energy fluxes at discrete spatial intervals for each unit cell. These fluxes are then used by PMC (Point-wise Multi-group Converter) module to collapse the point-wise continuous energy cross sections into multi-group cross sections for each nuclide in each material in the unit cell. CENTRM can be

used to explicitly model fuel or absorber materials in subdivided regions, such as concentric rings in a fuel pin, to more precisely model the spatial effect on the flux and cross sections. Other modules in SCALE 5, such as KENO, can then use these multi-group cross sections.

STARBUCS (Standardized Analysis of Reactivity for Burnup Credit using SCALE) is a sequence to perform criticality calculations for spent fuel systems employing burnup credit. STARBUCS automates the criticality analysis of spent fuel configurations by coupling the depletion and criticality aspects of the analysis, thereby eliminating the need to manually process the spent fuel nuclide compositions into a format compatible with criticality safety codes. STARBUCS automatically prepares the input for all codes in the analysis sequence, executes the codes through the SCALE driver, and performs all module interface and data management functions for the user. STARBUCS performs a depletion analysis calculation for each spatially varying burnup region (if an axial burnup profile is specified) of a spent fuel assembly using the ORIGEN-ARP methodology of SCALE. The ORIGEN-ARP methodology serves as a faster alternative to the SAS2H depletion analysis sequence in SCALE, while maintaining calculational accuracy. The spent fuel compositions are then used to generate resonance self-shielded cross sections for each burnup-dependent fuel region using the SCALE **C**riticality **S**afety **A**nalysis **S**equence (CSAS). Finally, a KENO criticality calculation is performed using the spatially varying cross sections to determine the neutron multiplication factor for the system.

ORIGEN-ARP is a sequence in SCALE that serves as a fast and easy to use system to perform nuclear irradiation and decay calculations with the ORIGEN-S code using problem dependent cross sections. ARP (Automatic Rapid Processing) uses an algorithm that allows the generation of cross section libraries for the ORIGEN-S code by interpolation over pre-generated cross section libraries. The interpolations are carried out on the following variables: burnup, enrichment, and moderator density.

ORIGEN has the capability to handle actinides with up to 30 explicit fission product yields. This capability allows for higher order actinides to address data requirements for actinide transmutation studies. These explicit yields improve fission product inventory and decay property predictions. In addition, ORIGEN-ARP methods allow the analysis of MOX fuel. It includes the MOX cross section libraries for most European MOX reactor types and fuel assembly designs [21].

NEWT (NEW Transport algorithm) module of SCALE 5 introduces two-dimensional analytical capability as a flexible mesh discrete ordinates code. Unlike traditional S_n codes, NEWT is not limited to Cartesian or cylindrical coordinate systems. NEWT's arbitrary geometry, or flexible mesh, allows users to combine orthogonal, radial, and other more unusual geometry shapes in the same model. NEWT is unique in the domain of discrete ordinates methods because it is based on a non-orthogonal, flexible mesh scheme that allows accurate representation of complex geometric configurations that are

normally impossible to model with discrete ordinates methods without significant approximations. Using a discrete ordinates approximation to the transport equation on an arbitrary grid, NEWT provides a rigorous deterministic solution for non-orthogonal configurations. Lower-order deterministic methods typically applied in lattice analyses (e.g., integral transport and collision probability methods) do not provide the angular resolution necessary to treat strongly anisotropic fluxes, such as those in the vicinity of strong absorbers or in high-leakage cores [22].

The SCALE package has been studied extensively for validation. Some of these validating studies are identified in [10]. In addition, the new features of the latest version of SCALE have been reviewed by several researchers. For example, the continuous energy version KENO-V.a and KENO-VI are investigated in [23], cross section libraries of ORIGEN-ARP is reviewed for validation in [24], and the fuel burnup and depletion capabilities of TRITON module are validated in [25, 26].

There are several other code packages such as DIF3D/VARIANT/REBUS3 that were developed at Argonne National Laboratory that function along the same lines as SCALE/TRITON/ORIGEN. A review of these codes along with some additional codes is provided in [10] and hence is not repeated here.

Finally, our literature review indicated that a fast and user friendly computational package V:BUDS (Visualize: Burnup, Depletion, Spectrum) was developed to provide a

scenario dependent material balances for fuel cycle systems studies. Even though V:BUDS does not replace the higher fidelity code packages such as SCALE, but its simple interface and very short computational time makes it a useful tool in parametric studies of different fuel cycles [10, 17]. Fuel element / moderator geometry and composition, reactor geometry, fuel residence time and target burnup are accepted as inputs and then the model calculates the buildup of 24 actinides, as well as fission products, along with the lethargy dependent neutron flux. V:BUDS operates at a unit cell level and couples a detailed multi-group treatment of energy dependence with a simplified collision probability model of spatial dependence. V:BUDS treats each of the fuel and moderator/coolant regions within the unit cell as uniform homogeneous volumes. V:BUDS relies on a multi-group formulation to treat energy dependence. V:BUDS is bundled with cross sections libraries for a wide range of potential constituents. The cross section libraries were developed from ENDF/B-VI data using NJOY99 processor at 5 different temperatures (300°K, 600°K, 900°K, 1200°K, and 1500°K). The results of VBUDS have been favorably compared against OECD/NEA benchmarks for homogeneous MOX and UOX LWR cores [27].

V:BUDS is driven by a graphical user interface (GUI). This interface allows the user to customize the geometry and composition of the unit cell under consideration that includes the isotopic contents and quantity of fuel material and moderator/coolant, the temporal parameters governing a burnup calculation and the desired output plots. Figures 2-1 and 2-2 represent a sample screenshots of the V:BUDS input parameters.

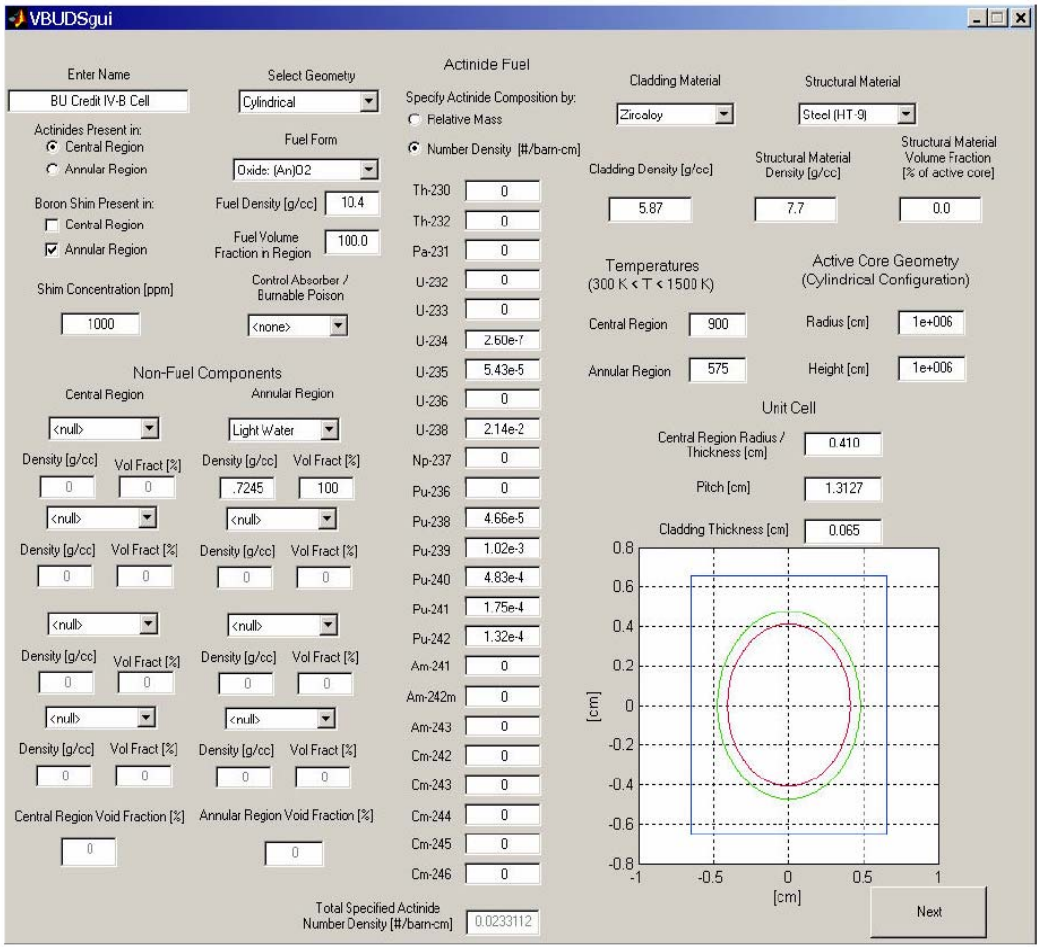

Figure 2- 1: V:BUDS GUI First Input Screen

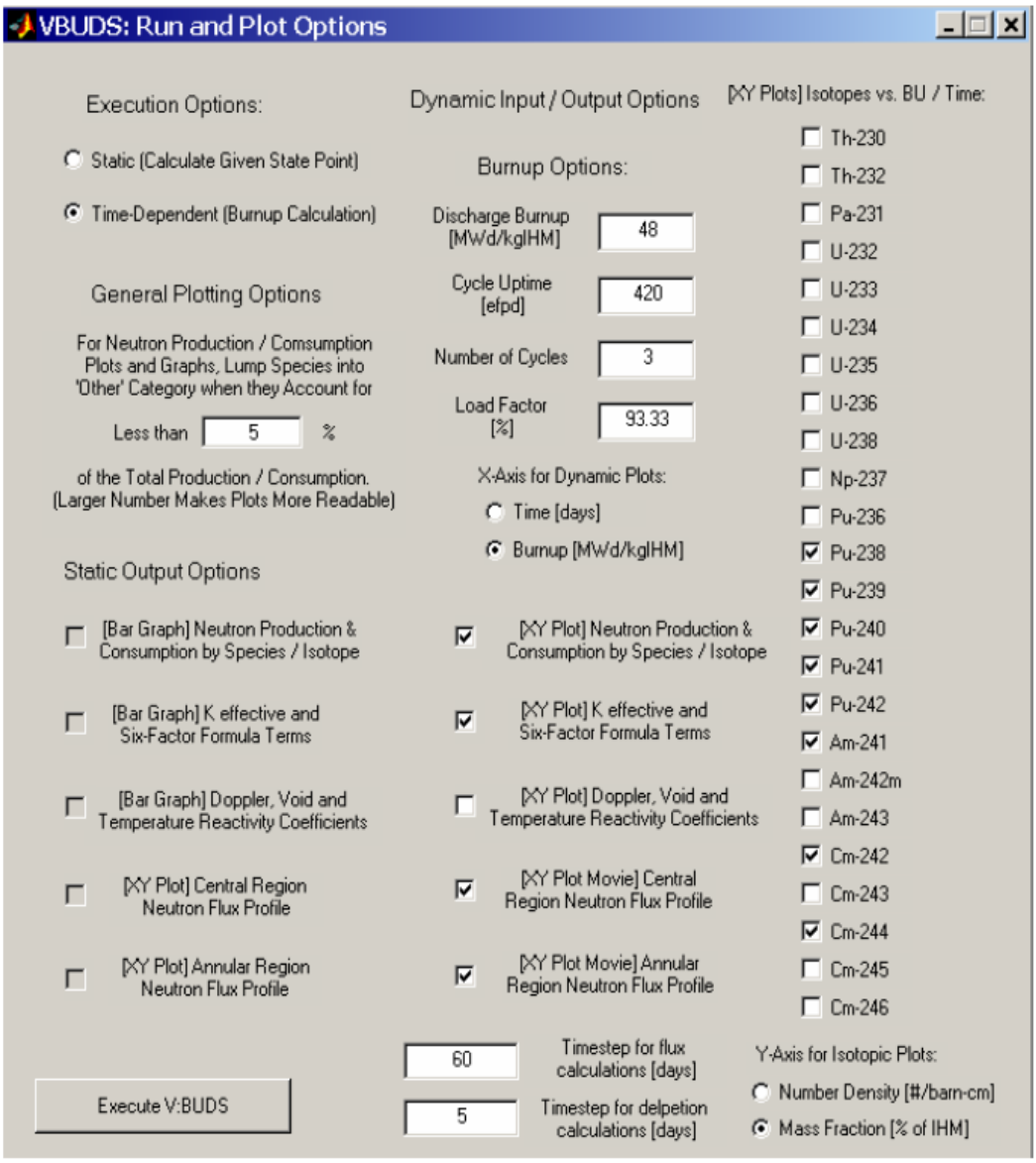

Figure 2- 2: V:BUDS GUI Second Input Screen

As indicated in Figure 2-2,V:BUDS offers two output options. First, the static (fuel burnup not simulated) option where spectral calculation is carried out for only the specified composition and second, time dependent option where burnup and depletion calculations are performed. As an output sample, the neutron energy spectra for fresh

fuel, within the fuel pin and the coolant/moderator annulus, are depicted in Figure 2-3. Figures 2-4 and 2-5 provide V:BUDS capabilities in demonstrating the burnup dependent effective multiplication factor for a given fuel composition and each of its contributing six factors and evolution of isotopic contents for a given fuel as a function of the fuel burnup. These capabilities are very appropriate in the studies of fuel cycle selection and nuclear non proliferation studies.

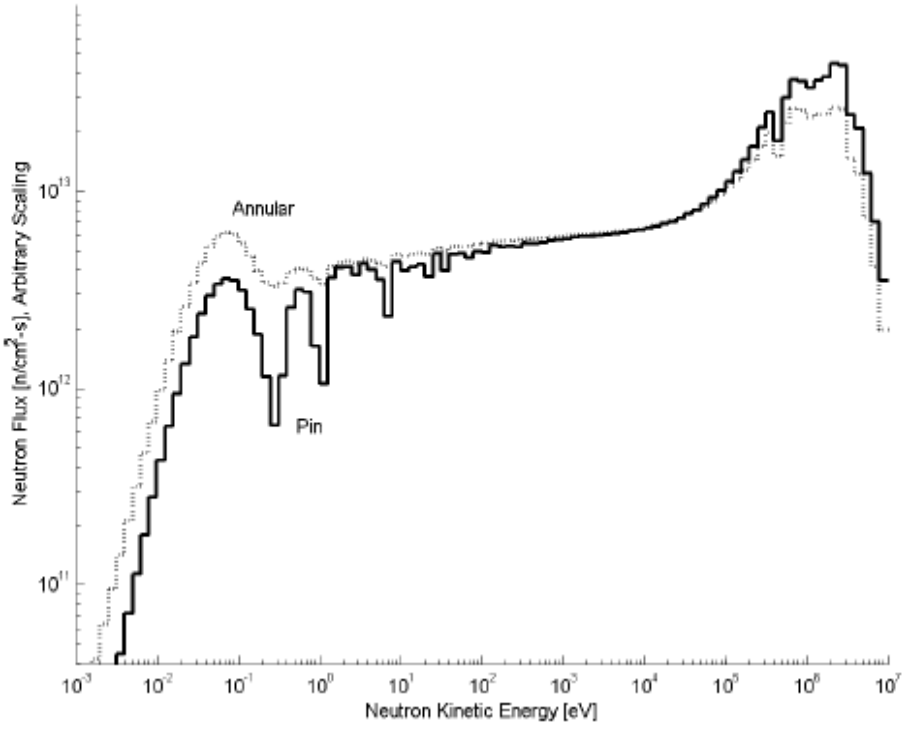

Figure 2- 3: V:BUDS Demonstration of Neutron Energy Spectra for a Fresh Fuel Composition

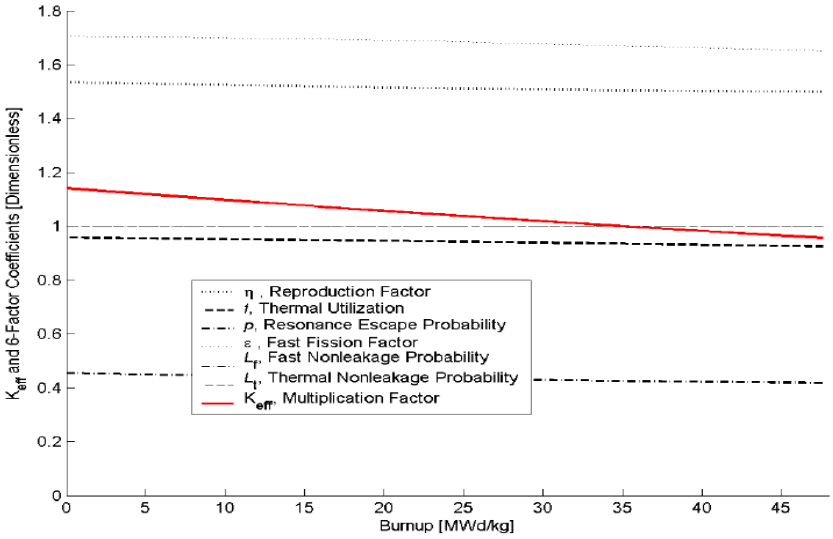

Figure 2- 4: V:BUDS Demonstration of Burnup Dependent k_{eff} and Six Factor Formula terms for Time Dependent Calculations

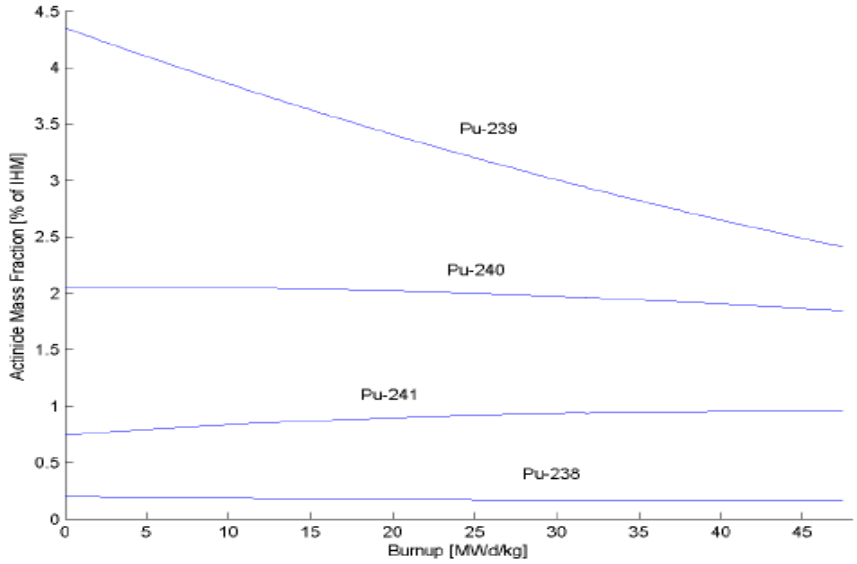

Figure 2- 5: V:BUDS Demonstration of Evolution of Isotopic Composition for a Selected Plutonium Fuel

Based on the review of the appropriate literature, we conclude that V:BUDS and its theoretical model will be best suited for our work and hence we will use this computational tool as a corner stone of our analyses for expanding and generalizing the collision probability theory to handle complicated problems.

3. Dissertation Description - Objectives and Problems

We have generalized the treatment of unit cell models using collision probability theory for fuel burnup studies in heterogeneous reactors by considering the fuel as a non-uniform multi-region area, and have developed an extension to the collision probability theory to situations where zero net neutron leakage across the unit cell boundaries is not appropriate.

The above outlined objectives are achieved by analyzing two complex problems with different geometries. Each complex problem in general is presented by an identification of its scope and statement of the problem, specific background and introduction, developed methodology, any benchmark problem as applicable, and results of the developed methodology and comparisons with the benchmark results as appropriate and concluding remarks.

3.1 Complex Problem # 1

3.1.1 Scope/Statement of Problem

We have developed approximate equations for neutron transport using collision probability theory for a unit square cell with an infinitely long cylindrical fuel pin located at the center of the cell where the fuel pin is treated as a non-homogeneous fuel medium to account for non-uniformity of neutron flux within the fuel medium.

The multi-region fuel area accounts for the non-uniformity/variability of the neutron flux and material properties across the fuel region which in turn affects the neutron transmission and escape probabilities inside the fuel region. The non-uniformity of the neutron flux and material properties better treats the self shielding effects inside the fuel region. The fuel within a reactor core is burned from outside surface toward inside of the fuel region and the developed treatment addresses this phenomenon.

3.1.2 Background/Introduction

A general form for the time independent neutron transport equation is:

$$\Omega \cdot \nabla \quad \phi(r,\ E,\ \Omega) + \Sigma_t\, \phi(r,\ E,\ \Omega) =$$

$$\int_{4\pi} d\Omega' \int_0^{\infty} dE'\ \Sigma_s(r,\ E' \rightarrow E,\ \Omega' \rightarrow \Omega)\phi(r,\ E',\ \Omega') +$$

$$\frac{\chi(E)}{4\pi} \int_0^{\infty} dE'\ \upsilon\ \Sigma_f(r, E')\phi(r,\ E') \qquad \text{(Eqn: 3.1-1)}$$

where;

Ω (ster): directional unit vector,

r (cm): positional vector,

E (eV): energy,

$\phi(r.E,\Omega)$ (n/cm^2/s/ster/eV): neutron flux per unit solid angle per unit energy

$\phi(r,E)$ (n/cm^2/s/eV): neutron flux per unit energy; $\phi(\mathrm{r},\mathrm{E}) = \int \mathrm{d}\Omega\phi(\mathrm{r},\mathrm{E},\Omega)$

$\Sigma_t(r,E,\Omega)$ (1/cm) : total macroscopic cross section

$\Sigma_s(r,E'\to E,\Omega'\to\Omega)$ (1/cm/eV/ster): cross section for scattering from (E',Ω') into (E,Ω)

$\Sigma_f(r,E')$ (1/cm): macroscopic fission cross section

$\chi(E)$ (1/eV): probability that a fission neutron is born at energy E

$\upsilon(r,E)$ (neutron per fission): fission yield

Collision probability theory solution of the integro-differential equation for neutron transport (Eqn: 3.1-1) for a given unit cell is accomplished by decoupling the spatial and energy effects. Two crucial assumptions are made in order to accomplish the subject decoupling.

First, elastic scattering is assumed to be linearly anisotropic in the center-of-mass system and for calculations involving the spatially-dependent flux, the total cross section is replaced by transport cross section as follows:

$$\Sigma_{tr} = \Sigma_a + \left(1 - \overline{\mu}\right)\Sigma_s \qquad \text{(Eqn: 3.1-2)}$$

where $\overline{\mu}$ is the average value of cosine of the scattering angle. For spatial transport modeling, scattering events devolve into a neglected forwarded scattering component with no energy transfer and an isotropic component governed by Σ_{tr}. Second, a unit cell consisting of homogeneous fuel region surrounded by a homogeneous moderator/coolant is assumed for the neutron transport between the fuel and moderator/coolant (two region model). The subject two region model is depicted in Figure 3.1-1.

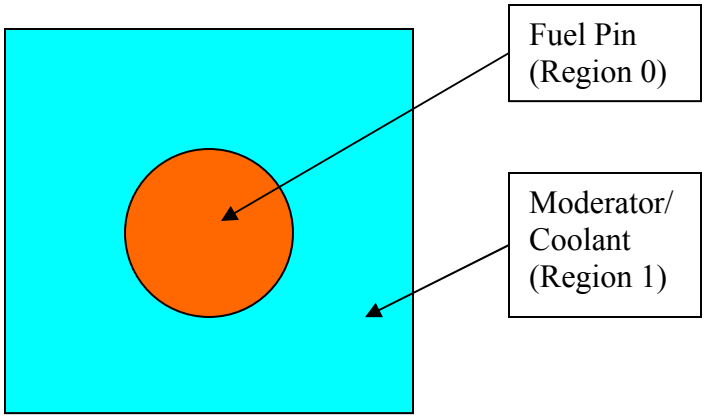

Figure 3.1- 1: Unit Cell Representing a Two Region Model

In the above two region model, the fuel region is considered to be homogeneous where the flux and properties are taken to be uniform Hence, the following transmission and

escape probabilities are defined for the fuel (region 0) and the moderator/coolant (region 1).

Table 3.1- 1: Transmission and Escape Probabilities for Unit Cell Two Region Model

P_0	Probability that a neutron having had its last interaction in the fuel, will escape the fuel without further interaction.
T_0	Probability that a neutron entering the fuel region is transmitted without interaction.
P_1	Probability that a neutron, having had its last interaction in the moderator/coolant, will escape the moderator/coolant without further interaction.
T_1	Probability that a neutron entering the moderator/coolant is transmitted without interaction (Dancoff factor)

Terms P_0, T_0, P_1 and T_1 are illustrated in Figure 3.1-2.

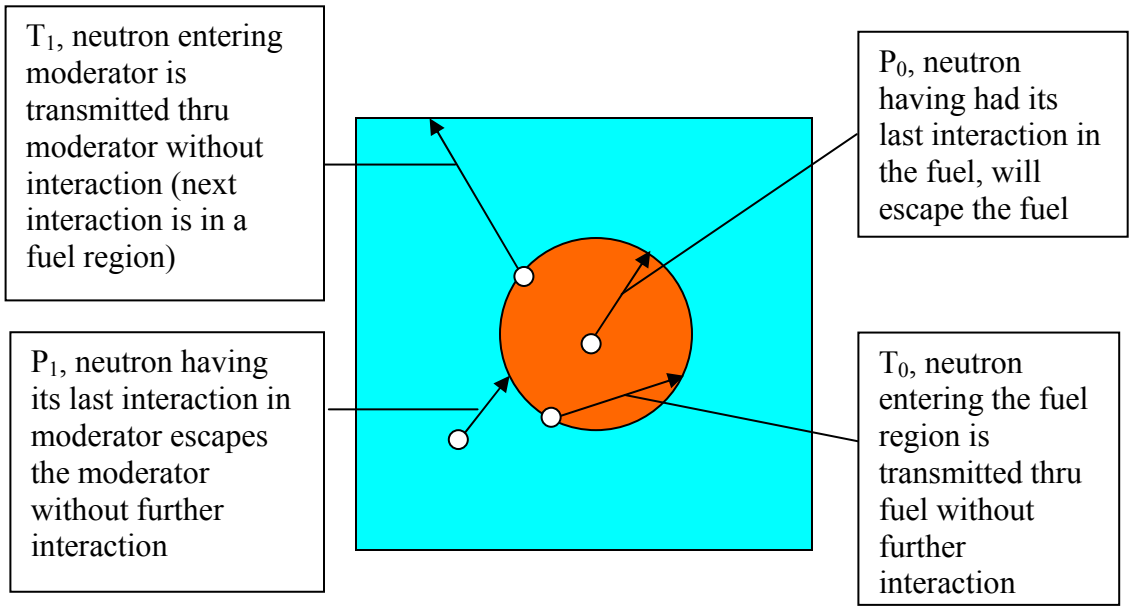

Figure 3.1- 2: Illustration of Terms P_0, T_0, P_1, and T_1 in a Two Region Unit Cell Model

Decoupling of spatial and energy effects in the neutron transport equation can now be accomplished using region to region neutron transmission probabilities Π_0 and Π_1. These transmission probabilities, Π_0 and Π_1, are defined in terms of P_0, T_0, P_1 and T_1 as follows:

Π_0 is defined as the probability that a neutron appearing in the fuel (region 0) at energy E will undergo its next interaction in the moderator/coolant (region 1).

Π_1 is defined as the probability that a neutron of energy E appearing in the moderator/coolant undergoes its next interaction in the fuel.

Π_0 and Π_1 are derived in [10] as;

$$\Pi_0 = P_0(1-T_1)\frac{1}{1-T_0T_1} \qquad \text{(Eqn: 3.1-3)}$$

$$\Pi_1 = P_1(1-T_0)\frac{1}{1-T_0T_1} \qquad \text{(Eqn: 3.1-4)}$$

Values of P_0, T_0, P_1 and T_1 for infinitely long cylinders with radius of R have been derived and are presented as follows. It is noted that this infinitely long cylinder represents the fuel region in the two region unit cell model.

The following closed form expression has been derived for T_0 by using diffusion theory to solve the pin-cell transport problem [9]. This derivation is based on isotropic neutron emission and constant cross section within the central fuel region. Equation 3.1-5 or similarly developed equations from reference [10] will be used to determine the transmission probability through the central region of the multi-region cylindrical fuel model developed in problem number 1 of this dissertation.

$$T_0 = 1 - \frac{2}{3}(\Sigma R)^2\left(\begin{array}{l} 2\Sigma R\left[K_0(\Sigma R)I_0(\Sigma R) + K_1(\Sigma R)I_1(\Sigma R)\right] - 2 + \dfrac{K_1(\Sigma R)I_1(\Sigma R)}{\Sigma R} \\ -K_0(\Sigma R)I_1(\Sigma R) + K_1(\Sigma R)I_0(\Sigma R) \end{array}\right)$$

(Eqn: 3.1-5)

where $K_i(\Sigma R)$ and $I_i(\Sigma R)$ are modified i^{th} order Bessel functions and Σ is the fuel total macroscopic interaction cross section.

P_0 is obtained by use of reciprocity relationship between T_0 and P_0.

$$1 - \mathrm{T}_0 = \frac{4\mathrm{V}_\mathrm{f}\Sigma}{\mathrm{A}_\mathrm{f}}\mathrm{P}_0 \qquad \text{(Eqn: 3.1-6)}$$

The volume to surface area ratio $\left(\frac{V_f}{A_f}\right)$ for an infinite cylinder is $\frac{R}{2}$. So, P_0 is derived for the fuel region as;

$$\mathrm{P}_0 = \frac{1 - \mathrm{T}_0}{2\Sigma\mathrm{R}} \qquad \text{(Eqn: 3.1-7)}$$

T_1, the probability that a neutron entering the moderator/coolant region from the fuel region will be transmitted without interaction is known as the Dancoff factor.

Computation of T_1 for cylindrical geometry is complicated. Fortunately, it has been determined for the subject configuration by several researchers. Dancoff factors have been obtained as functions of geometry and attenuation coefficient via ray tracing techniques and expressed in tabular form for parallel circular cylinders as a function of two dimensionless parameters; the pitch to pin radius ratio and the pin radius to the mean free path in the moderator ratio. This approach is encoded in V:BUDS. P_1 is then calculated by use of reciprocity relation between P_1 and T_1.

Now, by knowing $P_0, T_0, P_1, T_1, \Pi_0$ and Π_1, the transport equation can be solved to find uniform fluxes in the fuel and moderator/coolant regions. The decoupled transport equation for two region unit cell model where spatial and energy variables have been decoupled are then presented in the following approximate form;

For Fuel Region (Region 0):

$$[\Sigma_0(\mathrm{E}) + \mathrm{D(E)B}^2]\phi_0(\mathrm{E}) =$$
$$(1 - \Pi_0(\mathrm{E}))\left[\int_0^\infty d\mathrm{E}'\phi_0(\mathrm{E}')[\ \Sigma_{s,0}(\mathrm{E}' \to \mathrm{E}) + \Sigma_{f,0}(E')\chi_0(E' \to E)\nu_0(E')]\right] +$$
$$\frac{V_1}{V_0}\Pi_1(\mathrm{E})\left[\int_0^\infty d\mathrm{E}'\phi_1(\mathrm{E}')[\ \Sigma_{s,1}(\mathrm{E}' \to \mathrm{E}) + \Sigma_{f,1}(E')\chi_1(E' \to E)\nu_1(E')]\right] \qquad \text{(Eqn: 3.1-8)}$$

For Moderator/Coolant (Region 1):

$$[\Sigma_1(\mathrm{E}) + \mathrm{D(E)B}^2]\phi_1(\mathrm{E}) =$$
$$\frac{V_0}{V_1}\Pi_0(\mathrm{E})\left[\int_0^\infty d\mathrm{E}'\phi_0(\mathrm{E}')[\ \Sigma_{s,0}(\mathrm{E}' \to \mathrm{E}) + \Sigma_{f,0}(\mathrm{E}')\chi_0(\mathrm{E}' \to \mathrm{E})\nu_0(\mathrm{E}')]\right] +$$
$$(1 - \Pi_1(\mathrm{E}))\left[\int_0^\infty d\mathrm{E}'\phi_1(\mathrm{E}')[\ \Sigma_{s,1}(\mathrm{E}' \to \mathrm{E}) + \Sigma_{f,1}(\mathrm{E}')\chi_1(\mathrm{E}' \to \mathrm{E})\nu_1(\mathrm{E}')]\right] \qquad \text{(Eqn: 3.1-9)}$$

We improve the solution to the unit cell flux equations by using collision probability theory and treating the fuel area as a multi-region area. This multi-region concept will account for the effects of self shielding and can even count for use of different fuel type

in each sub-region of the fuel region. We will develop the methodology within section 3.1.3 of this dissertation.

3.1.3 Developed Methodology and Definitions for Solving Complex Problem Number 1

The methodology for solving the proposed problem is provided in the following sections. This methodology will provide a tool for examining the effects of variability of the flux and material properties across the fuel region which in turn will affect the neutron transmission and escape probabilities inside the fuel region. These probabilities help determine important reactor physical parameters such as the multiplication factor in the unit cell and the fuel burnup and production of different radionuclides during the fuel irradiation process.

We divide the cylindrical fuel region to several sub-regions. Then we determine the transmission and escape probabilities within each of these fuel sub-regions. The proposed multi-region fuel complicates the determination of transmission and escape probabilities in the fuel region. A model of this subdivision is depicted in the Figure 3.1-3.

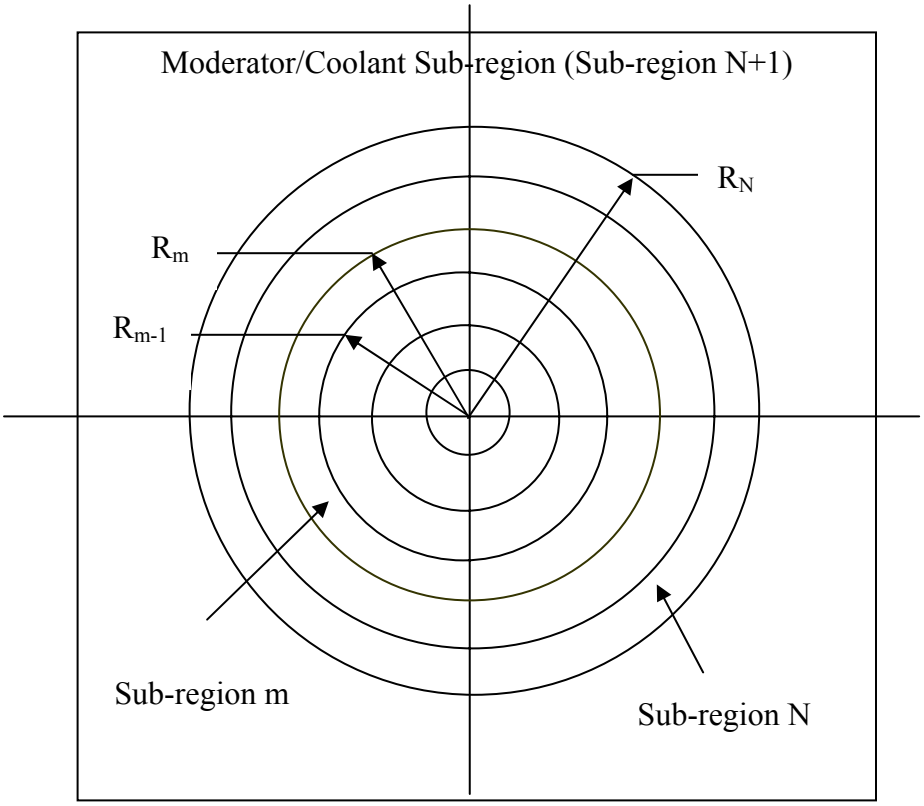

Figure 3.1- 3: Unit Cell with Multi-Region Fuel Model

Use of multi-region fuel area in a unit cell requires introduction of transmission and escape probabilities within each fuel sub-region. We use Figure 3.1-3 to derive these probabilities, $P_i^m, P_o^m, T_{i,o}^m, T_{o,i}^m, T_{o,o}^m$ and $\Pi_{m,n}$ based on the following definitions.

$T_{i,o}^m$ = probability that a neutron at energy E entering sub-region m from its inner surface is transmitted to its outer surface without interaction.

$T_{o,i}^{m}$ = probability that a neutron at energy E entering sub-region m from its outer surface is transmitted to its inner surface without interaction.

$T_{o,o}^{m}$ = probability that a neutron at energy E entering sub-region m from its outer surface is transmitted to its outer surface without interaction.

P_{i}^{m} = probability that a neutron at energy E, having had its last interaction in sub-region m, will escape through inner surface of sub-region m without further interaction.

P_{o}^{m} = probability that a neutron at energy E, having had its last interaction in sub-region m, will escape through outer surface of sub-region m without further interaction.

$\Pi_{m,n}$ = probability that a neutron appearing in sub-region m at energy E will undergo its next interaction in sub-region n.

For better understanding of the transmission and escape probabilities within each fuel sub-region m, these terms are depicted in Figure 3.1-4.

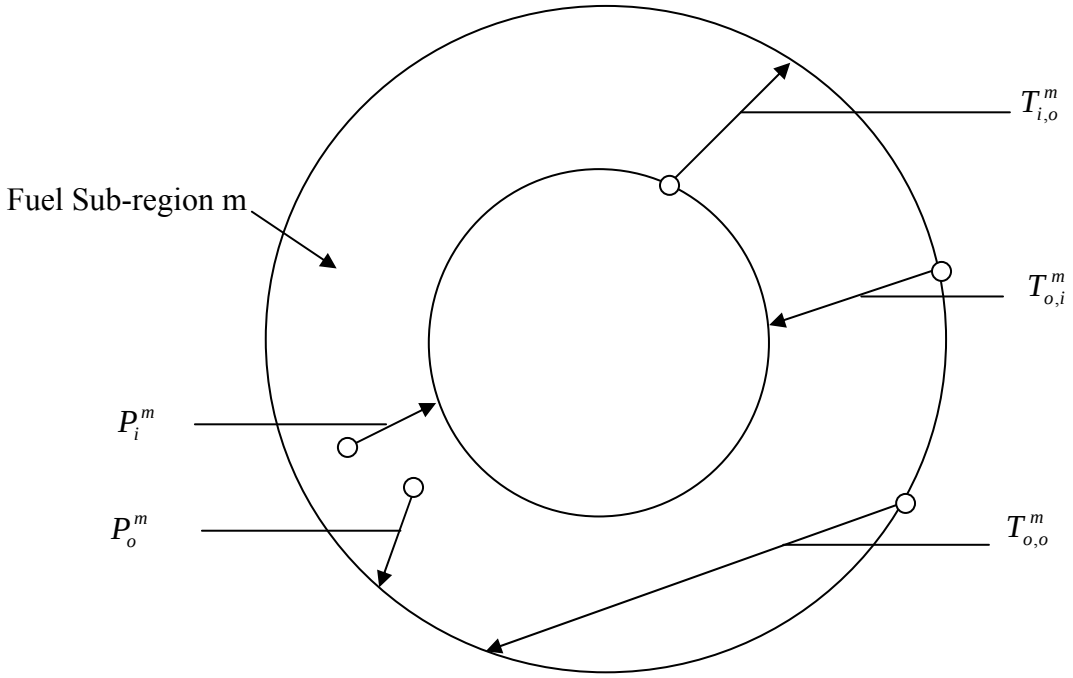

Figure 3.1- 4: Transmission and Escape Probabilities within Fuel Sub-Region m

3.1.4 Coordinate System for Solving Complex Problem # 1

Definition and selection of an appropriate set of coordinate systems is an absolute essential in the derivation of mathematical expressions for the transmission and escape probabilities in the fuel sub-regions. Use of the same coordinate system throughout the process of the mathematical derivation of transmission and escape probabilities will not result in mathematical expressions in their simplest possible form. Therefore, the coordinate system is carefully selected on a case by case basis for the derivation of each desired probability. These coordinate systems are depicted in the following sections.

3.1.5 Determination of P_i^m

The coordinate system for determination of P_i^m is shown in Figure 3.1-5. We take an arbitrary infinitesimal volume within region m (point of interest) of the fuel and define the following parameters;

r and z = radial and vertical coordinates

r_m and r_{m-1} = outer and inner radii of fuel sub-region m

L = distance between the point of interest and an arbitrary point on the inner cylinder with radius r_{m-1} (target point).

θ = L angle of declination from vertical

ω = angular distance between the target point and r axis.

R = radial distance between the fuel centerline and intersection of the vertical line from the point of interest and the horizontal plane that contains the target point. It is noted that the horizontal plane is perpendicular to z axis.

φ = angle between the line that connects the target point to the intersection of the vertical line from the point of interest and the horizontal plane containing the target point and the extension of the line that connects the target point and the fuel centerline.

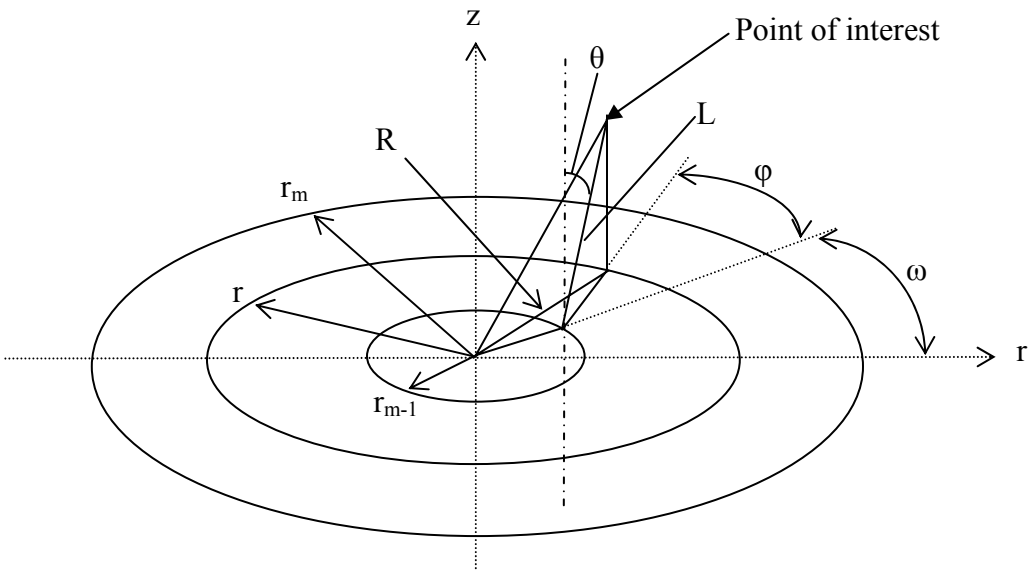

Figure 3.1- 5: Coordinate System for Determination of P_i^m

We will develop P_i^m by calculating the escape probability from a typical point of interest as shown in Figure 3.1-5 into a target point on the cylindrical region with radius r_{m-1} and move the target point all over the inner cylinder where there is a line of sight between the point of interest and the inner cylinder. Then the point of interest is moved throughout the m sub-region and the above process is repeated. This process is accomplished by triple integrals as shown in the numerator of equation 3.1-10. Then the overall escape probability is obtained by dividing the result of this triple integrals by the total neutron source within sub-region m. As part of the analysis, it is assumed that the neutron source (q) is uniform and isotropic in the annular region between r_{m-1} and r_m (region m) including the boundaries and the annular cylindrical region is infinite in the z direction. The concept of the above derivation is similar to derivation of view factors between two

surfaces however it includes the attenuation factor between the two surfaces which complicates the derivation tremendously.

$$P_i^m = \frac{4\int_{\varphi=0}^{\frac{\pi}{2}}\int_{\theta=0}^{\frac{\pi}{2}}\int_{L=0}^{L_{\max}}(q)\left(L^2\sin\theta d\varphi d\theta dL\right)e^{-\Sigma_m L}\int_{\omega=0}^{2\pi}\frac{\sin\theta\cos\varphi}{4\pi L^2}r_{m-1}d\omega}{(q)\pi\left(r_m^2 - r_{m-1}^2\right)} \qquad \text{(Eqn: 3.1-10)}$$

By using law of cosines,

$$R^2 = r_{m-1}^2 + L^2\sin^2\theta - 2r_{m-1}L\sin\theta\cos(\pi-\varphi) \qquad \text{(Eqn: 3.1-11)}$$

$$R^2 = r_{m-1}^2 + L^2\sin^2\theta + 2r_{m-1}L\sin\theta\cos\varphi \qquad \text{(Eqn: 3.1-12)}$$

L_{max} for a given (φ, θ) is found when the point of interest is located on the surface of cylinder with radius r_m. Hence,

$$r_m^2 = r_{m-1}^2 + L_{\max}^2\sin^2\theta + 2r_{m-1}L_{\max}\sin\theta\cos\varphi \qquad \text{(Eqn: 3.1-13)}$$

L_{max} is obtained as follows by solving equation 3.1-13.

$$L_{\max} = \frac{-r_{m-1}\cos\varphi + \sqrt{r_m^2 - r_{m-1}^2\sin^2\varphi}}{\sin\theta} = f(\varphi)\csc\theta \qquad \text{(Eqn: 3.1-14)}$$

where we have defined $f(\varphi)$ as follows for simplifying the appearance of the derived equations.

$$f(\varphi) = -r_{m-1}\cos\varphi + \sqrt{r_m^2 - r_{m-1}^2\sin^2\varphi} \qquad \text{(Eqn: 3.1-15)}$$

By integrating and simplifying equation 3.1-10, we get;

$$P_i^m = \frac{2r_{m-1}}{\pi\left(r_m^2 - r_{m-1}^2\right)}\left[\int_{\varphi=0}^{\frac{\pi}{2}} d\varphi \int_{\theta=0}^{\frac{\pi}{2}} d\theta \sin^2\theta \cos\varphi \int_{L=0}^{f(\varphi)\csc\theta} e^{-\Sigma_m L} dL\right] \qquad \text{(Eqn: 3.1-16)}$$

$$P_i^m = \frac{2r_{m-1}}{\pi\left(r_m^2 - r_{m-1}^2\right)\Sigma_m}\left[\int_{\varphi=0}^{\frac{\pi}{2}} d\varphi \int_{\theta=0}^{\frac{\pi}{2}} d\theta \sin^2\theta \cos\varphi - \int_{\varphi=0}^{\frac{\pi}{2}} d\varphi \int_{\theta=0}^{\frac{\pi}{2}} d\theta \sin^2\theta \cos\varphi . e^{-\Sigma_m f(\varphi)\csc\theta}\right]$$

(Eqn: 3.1-17)

For further simplification, define Bickley function [Ref. 5] as;

$$Ki_3\left(\Sigma_m f(\varphi)\right) = \int_{\theta=0}^{\frac{\pi}{2}} d\theta \sin^2\theta . e^{-\Sigma_m f(\varphi)\csc\theta} \qquad \text{(Eqn: 3.1-18)}$$

Hence the final form of the escape probability P_i^m is derived as:

$$P_i^m = \frac{2r_{m-1}}{\pi\left(r_m^2 - r_{m-1}^2\right)\Sigma_m}\left[\frac{\pi}{4} - \int_{\varphi=0}^{\frac{\pi}{2}} d\varphi \cos\varphi Ki_3\left(\Sigma_m f(\varphi)\right)\right] \qquad \text{(Eqn: 3.1-19)}$$

Examination of equation 3.1-19 indicates that P_i^m can be expressed in terms of two dimensionless variables $\frac{r_m}{r_{m-1}}$ and $\Sigma_m r_{m-1}$. Therefore we will plot P_i^m in terms of these two variables in order to verify the limiting behavior of P_i^m. Mathcad version 11 software is

used within this dissertation to obtain the values for the escape and transmission probabilities that are only used for plotting purposes. An adaptive quadrature integration method is used that is appropriate for use with functions that have the potential to change rapidly over an interval of interest such as our escape and transmission probabilities.

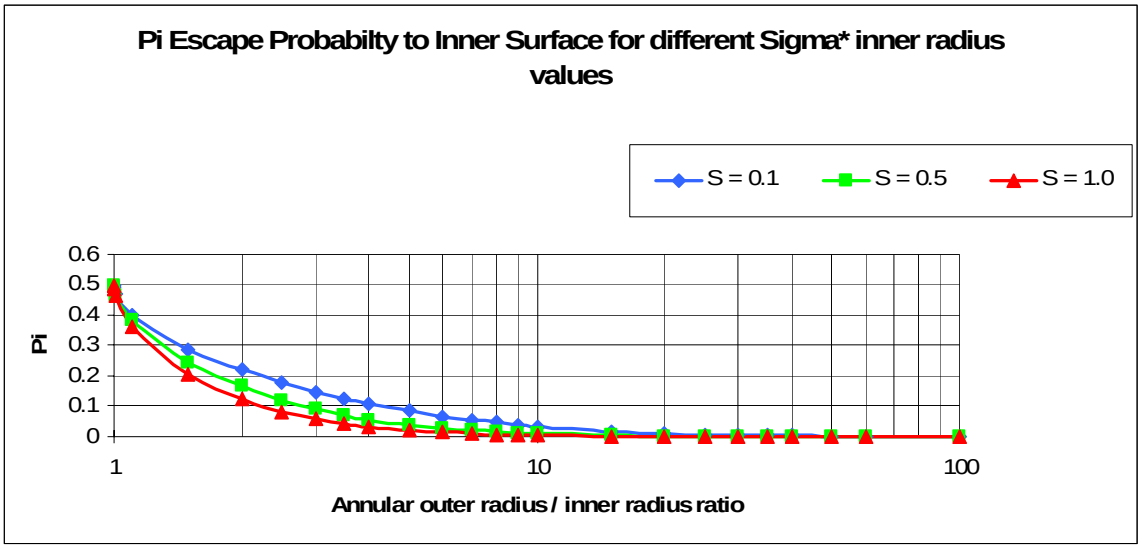

Figure 3.1- 6: P_i^m Escape Probability vs. $\frac{r_m}{r_{m-1}}$ Ratio for Several S=$\Sigma_m r_{m-1}$ Values

P_i^m exhibits the correct behavior as it approaches a value of 0.5 as $\frac{r_m}{r_{m-1}}$ approaches unity. This is because for $\frac{r_m}{r_{m-1}}$ of 1, which means that the sub-region m is extremely thin, half the neutrons will escape to the inner surface and the other half will escape to the outer

surface and there will be virtually no attenuation due to very small travel distance. As $\frac{r_m}{r_{m-1}}$ gets larger, the escape probability gets smaller due to larger travel distance.

Therefore, we conclude the validity of equation 3.1-19.

3.1.6 Determination of P_o^m

The following calculations show how P_o^m is derived. The methodology is similar to those for derivation of P_i^m so some of the intermediate steps are not shown for presentation simplicity reasons. The utilized coordination is shown in the figure below. We take an arbitrary infinitesimal volume within region m (point of interest) of the fuel and define the following parameters;

r and z = radial and vertical coordinates

r_m and r_{m-1} = outer and inner radii of fuel sub-region m

L = distance between the point of interest and an arbitrary point on the outer cylinder with radius r_m (target point).

θ = L angle of declination from vertical

ω = angular distance between the target point and r axis.

R = radial distance between the fuel centerline and intersection of the vertical line from the point of interest and the horizontal plane that contains the target point. It is noted that the horizontal plane is perpendicular to z axis.

φ = angle between the line that connects the target point to the intersection of the vertical line from the point of interest and the horizontal plane containing the target point and the line that connects the target point and the fuel centerline.

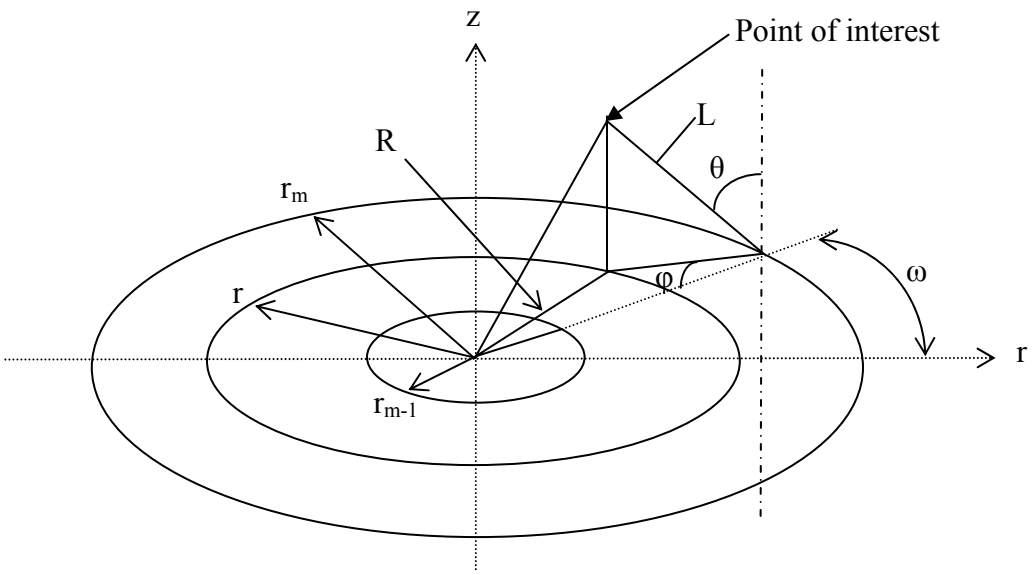

Figure 3.1- 7: Coordinate System for Determination of P_o^m

Derivation of P_o^m within equation 3.1-20 is similar to derivation of P_i^m in equation 3.1-10 except for the fact that the target point is now located on the outer surface with radius r_m. The results are as follows.

$$P_o^m = \frac{4\int_{\varphi=0}^{\frac{\pi}{2}}\int_{\theta=0}^{\frac{\pi}{2}}\int_{L=0}^{L_{\max}}(q)\left(L^2\sin\theta d\varphi d\theta dL\right)e^{-\Sigma_m L}\int_{\omega=0}^{2\pi}\frac{\sin\theta\cos\varphi}{4\pi L^2}r_m d\omega}{(q)\pi\left(r_m^2 - r_{m-1}^2\right)} \qquad \text{(Eqn: 3.1-20)}$$

Using Figure 3.1-7 and law of cosines we get;

$$R^2 = r_m^2 + L^2\sin^2\theta - 2r_m L\sin\theta\cos\varphi \qquad \text{(Eqn: 3.1-21)}$$

L_{max} for a given (φ, θ) and when $0 \le \varphi \le \arcsin\frac{r_{m-1}}{r_m}$ is found by putting the point of interest on the surface of cylinder with radius r_{m-1} (R = r_{m-1}). Hence,

$$r_{m-1}^2 = r_m^2 + L_{\max}^2\sin^2\theta - 2r_m L_{\max}\sin\theta\cos\varphi \quad \text{for} \quad 0 \le \varphi \le \arcsin\frac{r_{m-1}}{r_m}$$

(Eqn: 3.1-22)

$$L_{\max} = \frac{r_m\cos\varphi - \sqrt{r_{m-1}^2 - r_m^2\sin^2\varphi}}{\sin\theta} = g(\varphi)\csc\theta \quad \text{for} \quad 0 \le \varphi \le \arcsin\frac{r_{m-1}}{r_m}$$

(Eqn: 3.1-23)

where;

$$g(\varphi) = r_m\cos\varphi - \sqrt{r_{m-1}^2 - r_m^2\sin^2\varphi} \qquad \text{(Eqn: 3.1-24)}$$

$L_{\max}$ for a given (φ, θ) and when $\frac{\pi}{2} \geq \varphi > \arcsin\frac{r_{m-1}}{r_m}$ is found by putting the point of interest on the surface of cylinder with radius r_m (R = r_m). Hence,

$$r_m^2 = r_m^2 + L_{\max}^2 \sin^2\theta - 2r_m L_{\max} \sin\theta\cos\varphi \qquad \text{for} \qquad \frac{\pi}{2} \geq \varphi > \arcsin\frac{r_{m-1}}{r_m}$$

(Eqn: 3.1-25)

$$L_{\max} = \frac{2r_m}{\sin\theta}\cos\varphi = 2r_m\cos\varphi\csc\theta = h(\varphi)\csc\theta \quad \text{for} \quad \frac{\pi}{2} \geq \varphi > \arcsin\frac{r_{m-1}}{r_m}$$

(Eqn: 3.1-26)

where;

$$h(\varphi) = 2r_m\cos\varphi \qquad \text{(Eqn: 3.1-27)}$$

By plugging values of $L_{\max}$ from equations 3.1-23 and 3.1-26 into equation 3.1-20 and simplification, we obtain;

$$P_o^m = \frac{2r_m}{\pi\left(r_m^2 - r_{m-1}^2\right)}\left[\begin{array}{l}\displaystyle\int_{\varphi=0}^{\arcsin\frac{r_{m-1}}{r_m}} d\varphi\cos\varphi\int_{\theta=0}^{\frac{\pi}{2}} d\theta\sin^2\theta\int_{L=0}^{g(\varphi)\csc\theta} dL.e^{-\Sigma_m L} + \\ \displaystyle\int_{\varphi=\arcsin\frac{r_{m-1}}{r_m}}^{\frac{\pi}{2}} d\varphi\cos\varphi\int_{\theta=0}^{\frac{\pi}{2}} d\theta\sin^2\theta\int_{L=0}^{h(\varphi)\csc\theta} dL.e^{-\Sigma_m L}\end{array}\right] \qquad \text{(Eqn: 3.1-28)}$$

We have;

$$\int_{L=0}^{L_{\max}} dL.e^{-\Sigma_m L} = \frac{1}{\Sigma_m}\left[1 - e^{-\Sigma_m L_{\max}}\right] \qquad \text{(Eqn: 3.1-29)}$$

$$P_o^m = \frac{2r_m}{\pi\left(r_m^2 - r_{m-1}^2\right)\Sigma_m}\left[\begin{array}{l} \int_{\varphi=0}^{\arcsin\frac{r_{m-1}}{r_m}} d\varphi\cos\varphi \int_{\theta=0}^{\frac{\pi}{2}} d\theta \sin^2\theta - \\ \int_{\varphi=0}^{\arcsin\frac{r_{m-1}}{r_m}} d\varphi\cos\varphi \int_{\theta=0}^{\frac{\pi}{2}} d\theta \sin^2\theta e^{-\Sigma_m g(\varphi)\csc\theta} + \\ \int_{\varphi=\arcsin\frac{r_{m-1}}{r_m}}^{\frac{\pi}{2}} d\varphi\cos\varphi \int_{\theta=0}^{\frac{\pi}{2}} d\theta \sin^2\theta - \\ \int_{\varphi=\arcsin\frac{r_{m-1}}{r_m}}^{\frac{\pi}{2}} d\varphi\cos\varphi \int_{\theta=0}^{\frac{\pi}{2}} d\theta \sin^2\theta e^{-\Sigma_m h(\varphi)\csc\theta} \end{array}\right] \qquad \text{(Eqn: 3.1-30)}$$

$$P_o^m = \frac{2r_m}{\pi\left(r_m^2 - r_{m-1}^2\right)\Sigma_m}\left[\begin{array}{l} \frac{\pi}{4}\left[\int_{\varphi=0}^{\arcsin\frac{r_{m-1}}{r_m}} d\varphi\cos\varphi + \int_{\varphi=\arcsin\frac{r_{m-1}}{r_m}}^{\frac{\pi}{2}} d\varphi\cos\varphi\right] - \\ \int_{\varphi=0}^{\arcsin\frac{r_{m-1}}{r_m}} d\varphi\cos\varphi \int_{\theta=0}^{\frac{\pi}{2}} d\theta \sin^2\theta e^{-\Sigma_m g(\varphi)\csc\theta} \\ - \int_{\varphi=\arcsin\frac{r_{m-1}}{r_m}}^{\frac{\pi}{2}} d\varphi\cos\varphi \int_{\theta=0}^{\frac{\pi}{2}} d\theta \sin^2\theta e^{-\Sigma_m h(\varphi)\csc\theta} \end{array}\right] \qquad \text{(Eqn: 3.1-31)}$$

$$P_o^m = \frac{2r_m}{\pi\left(r_m^2 - r_{m-1}^2\right)\Sigma_m}\left[\frac{\pi}{4} - \int_{\varphi=0}^{\arcsin\frac{r_{m-1}}{r_m}} d\varphi\cos\varphi\int_{\theta=0}^{\frac{\pi}{2}} d\theta\sin^2\theta e^{-\Sigma_m g(\varphi)\csc\theta} - \int_{\varphi=\arcsin\frac{r_{m-1}}{r_m}}^{\frac{\pi}{2}} d\varphi\cos\varphi\int_{\theta=0}^{\frac{\pi}{2}} d\theta\sin^2\theta e^{-\Sigma_m h(\varphi)\csc\theta}\right] \qquad \text{(Eqn: 3.1-32)}$$

$$P_o^m = \frac{2r_m}{\pi\left(r_m^2 - r_{m-1}^2\right)\Sigma_m}\left[\begin{array}{l}\frac{\pi}{4} - \int_{\varphi=0}^{\arcsin\frac{r_{m-1}}{r_m}} d\varphi\cos\varphi\int_{\theta=0}^{\frac{\pi}{2}} d\theta\sin^2\theta e^{-\Sigma_m g(\varphi)\csc\theta} \\ - \int_{\varphi=0}^{\frac{\pi}{2}} d\varphi\cos\varphi\int_{\theta=0}^{\frac{\pi}{2}} d\theta\sin^2\theta e^{-\Sigma_m h(\varphi)\csc\theta} + \\ \int_{\varphi=0}^{\arcsin\frac{r_{m-1}}{r_m}} d\varphi\cos\varphi\int_{\theta=0}^{\frac{\pi}{2}} d\theta\sin^2\theta e^{-\Sigma_m h(\varphi)\csc\theta}\end{array}\right] \qquad \text{(Eqn: 3.1-33)}$$

To further simplify the expression for P_o^m, we will introduce the following transformation in order to change the ($\arcsin\frac{r_{m-1}}{r_m}$) integral limit to ($\frac{\pi}{2}$).

$$\sin\varphi = \frac{r_{m-1}}{r_m}\sin\psi \qquad \text{(Eqn: 3.1-34)}$$

$$d\varphi\cos\varphi = \frac{r_{m-1}}{r_m}d\psi\cos\psi \qquad \text{(Eqn: 3.1-35)}$$

Hence when $\varphi \to \arcsin\frac{r_{m-1}}{r_m}$, then $\psi \to \frac{\pi}{2}$ and when $\varphi \to 0$, then $\psi \to 0$. Substituting these transformations in $g(\varphi)$ and $h(\varphi)$, we get;

$$h(\varphi) = 2r_m \cos\varphi = 2\sqrt{r_m^2\left(1-\sin^2\varphi\right)} = 2\sqrt{r_m^2 - r_m^2\sin^2\varphi} = 2\sqrt{r_m^2 - r_{m-1}^2\sin^2\psi} = k(\psi)$$

(Eqn: 3.1-36)

where;

$$k(\psi) = 2\sqrt{r_m^2 - r_{m-1}^2\sin^2\psi} \qquad \text{(Eqn: 3.1-37)}$$

$$g(\varphi) = r_m\cos\varphi - \sqrt{r_{m-1}^2 - r_m^2\sin^2\varphi} = \sqrt{r_m^2\cos^2\varphi} - \sqrt{r_{m-1}^2 - r_{m-1}^2\sin^2\psi} \qquad \text{(Eqn: 3.1-38)}$$

$$g(\varphi) = \sqrt{r_m^2\left(1-\sin^2\varphi\right)} - \sqrt{r_{m-1}^2\cos^2\psi} = \sqrt{r_m^2 - r_{m-1}^2\sin^2\psi} - r_{m-1}\cos\psi = p(\psi)$$

(Eqn: 3.1-39)

where;

$$p(\psi) = \sqrt{r_m^2 - r_{m-1}^2\sin^2\psi} - r_{m-1}\cos\psi = f(\psi) \qquad \text{(Eqn: 3.1-40)}$$

Equation 3.1-33 can now be simplified as,

$$P_o^m = \frac{2r_m}{\pi\left(r_m^2 - r_{m-1}^2\right)\Sigma_m}\left[\begin{array}{l} \frac{\pi}{4} - \int_{\psi=0}^{\frac{\pi}{2}} \frac{r_{m-1}}{r_m} d\psi \cos\psi \int_{\theta=0}^{\frac{\pi}{2}} d\theta \sin^2\theta e^{-\Sigma_m f(\psi)\csc\theta} \\ - \int_{\varphi=0}^{\frac{\pi}{2}} d\varphi \cos\varphi \int_{\theta=0}^{\frac{\pi}{2}} d\theta \sin^2\theta e^{-\Sigma_m h(\varphi)\csc\theta} \\ + \int_{\psi=0}^{\frac{\pi}{2}} \frac{r_{m-1}}{r_m} d\psi \cos\psi \int_{\theta=0}^{\frac{\pi}{2}} d\theta \sin^2\theta e^{-\Sigma_m k(\psi)\csc\theta} \end{array}\right] \qquad \text{(Eqn: 3.1-41)}$$

Based on the definition for Bickley function [Ref. 5], the P_o^m can be further simplified.

$$P_o^m = \frac{2r_m}{\pi\left(r_m^2 - r_{m-1}^2\right)\Sigma_m}\left[\begin{array}{l} \frac{\pi}{4} - \int_{\psi=0}^{\frac{\pi}{2}} \frac{r_{m-1}}{r_m} d\psi \cos\psi Ki_3\left(\Sigma_m f(\psi)\right) - \int_{\varphi=0}^{\frac{\pi}{2}} d\varphi \cos\varphi Ki_3\left(\Sigma_m h(\varphi)\right) \\ + \int_{\psi=0}^{\frac{\pi}{2}} \frac{r_{m-1}}{r_m} d\psi \cos\psi Ki_3\left(\Sigma_m k(\psi)\right) \end{array}\right]$$

(Eqn: 3.1-42)

$$P_o^m = \frac{2r_m}{\pi\left(r_m^2 - r_{m-1}^2\right)\Sigma_m}\left[\begin{array}{l} \frac{\pi}{4} - \\ \int_{\varphi=0}^{\frac{\pi}{2}} d\varphi \cos\varphi\left[\frac{r_{m-1}}{r_m} Ki_3\left(\Sigma_m f(\varphi)\right) + Ki_3\left(\Sigma_m h(\varphi)\right) - \frac{r_{m-1}}{r_m} Ki_3\left(\Sigma_m k(\varphi)\right)\right] \end{array}\right]$$

(Eqn: 3.1-43)

Equation 3.1-43 above is the simplest closed form representation of P_o^m.

Examination of equation 3.1-43 indicates that P_o^m can be expressed in terms of two dimensionless variables $\frac{r_m}{r_{m-1}}$ and $\Sigma_m r_m$. Therefore we will plot P_o^m in terms of these two variables in order to verify the limiting behavior of P_o^m.

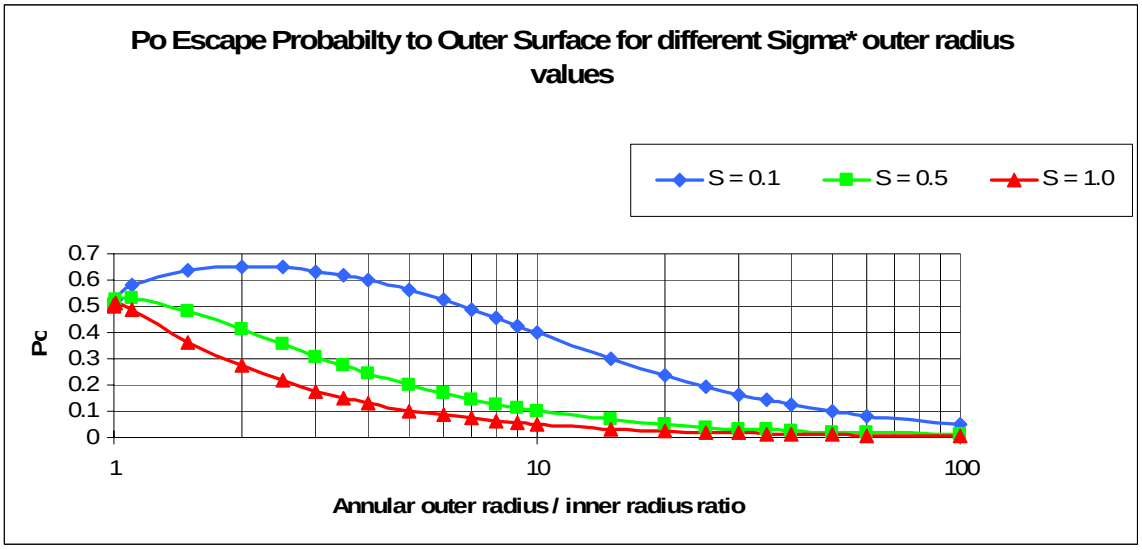

Figure 3.1- 8: Escape Probability vs. $\frac{r_m}{r_{m-1}}$ Ratio for Several S=$\Sigma_m r_m$ Values

P_o^m exhibits the correct behavior as it approaches a value of 0.5 as $\frac{r_m}{r_{m-1}}$ approaches unity. This is because for $\frac{r_m}{r_{m-1}}$ of 1, which means that the sub-region m is extremely thin, half the neutrons will escape to the inner surface and the other half will escape to the outer surface and there will be virtually no attenuation due to very small travel distance. As

$\frac{r_m}{r_{m-1}}$ gets larger, the escape probability gets smaller due to larger travel distance. It is also noted that for small values of $\Sigma_m r_m$, as $\frac{r_m}{r_{m-1}}$ starts increasing over unity, P_o^m initially increases above 0.5 value due to a larger subtended angle towards the outer surface when compared to the inner surface, then P_o^m decreases due to larger traversed distance to the outer surface. Therefore, we conclude the validity of equation 3.1-43.

3.1.7 Determination of T_{io}^m

Now we will turn our attention in calculations of the transmission probabilities in the cylindrical annular region. We take an arbitrary infinitesimal surface area on the inner cylinder with radius r_{m-1} (point of interest) and define the following parameters;

r and z = radial and vertical coordinates

r_m and r_{m-1} = outer and inner radii of fuel sub-region m

L = distance between the point of interest and an arbitrary point on the outer cylinder with radius r_m (target point).

θ = L angle of declination from vertical

φ = angle between the horizontal projection of line L and r axis.

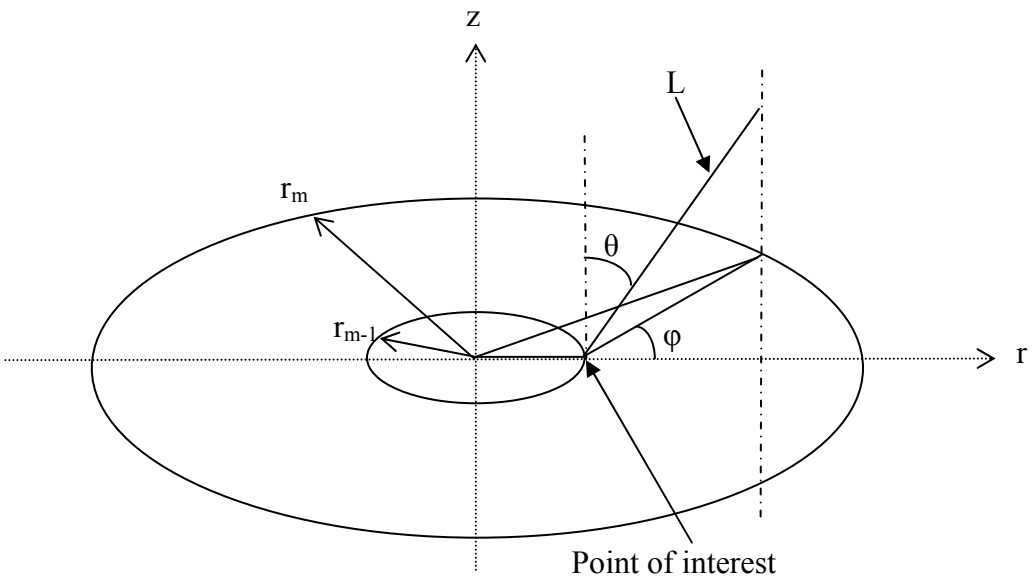

Figure 3.1- 9: Coordinate System for Determination of T_{io}^{m}

We will develop T_{io}^{m} by calculating the transmission probability from a typical point on the inner cylinder with radius r_{m-1} as shown in Figure 3.1-9 into the outer cylindrical region with radius r_m as shown in equation 3.1-44. In this approach, the transmission probability is determined by finding the transmission probability from the point of interest to a target point on the outer surface where there is a line of sight from the point of interest.

$$T_{io}^{m} = \frac{\int_{\varphi=0}^{\frac{\pi}{2}} \int_{\theta=0}^{\frac{\pi}{2}} d\varphi d\theta \cos\varphi \sin^2\theta e^{-\Sigma_m L}}{\int_{\varphi=0}^{\frac{\pi}{2}} \int_{\theta=0}^{\frac{\pi}{2}} d\varphi d\theta \cos\varphi \sin^2\theta} \qquad \text{(Eqn: 3.1-44)}$$

$$T_{io}^{m} = \frac{4}{\pi} \int_{\varphi=0}^{\frac{\pi}{2}} \int_{\theta=0}^{\frac{\pi}{2}} d\varphi d\theta \cos\varphi \sin^2\theta e^{-\Sigma_m L} \qquad \text{(Eqn: 3.1-45)}$$

L can be found by using law of cosines in Figure 3.1-9.

$$r_m^2 = r_{m-1}^2 + L^2 \sin^2\theta - 2 r_{m-1} L \sin\theta \cos(\pi - \varphi) \qquad \text{(Eqn: 3.1-46)}$$

Solution for the above equation is;

$$L = \frac{-r_{m-1}\cos\varphi + \sqrt{r_m^2 - r_{m-1}^2 \sin^2\varphi}}{\sin\theta} = f(\varphi)\csc\theta \qquad \text{(Eqn: 3.1-47)}$$

Therefore the transmission probability is;

$$T_{io}^{m} = \frac{4}{\pi} \int_{\varphi=0}^{\frac{\pi}{2}} d\varphi \cos\varphi \int_{\theta=0}^{\frac{\pi}{2}} d\theta \sin^2\theta e^{-\Sigma_m f(\varphi)\csc\theta} \qquad \text{(Eqn: 3.1-48)}$$

$$T_{io}^{m} = \frac{4}{\pi} \int_{\varphi=0}^{\frac{\pi}{2}} d\varphi \cos\varphi Ki_3\left(\Sigma_m f(\varphi)\right) \qquad \text{(Eqn: 3.1-49)}$$

Examination of equation 3.1-49 indicates that T_{io}^{m} can be expressed in terms of two dimensionless variables $\frac{r_m}{r_{m-1}}$ and $\Sigma_m r_{m-1}$. Therefore we will plot T_{io}^{m} in terms of these two variables in order to verify the limiting behavior of T_{io}^{m}.

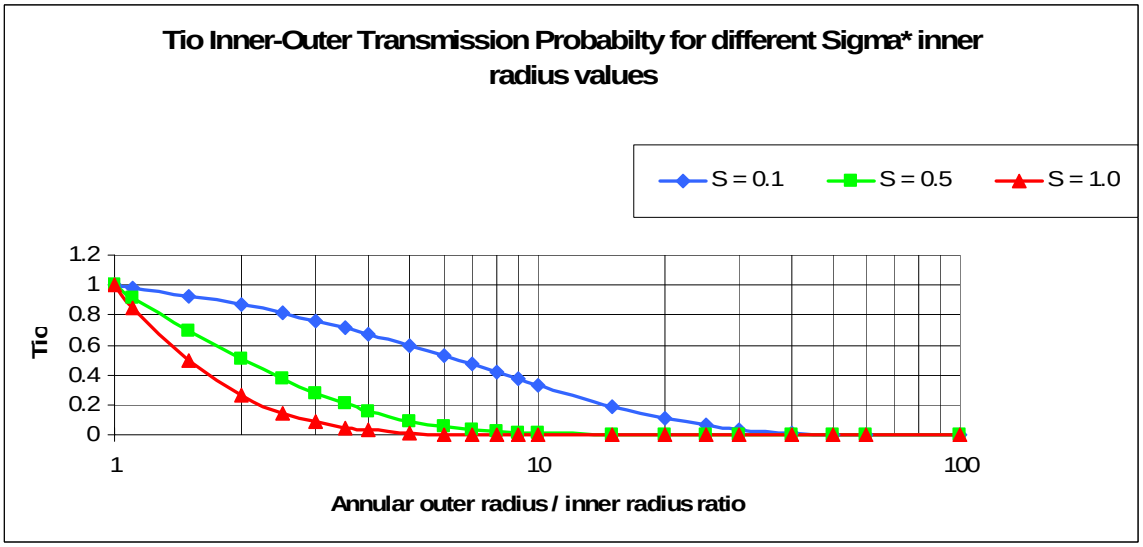

Figure 3.1- 10: T_{io}^{m} Transmission Probability vs. $\frac{r_m}{r_{m-1}}$ Ratio for Several S=$\Sigma_m r_{m-1}$ Values

T_{io}^{m} exhibits the correct behavior as it approaches a value of 1.0 as $\frac{r_m}{r_{m-1}}$ approaches unity. This is because for $\frac{r_m}{r_{m-1}}$ of 1, which means that the sub-region m is extremely thin, nearly all the neutrons will transmit to the outer surface un-interacted. As $\frac{r_m}{r_{m-1}}$ gets larger, the

transmission probability gets smaller due to larger travel distance. Therefore, we conclude the validity of equation 3.1-49.

3.1.8 Determination of T_{oi}^{m}

We take an arbitrary infinitesimal surface area on the outer cylinder with radius r_m (point of interest) and define the following parameters;

r and z = radial and vertical coordinates

r_m and r_{m-1} = outer and inner radii of fuel sub-region m

L = distance between the point of interest and an arbitrary point on the inner cylinder with radius r_{m-1} (target point).

θ = L angle of declination from vertical

φ = angle between the horizontal projection of line L and r axis.

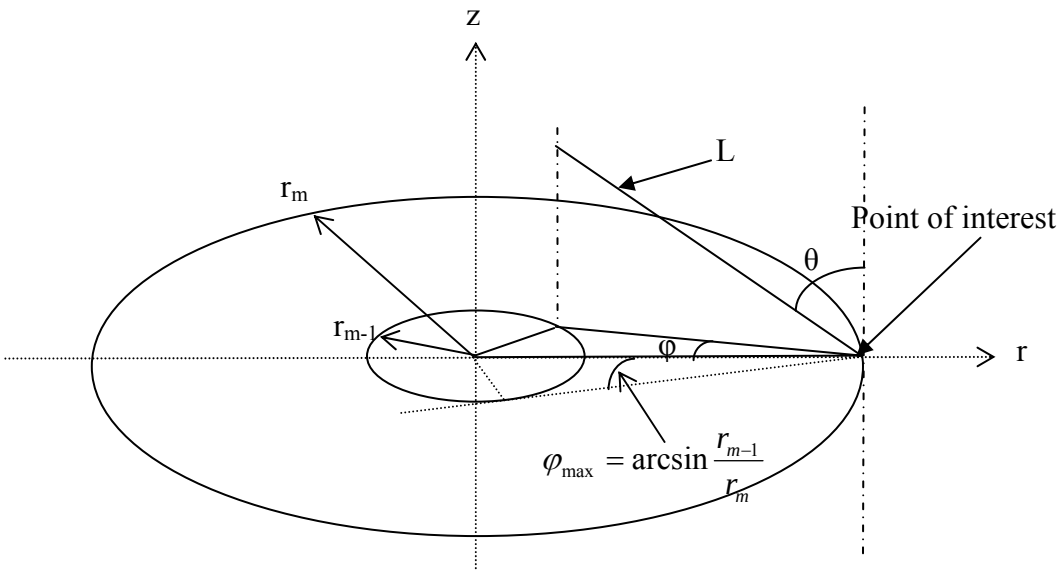

Figure 3.1- 11: Coordinate System for Determination of T_{oi}^m

The derivation of T_{oi}^m is similar to that for T_{io}^m as derived below.

$$T_{oi}^m = \frac{\int_{\varphi=0}^{\arcsin\frac{r_{m-1}}{r_m}} \int_{\theta=0}^{\frac{\pi}{2}} d\varphi d\theta \cos\varphi \sin^2\theta e^{-\Sigma_m L}}{\int_{\varphi=0}^{\arcsin\frac{r_{m-1}}{r_m}} \int_{\theta=0}^{\frac{\pi}{2}} d\varphi d\theta \cos\varphi \sin^2\theta} \qquad \text{(Eqn: 3.1-50)}$$

$$T_{oi}^m = \frac{4}{\pi} \int_{\varphi=0}^{\arcsin\frac{r_{m-1}}{r_m}} \int_{\theta=0}^{\frac{\pi}{2}} d\varphi d\theta \cos\varphi \sin^2\theta e^{-\Sigma_m L} \qquad \text{(Eqn: 3.1-51)}$$

By using the law of cosines and Figure 3.1-11;

$$r_m^2 = r_{m-1}^2 + L^2 \sin^2\theta - 2r_m L \sin\theta\cos\varphi \qquad \text{(Eqn: 3.1-52)}$$

$$L = \frac{r_m \cos\varphi - \sqrt{r_{m-1}^2 - r_m^2 \sin^2\theta}}{\sin\theta} = g(\varphi)\csc\theta \qquad \text{(Eqn: 3.1-53)}$$

Using a similar transformation as shown in equations 3.1-34 and 3.1-35, we get;

$$\sin\varphi = \frac{r_{m-1}}{r_m}\sin\psi \qquad \text{(Eqn: 3.1-54)}$$

$$g(\varphi) = \sqrt{r_m^2 - r_{m-1}^2 \sin^2\psi} - r_{m-1}\cos\psi = f(\psi) \qquad \text{(Eqn: 3.1-55)}$$

So the transmission probability from equation 3.1-50 becomes;

$$T_{oi}^m = \frac{4}{\pi}\int_{\psi=0}^{\frac{\pi}{2}} \frac{r_{m-1}}{r_m} d\psi \cos\psi \int_{\theta=0}^{\frac{\pi}{2}} d\theta \sin^2\theta e^{-\Sigma_m p(\psi)\csc\theta} = \frac{r_{m-1}}{r_m}\frac{4}{\pi}\int_{\psi=0}^{\frac{\pi}{2}} d\psi \cos\psi Ki_3(\Sigma_m p(\psi))$$

(Eqn: 3.1-56)

$$T_{oi}^m = \frac{r_{m-1}}{r_m}\frac{4}{\pi}\int_{\psi=0}^{\frac{\pi}{2}} d\psi \cos\psi Ki_3(\Sigma_m f(\psi)) \qquad \text{(Eqn: 3.1-57)}$$

$$T_{oi}^m = \frac{r_{m-1}}{r_m}\frac{4}{\pi}\int_{\varphi=0}^{\frac{\pi}{2}} d\varphi \cos\varphi Ki_3(\Sigma_m f(\varphi)) \qquad \text{(Eqn: 3.1-58)}$$

Examination of equation 3.1-58 indicates that T_{oi}^{m} can be expressed in terms of two dimensionless variables $\frac{r_m}{r_{m-1}}$ and $\Sigma_m r_{m-1}$. Therefore we will plot T_{oi}^{m} in terms of these two variables in order to verify the limiting behavior of T_{oi}^{m}.

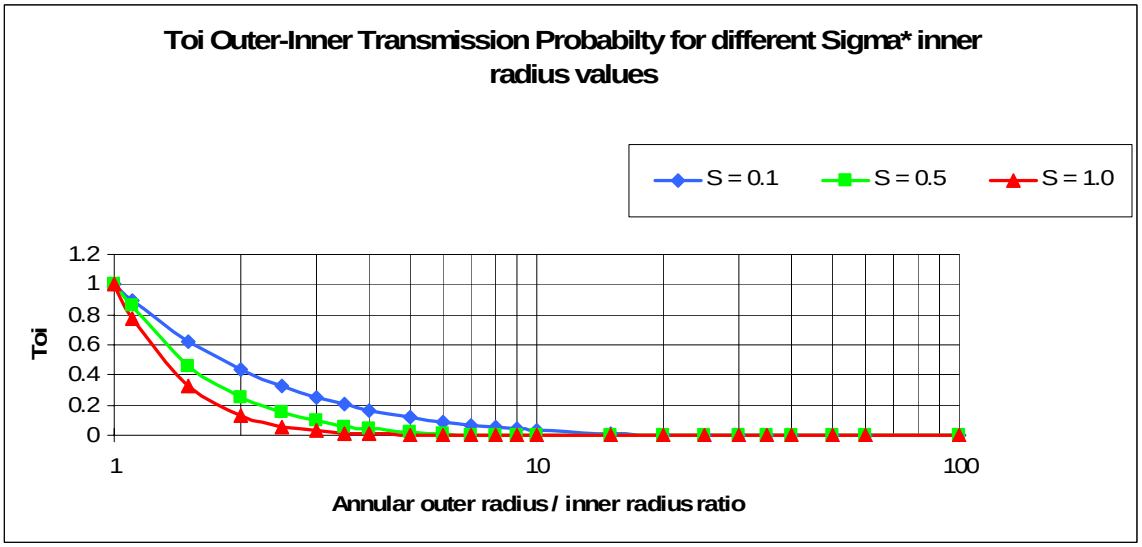

Figure 3.1- 12: T_{oi}^{m} Transmission Probability vs. $\frac{r_m}{r_{m-1}}$ Ratio for Several S=$\Sigma_m r_{m-1}$ Values

T_{oi}^{m} exhibits the correct behavior as it approaches a value of 1.0 as $\frac{r_m}{r_{m-1}}$ approaches unity. This is because for $\frac{r_m}{r_{m-1}}$ of 1, which means that the sub-region m is extremely thin, nearly

all the neutrons will transmit to the inner surface un-interacted. As $\frac{r_m}{r_{m-1}}$ gets larger, the transmission probability gets smaller due to larger travel distance. Therefore, we conclude the validity of equation 3.1-58.

3.1.9 Determination of T_{oo}^{m}

We take an arbitrary infinitesimal surface area on the outer cylinder with radius r_m (point of interest) and define the following parameters;

r and z = radial and vertical coordinates

r_m and r_{m-1} = outer and inner radii of fuel sub-region m

L = distance between the point of interest and an arbitrary point on the outer cylinder with radius r_m (target point).

θ = L angle of declination from vertical

φ = angle between the horizontal projection of line L and r axis.

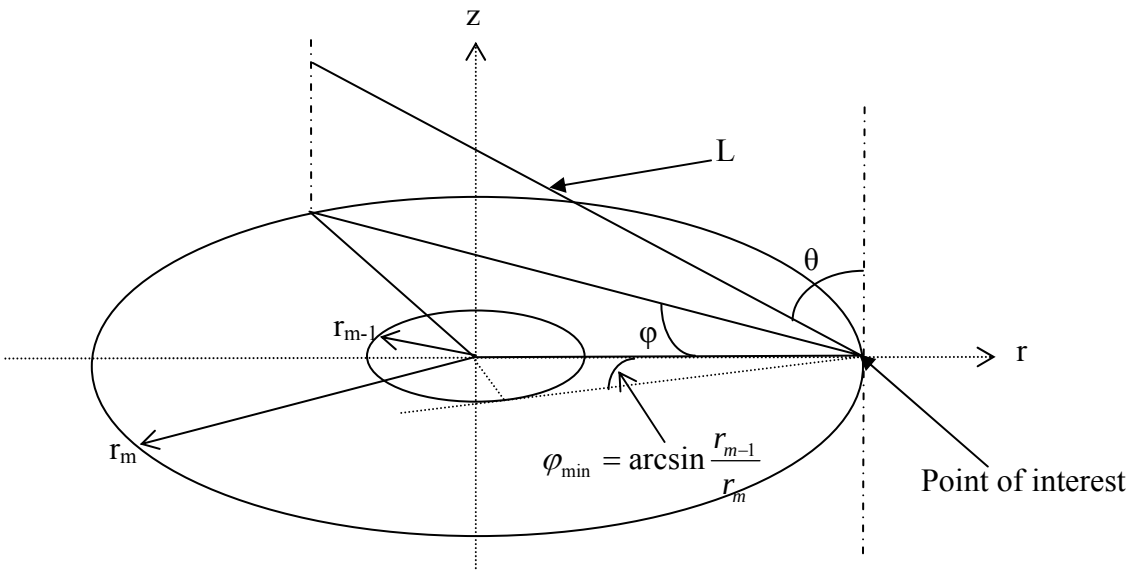

Figure 3.1- 13: Coordinate System for Determination of T_{oo}^{m}

We will develop T_{oo}^{m} by calculating the transmission probability from a typical point on the outer cylinder with radius r_m as shown in Figure 3.1-13 to another outer cylinder area with radius r_m as shown in equation 3.1-59. In this approach, the transmission probability is determined by finding the transmission probability from the point of interest on the outer cylinder to a target point on the outer cylinder where there is a line of sight from the point of interest.

$$T_{oo}^{m}=\frac{\int_{\varphi=\arcsin\frac{r_{m-1}}{r_m}}^{\frac{\pi}{2}}\int_{\theta=0}^{\frac{\pi}{2}}d\varphi d\theta\cos\varphi\sin^2\theta e^{-\Sigma_m L}}{\int_{\varphi=\arcsin\frac{r_{m-1}}{r_m}}^{\frac{\pi}{2}}\int_{\theta=0}^{\frac{\pi}{2}}d\varphi d\theta\cos\varphi\sin^2\theta}=\frac{4}{\pi}\int_{\varphi=\arcsin\frac{r_{m-1}}{r_m}}^{\frac{\pi}{2}}\int_{\theta=0}^{\frac{\pi}{2}}d\varphi d\theta\cos\varphi\sin^2\theta e^{-\Sigma_m L}$$

(Eqn: 3.1-59)

$$T_{oo}^{m}=\frac{4}{\pi}\left[\int_{\varphi=0}^{\frac{\pi}{2}}d\varphi\cos\varphi\int_{\theta=0}^{\frac{\pi}{2}}d\theta\sin^2\theta e^{-\Sigma_m L}-\int_{\varphi=0}^{\arcsin\frac{r_{m-1}}{r_m}}d\varphi\cos\varphi\int_{\theta=0}^{\frac{\pi}{2}}d\theta\sin^2\theta e^{-\Sigma_m L}\right]$$

(Eqn: 3.1-60)

For a given (φ,θ), value of L is obtained by using the law of cosines.

$$r_m^2=r_m^2+L^2\sin^2\theta-2r_m L\sin\theta\cos\varphi \qquad \text{(Eqn: 3.1-61)}$$

$$L=\frac{2r_m\cos\varphi}{\sin\theta}=h(\varphi)\csc\theta \qquad \text{(Eqn: 3.1-62)}$$

where;

$$h(\varphi)=2r_m\cos\varphi \qquad \text{(Eqn: 3.1-63)}$$

By using transformation as used before, we can get a simplified form for T_{oo}^{m}.

$$\sin\varphi = \frac{r_{m-1}}{r_m}\sin\psi \qquad \text{(Eqn: 3.1-64)}$$

$$T_{oo}^{m} = \frac{4}{\pi}\left[\int_{\varphi=0}^{\frac{\pi}{2}} d\varphi\cos\varphi\int_{\theta=0}^{\frac{\pi}{2}} d\theta\sin^2\theta e^{-\Sigma_m h(\varphi)\csc\theta} - \int_{\psi=0}^{\frac{\pi}{2}} \frac{r_{m-1}}{r_m} d\psi\cos\psi\int_{\theta=0}^{\frac{\pi}{2}} d\theta\sin^2\theta e^{-\Sigma_m k(\psi)\csc\theta}\right]$$

(Eqn: 3.1-65)

$$T_{oo}^{m} = \frac{4}{\pi}\left[\int_{\varphi=0}^{\frac{\pi}{2}} d\varphi\cos\varphi Ki_3\left(\Sigma_m h(\varphi)\right) - \frac{r_{m-1}}{r_m}\int_{\psi=0}^{\frac{\pi}{2}} d\psi\cos\psi Ki_3\left(\Sigma_m k(\psi)\right)\right] \qquad \text{(Eqn: 3.1-66)}$$

$$T_{oo}^{m} = \frac{4}{\pi}\left[\int_{\varphi=0}^{\frac{\pi}{2}} d\varphi\cos\varphi\left[Ki_3\left(\Sigma_m h(\varphi)\right) - \frac{r_{m-1}}{r_m}Ki_3\left(\Sigma_m k(\varphi)\right)\right]\right] \qquad \text{(Eqn: 3.1-67)}$$

Examination of equation 3.1-67 indicates that T_{oo}^{m} can be expressed in terms of two dimensionless variables $\frac{r_m}{r_{m-1}}$ and $\Sigma_m r_{m-1}$. Therefore we will plot T_{oo}^{m} in terms of these two variables in order to verify the limiting behavior of T_{oo}^{m}.

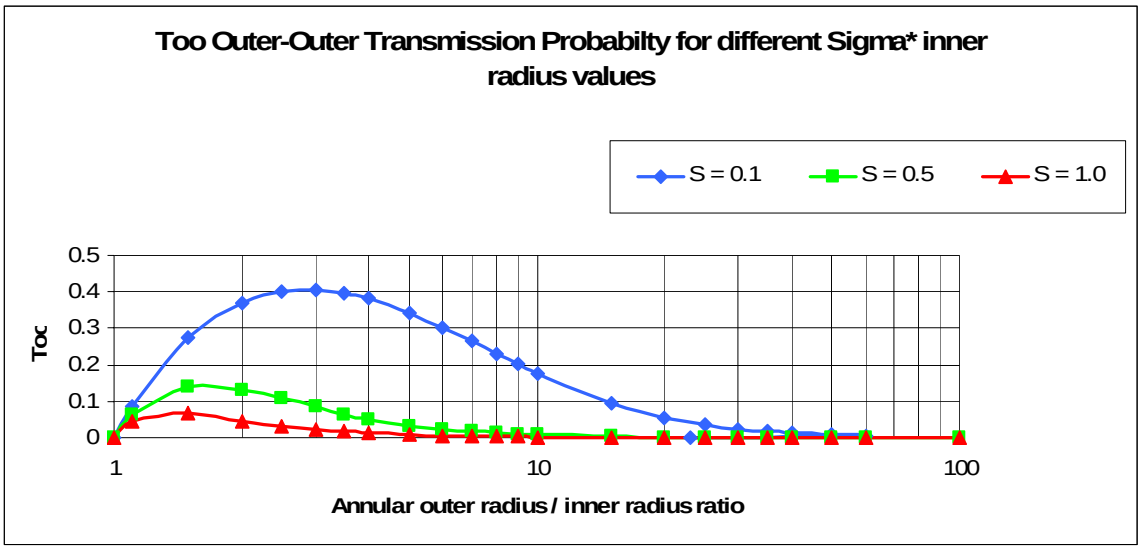

Figure 3.1- 14: T_{oo}^{m} Transmission Probability vs. $\frac{r_m}{r_{m-1}}$ Ratio for Several S=$\Sigma_m r_{m-1}$ Values

T_{oo}^{m} exhibits the correct behavior as it approaches a value of 0.0 as $\frac{r_m}{r_{m-1}}$ approaches unity. This is because for $\frac{r_m}{r_{m-1}}$ of 1, which means that the sub-region m is extremely thin or the inner and outer radii are very close to each other, nearly all the neutrons will transmit to the inner surface un-interacted and not many of these neutrons will reach the outer surface again. As $\frac{r_m}{r_{m-1}}$ gets larger, the transmission probability gets smaller due to larger travel distance. It is noted again that as $\frac{r_m}{r_{m-1}}$ starts increasing over unity, T_{oo}^{m} initially increases above zero due to a larger subtended angle towards the outer surface when

compared to the inner surface, then T_{oo}^{m} decreases due to larger traversed distance to the outer surface. This effect is more pronounced for the smaller values of $\Sigma_m r_{m-1}$ .Therefore, we conclude the validity of equation 3.1-67.

3.1.10 Correlations between the Transmission and Escape Probabilities

The following section summaries the results for the transmission and escape probabilities and establishes the correlation between these probabilities. These derived equations are consistent with the results presented in Reference [37] for the transmission and escape probabilities for annular regions.

$$T_{io}^{m} = \frac{4}{\pi} \int_{\varphi=0}^{\frac{\pi}{2}} d\varphi \cos\varphi Ki_3\left(\Sigma_m f(\varphi)\right) \qquad \text{(Eqn: 3.1-68)}$$

where;

$$f(\varphi) = -r_{m-1}\cos\varphi + \sqrt{r_m^2 - r_{m-1}^2 \sin^2\varphi} \qquad \text{(Eqn: 3.1-69)}$$

$$T_{oi}^{m} = \frac{r_{m-1}}{r_m}\frac{4}{\pi} \int_{\varphi=0}^{\frac{\pi}{2}} d\varphi \cos\varphi Ki_3\left(\Sigma_m f(\varphi)\right) \qquad \text{(Eqn: 3.1-70)}$$

Therefore;

$$T_{oi}^{m} = \frac{r_{m-1}}{r_m} T_{io}^{m} \qquad \text{(Eqn: 3.1-71)}$$

$$T_{oo}^{m} = \frac{4}{\pi}\left[\int_{\varphi=0}^{\frac{\pi}{2}} d\varphi \cos\varphi \left[Ki_3\left(\Sigma_m h(\varphi)\right) - \frac{r_{m-1}}{r_m} Ki_3\left(\Sigma_m k(\varphi)\right)\right]\right] \qquad \text{(Eqn: 3.1-72)}$$

where;

$$h(\varphi) = 2r_m \cos\varphi \qquad \text{(Eqn: 3.1-73)}$$

$$k(\varphi) = 2\sqrt{r_m^2 - r_{m-1}^2 \sin^2\varphi} \qquad \text{(Eqn: 3.1-74)}$$

$$P_i^m = \frac{2r_{m-1}}{\pi\left(r_m^2 - r_{m-1}^2\right)\Sigma_m}\left[\frac{\pi}{4} - \int_{\varphi=0}^{\frac{\pi}{2}} d\varphi \cos\varphi Ki_3\left(\Sigma_m f(\varphi)\right)\right] \qquad \text{(Eqn: 3.1-75)}$$

$$P_o^m = \frac{2r_m}{\pi\left(r_m^2 - r_{m-1}^2\right)\Sigma_m}\left[\frac{\pi}{4} - \int_{\varphi=0}^{\frac{\pi}{2}} d\varphi \cos\varphi \left[\frac{r_{m-1}}{r_m} Ki_3\left(\Sigma_m f(\varphi)\right) + Ki_3\left(\Sigma_m h(\varphi)\right) - \frac{r_{m-1}}{r_m} Ki_3\left(\Sigma_m k(\varphi)\right)\right]\right]$$

(Eqn: 3.1-76)

Substitution of equations 3.1-68, 3.1-70, and 3.1-71 into equations 3.1-75 and 3.1-76 will provide the escape probabilities in terms of transmission probabilities.

$$P_i^m = \frac{r_{m-1}}{2\Sigma_m\left(r_m^2 - r_{m-1}^2\right)}\left(1 - T_{io}^{m}\right) \qquad \text{(Eqn: 3.1-77)}$$

$$P_o^m = \frac{r_m}{2\Sigma_m\left(r_m^2 - r_{m-1}^2\right)}\left(1 - T_{oo}^m - T_{oi}^m\right) \qquad \text{(Eqn: 3.1-78)}$$

As a final note, examination of equation 3.1-71, reveals the fact that the reciprocity theorem applies to inner to outer and outer to inner transmission probabilities. This is similar to reciprocity theorem between two surfaces that exchange radiative heat transfer. In this case the product of the surface area and the transmission probability (similar to a view factor) follows the following correlation;

$$A_i T_{io}^m = A_o T_{oi}^m \qquad \text{(Eqn: 3.1-79)}$$

or;

$$\frac{T_{io}^m}{T_{oi}^m} = \frac{A_o}{A_i} = \frac{2\pi r_m l}{2\pi r_{m-1} l} = \frac{r_m}{r_{m-1}} \qquad \text{(Eqn: 3.1-80)}$$

3.1.11 Calculation of Π_0 for Problem # 1

We will extend the definition of Π_0 to be the probability that a neutron appearing in any fuel sub-region (sub-regions 1, 2, …, N) as demonstrated in Figure 3.1-3 at energy E will undergo its next interaction in the moderator/coolant (sub-region N+1). Computation of Π_0 consists of two elements. The first one is P_f, the probability of a neutron being born in any of the fuel sub-regions to escape the outer boundary of the outer most fuel sub-

region (sub-region N) and the second one is the probability that a neutron entering the moderator/coolant sub-region (sub-region N+1) will interact with the moderator. Multiplication of these two probabilities will determine Π_0.

For determination of the P_f, we will start with a fuel area divided in three annular regions (N=3) and after determination of P_f for three sub-regions, we will generalize it to N sub-regions.

i) For neutron born in sub-region 1 (P_{f1});

$$P_{f1} = P_o^1 T_{io}^2 T_{io}^3 \qquad \text{(Eqn: 3.1-81)}$$

ii) For neutron born in sub-region 2 (P_{f2});

$$P_{f2} = P_o^2 T_{io}^3 + P_i^2 T_{oo}^1 T_{io}^2 T_{io}^3 \qquad \text{(Eqn: 3.1-82)}$$

iii) For neutron born in sub-region 3 (P_{f3});

$$P_{f3} = P_o^3 + P_i^3 \left(T_{oo}^2 T_{io}^3 + T_{oi}^2 T_{oo}^1 T_{io}^2 T_{io}^3 \right) \qquad \text{(Eqn: 3.1-83)}$$

The overall escape probability of P_f can then be obtained by summing the weighted fraction of P_{f1}, P_{f2} and P_{f3}. The weighing factor for each region is necessary to normalize the total number of neutrons that are originated in all fuel sub-regions to 1. The developed equation will then give us the equivalent escape probability from the entire

fuel region for a neutron that is originated anywhere within the fuel. We will designate the weighing factor for each fuel sub-region m as ω_m where;

$$\sum_{m=1}^{N} \omega_m = 1 \qquad \text{(Eqn: 3.1-84)}$$

$$P_f = \omega_1 P_{f1} + \omega_2 P_{f2} + \omega_3 P_{f3} \qquad \text{(Eqn: 3.1-85)}$$

$$P_f = \left(\omega_1 P_o^1 T_{io}^2 T_{io}^3 + \omega_2 P_o^2 T_{io}^3\right) + \left(\omega_2 P_i^2 T_{oo}^1 T_{io}^2 T_{io}^3\right) + \left(\omega_3 P_i^3 T_{oo}^2 T_{io}^3 + \omega_3 P_i^3 T_{oi}^2 T_{oo}^1 T_{io}^2 T_{io}^3\right) + \omega_3 P_o^3$$

(Eqn: 3.1-86)

Based on the examination of the patterns of the terms in equation 3.1-86, the escape probability P_f is generalized for N fuel sub-regions as follows;

$$P_f = \sum_{j=1}^{N-1} \omega_j P_o^j \prod_{k=j+1}^{N} T_{io}^k + \sum_{j=2}^{N} \omega_j P_i^j T_{oo}^{j-1} \prod_{l=j}^{N} T_{io}^l + \sum_{j=3}^{N} \omega_j P_i^j \sum_{k=2}^{j-1} \left[\left(\prod_{l=k}^{j-1} T_{oi}^l \right) T_{oo}^{k-1} \left(\prod_{l=k}^{N} T_{io}^l \right) \right] + \omega_N P_o^N$$

(Eqn: 3.1-87)

Determination of the second element requires that we calculate the probability of a neutron entering the outer most fuel sub-region from outside will pass through the entire fuel without any interaction. Similar to the methodology for determination P_f, we will calculate this transmission probability T_f for a three fuel sub-regions and then we will generalize the results for N fuel sub-regions.

$$T_f = T_{oo}^3 + \left(1 - T_{oo}^3\right)\left(T_{oo}^2 T_{io}^3 + \left(1 - T_{oo}^2\right)\left(T_{oo}^1 T_{io}^2 T_{io}^3\right)\right) \quad \text{(Eqn: 3.1-88)}$$

The above equation is rearranged for the purpose of pattern recognition.

$$T_f = T_{oo}^3 + \left(1 - T_{oo}^2\right)\left(1 - T_{00}^3\right) T_{oo}^1 T_{io}^2 T_{io}^3 + \left(1 - T_{oo}^3\right) T_{oo}^2 T_{io}^3 \quad \text{(Eqn: 3.1-89)}$$

The general equation for the fuel transmission probability is then derived.

$$T_f = T_{oo}^N + \sum_{j=1}^{N-1} T_{oo}^j \prod_{k=j+1}^{N} T_{io}^k \left(1 - T_{oo}^k\right) \quad \text{(Eqn: 3.1-90)}$$

Now based on the two P_f and T_f elements as derived above, the escape probability Π_o is calculated.

$$\Pi_o = P_f\left(1 - T^{N+1}\right) + P_f T^{N+1} T_f \left(1 - T^{N+1}\right) + \ldots = \sum_{i=0}^{\infty} P_f \left(1 - T^{N+1}\right)\left(T^{N+1} T_f\right)^i \quad \text{(Eqn: 3.1-91)}$$

$$\Pi_o = P_f\left(1 - T^{N+1}\right)\frac{1}{1 - T^{N+1} T_f} \quad \text{(Eqn: 3.1-92)}$$

where T^{N+1} is the Dancoff factor (transmission probability through the moderator/coolant) and as stated in the problem statement, the Dancoff factor as derived in reference [10] will be used in this work.

At this point, we will derive the weighing factor ω_m for each fuel sub-region. In a case where the neutron flux is taken as uniform throughout the fuel, weighting factor for each

fuel sub-region is equal to the fraction of the fuel sub-region volume to the total fuel volume.

$$\omega_m = \frac{\pi\left(r_m^2 - r_{m-1}^2\right)}{\pi r_N^2} = \frac{r_m^2 - r_{m-1}^2}{R^2} \qquad \text{(Eqn: 3.1-93)}$$

We will attempt to refine ω_m further for our calculations. For this purpose, we need to develop the weighing factors for neutrons that interact in each fuel sub-region, ω_m, as shown in equation 3.1-87. First, ω_m is defined as the ratio of number of neutron interactions within fuel sub-region m to the total number of neutron interactions within the entire fuel.

$$\omega_m = \frac{\int_{E=0}^{\infty}\int_{r=r_{m-1}}^{r_m} dEdr2\pi r\Sigma(r,E,t)\phi(r,E,t)}{\int_{E=0}^{\infty}\int_{r=0}^{R} dEdr2\pi r\Sigma(r,E,t)\phi(r,E,t)} \qquad \text{(Eqn: 3.1-94)}$$

We make the following simplifying assumptions in order to solve equation 3.1-94; (1) for addressing the issue of energy dependence of the interaction rate, we use an average cross section value within equation 3.1-94. The average total interaction cross section is taken to be constant throughout the fuel region and does not change significantly with the fuel burnup, (2) The rate of interaction of fast and epithermal neutrons within the fuel is assumed to be insignificant when compared to those for thermal neutrons.

The thermal flux within a fuel rod in a two region cell is determined by use of equation 3.1-95 [14].

$$\phi(r) = AI_0(\tau r) \qquad \text{(Eqn: 3.1-95)}$$

where A is a constant associated with the power level of the fuel rod and $\tau = \sqrt{\frac{\Sigma_a}{D}}$ is the reciprocal of the thermal diffusion length in the fuel. Based on these assumptions, equation 3.1-94 is simplified as follows.

$$\omega_m = \frac{\int_{r=r_{m-1}}^{r_m} rI_0(\tau r)dr}{\int_{r=0}^{R} rI_0(\tau r)dr} \qquad \text{(Eqn: 3.1-96)}$$

The reasonableness of the above assumptions are discussed below. The weighing factors as derived from equation 3.1-96 will be used in for solving the current subject problem. We used the modified V:BUDS code to calculate the values τ based on averaged total absorption cross section and diffusion coefficient from equations 3.1-97 and 3.1-98 for the multiplication factor benchmark problems for the fresh and irradiated fuel using the input parameters from Reference [29].

$$\Sigma_a = \frac{\int_{E=0}^{\infty} dE \Sigma_a(E)\phi(E)}{\int_{E=0}^{\infty} dE \phi(E)} \qquad \text{(Eqn: 3.1-97)}$$

$$D = \frac{1}{3\Sigma_{tr}} = \frac{\int_{E=0}^{\infty} dE \phi(E)}{3\int_{E=0}^{\infty} dE \Sigma_{tr}(E)\phi(E)} \qquad \text{(Eqn: 3.1-98)}$$

Calculated τ and averaged total interaction cross sections are included in Table 3.1-2.

Table 3.1- 2: Calculated Σ_{avg} for Multiplication Factor Benchmark Problems Using V:BUDS

Level of Fuel Irradiation (MWd/kg)	$\tau - cm^{-1}$	$\Sigma_{avg} - cm^{-1}$
0 (fresh fuel)	0.118646	0.149309
20	0.116728	0.147949
40	0.114415	0.146400
60	0.112192	0.144906

Results of Table 3.1-2 validate the reasonableness of the constant average total interaction cross section assumption in the subject calculations. Also, incorporation of the average τ and the fuel radius of the benchmark problem into equation 3.1-96 shows that

the values of ω_m is very close to the values ω_m that are obtained by assuming a uniform flux within the fuel region. Review of existing literature such as References [34] and [35] indicate that in closely packed cells with light nuclide moderator and small fuel diameter such as our benchmark problem and actual fuel assemblies of power reactor core, the uniform flux assumption is reasonable. These conclusions justify the adequacy of the assumptions we used in deriving values of ω_m for use in equation 3.1-87.

Π_1 will be derived based on the reciprocity theorem as follows;

$$\Pi_0 V_f \Sigma_f = \Pi_1 V_{N+1} \Sigma_{N+1} \qquad \text{(Eqn: 3.1-99)}$$

where;

Σ_f = total macroscopic cross section of the fuel

V_f = volume of the fuel region

Σ_{N+1} = total macroscopic cross section of the moderator/coolant

V_{N+1} = volume of the moderator/coolant

At this point all the terms as defined in the statement of problem are derived and hence the decoupled flux equations as shown in equations 3.1-8 and 3.1-9 can be solved using the expanded V:BUDS computer code.

The V:BUDS computer code is expanded by allowing the code to recognize the multi-region fuel, obtaining the geometry and material properties for each of the fuel sub-regions, calculating the transmission and escape probabilities for each fuel sub-region using numerical integrations, calculating P_f and T_f values for the fuel and then calculating the equivalent Π_o and Π_1. As a last point in the development of the subject problem, we note that the characteristics length or mean chord length of the fuel sub-region should be similar to or larger than the mean free path for the thermal neutrons within the fuel, otherwise, inaccuracies will be introduced into the calculations due to the imposed boundary conditions at each fuel sub-region. These inaccuracies will increase as the fuel sub-region characteristic length gets smaller when compared to the thermal neutron mean free path within the fuel. Hence, care should be taken when selecting the number of the fuel sub-regions. This point is illustrated in Table 3.1-12 of section 3.1-14.

3.1.12 Determination of fuel sub-region to sub-region escape probability $\Pi_{m,n}$

The purpose of this section is to determine the escape probability from sub-region m to sub-region n of the fuel for the purpose of providing a methodology for solving equations 3.1-8 and 3.1-9. This determination depends on location of m sub-region in relation to n sub-region. Therefore two escape probabilities will be determined based on whether m>n or m<n.

Case (1): m<n

Figure 3.1-3 will be used as guide for this determination. The subject probability will be the sum of the following series of probabilities; (i) probability of a neutron being born in sub-region m will travel to sub-region n and will have its first interaction there, (ii) probability of neutron born in sub-region m will leave the fuel pin and travel through the moderator/coolant without any interaction and then enter another fuel pin and travel to sub-region n of that fuel and have its first interaction there, (iii) probability of neutron born in sub-region m leaving the fuel and moderator/coolant un-interacted entering another fuel pin and traversing it un-interacted and entering the moderator/coolant for the second time and traversing it un-interacted and then enter another fuel pin where it has into first interaction in sub-region n of that fuel pin. This process will be repeated infinite times. We will demonstrate the derivation for a six sub-region fuel model (N=6) where m=3 and n=5 for illustration purposes and then generalize the resulting probability correlation. Six fuel sub-regions were chosen in order to generate adequate number of terms for the purpose of pattern recognition. Each of the possible escape probabilities from region m to region n will be identified as P_i as shown below and the total escape probability from region m into region n will be the sum of all $P_i's$.

$$P_1 = P_o^3 T_{io}^4 \left(1 - T_{io}^5\right) \qquad \text{(Eqn: 3.1-100)}$$

$$P_2 = P_i^3 T_{oi}^2 T_{oo}^1 T_{io}^2 T_{io}^3 T_{io}^4 \left(1 - T_{io}^5\right) \quad \text{(Eqn: 3.1-101)}$$

$$P_3 = P_i^3 T_{oo}^2 T_{io}^3 T_{io}^4 \left(1 - T_{io}^5\right) \quad \text{(Eqn: 3.1-102)}$$

$P_1 + P_2 + P_3$ constitutes (generally shown as $P_{m,n}^m$) the item (i) above. For calculating probabilities in items (ii), (iii) and on we will first calculate the neutron escape probability from the Nth sub-region for a neutron that was born in sub-region m.

$$P_4 = P_o^3 T_{io}^4 T_{io}^5 T_{io}^6 \quad \text{(Eqn: 3.1-103)}$$

$$P_5 = P_i^3 T_{oi}^2 T_{oo}^1 T_{io}^2 T_{io}^3 T_{io}^4 T_{io}^5 T_{io}^6 \quad \text{(Eqn: 3.1-104)}$$

$$P_6 = P_i^3 T_{00}^2 T_{io}^3 T_{io}^4 T_{io}^5 T_{io}^6 \quad \text{(Eqn: 3.1-105)}$$

$P_4 + P_5 + P_6$ constitutes probability that a neutron that was born in sub-region m=3 will escape the fuel pin it was born in. We will designate this probability as P_e^m.

Study of $P_1 + P_2 + P_3$ shows that it can be generalized as follows:

$$P_{m,n}^{m} = P_o^m \prod_{j=m}^{n-1} T_{io}^{j}\left(1-T_{io}^{n}\right)+ P_i^m \left(1-T_{io}^{n}\right)\left[\sum_{j=1}^{m-1}\left(\prod_{k=j+1}^{m-1} T_{oi}^{k}\right)T_{oo}^{j}\left(\prod_{l=j+1}^{n-1} T_{io}^{l}\right)\right] \quad \text{(Eqn: 3.1-106)}$$

$$P_e^m = P_o^m \prod_{j=m+1}^{N} T_{io}^{j} + P_i^m \left[\sum_{j=1}^{m-1}\left(\prod_{k=j+1}^{m-1} T_{oi}^{k}\right)T_{oo}^{j}\left(\prod_{l=j+1}^{N} T_{io}^{l}\right)\right] \quad \text{(Eqn: 3.1-107)}$$

Now, probability for the neutron that just escaped the fuel pin where it was originated, to enter back into the fuel region and have its first interaction in sub-region n (say n=5) (P_7) will be;

$$P_7 = P_e^m \left(T^{N+1}\right)T_{oi}^{6}\left(1-T_{oi}^{5}\right) \quad \text{(Eqn: 3.1-108)}$$

P_7 constitutes item (ii) as discussed above. Now, to determine item (iii) and the consecutive iterations (P_8) from above discussion, we recall from equation 3.1-90 that the probability for a neutron entering a fuel region from its outer surface and traversing it un-interacted is T_f .

$$T_f = T_{oo}^{N} + \sum_{j=1}^{N-1} T_{oo}^{j} \prod_{k=j+1}^{N} T_{io}^{k}\left(1-T_{oo}^{k}\right) \quad \text{(Eqn: 3.1-109)}$$

$$T_8 = P_e^m \left(T^{N+1}\right)T_f \left(T^{N+1}\right)T_{oi}^{6}\left(1 - T_{oi}^{5}\right) \quad \text{(Eqn: 3.1-110)}$$

Hence the probabilities for items (ii) and (iii) and so on are;

$$P_7 + P_8 + \ldots = P_e^m \left(T^{N+1}\right) T_{oi}^6 \left(1 - T_{oi}^5\right) + P_e^m \left(T^{N+1}\right) T_f \left(T^{N+1}\right) T_{oi}^6 \left(1 - T_{oi}^5\right) + \ldots \qquad \text{(Eqn: 3.1-111)}$$

$$P_7 + P_8 + \ldots = P_e^m T^{N+1} T_{oi}^6 \left(1 - T_{oi}^5\right) \sum_{i=0}^{\infty} \left(T_f T^{N+1}\right)^i \qquad \text{(Eqn: 3.1-112)}$$

Equation 3.1-112 can be generalized for a target fuel sub-region n where the subject neutron is interacted as follows;

$$P_7 + P_8 + \ldots = P_e^m T^{N+1} \left(\prod_{j=n+1}^{N} T_{oi}^j \right) \left(1 - T_{oi}^n\right) \sum_{i=0}^{\infty} \left(T_f T^{N+1}\right)^i \qquad \text{(Eqn: 3.1-113)}$$

Therefore, $\Pi_{m,n}$ for a case where m<n can be derived by combining equations 3.1-106 and 3.1-113.

$$\begin{aligned} \Pi_{m,n} = {} & P_o^m \prod_{j=m}^{n-1} T_{io}^j \left(1 - T_{io}^n\right) + P_i^m \left(1 - T_{io}^n\right) \left[\sum_{j=1}^{m-1} \left(\prod_{k=j+1}^{m-1} T_{oi}^k \right) T_{oo}^j \left(\prod_{l=j+1}^{n-1} T_{io}^l \right) \right] \\ & + P_e^m T^{N+1} \left(\prod_{j=n+1}^{N} T_{oi}^j \right) \left(1 - T_{oi}^n\right) \sum_{i=0}^{\infty} \left(T_f T^{N+1}\right)^i \end{aligned} \qquad \text{(Eqn: 3.1-114)}$$

or;

$$\Pi_{m,n} = P_o^m \prod_{j=m}^{n-1} T_{io}^j \left(1 - T_{io}^n\right) + P_i^m \left(1 - T_{io}^n\right) \left[\sum_{j=1}^{m-1} \left(\prod_{k=j+1}^{m-1} T_{oi}^k \right) T_{oo}^j \left(\prod_{l=j+1}^{n-1} T_{io}^l \right) \right] \quad \text{for m<n}$$
$$+ P_e^m T^{N+1} \left(\prod_{j=n+1}^{N} T_{oi}^j \right) \left(1 - T_{oi}^n\right) \frac{1}{1 - T_f T^{N+1}}$$

(Eqn: 3.1-115)

Case (2): m>n

Development of $\Pi_{m,n}$ is similar to the previous case and hence all the developmental steps are not repeated here. The result for this case is given as;

$$\Pi_{m,n} = P_i^m \left(1 - T_{oi}^n - T_{oo}^n\right) \left(\prod_{j=n+1}^{m-1} T_{oi}^j \right) + P_e^m T^{N+1} \left(\prod_{j=n+1}^{N} T_{oi}^j \right) \left(1 - T_{oi}^n\right) \frac{1}{1 - T_f T^{N+1}} \quad \text{for m>n}$$

(Eqn: 3.1-116)

Determination $\Pi_{m,n}$ allows for the determination of flux distribution by solving the neutron transport equation as derived in this section.

It is noted that derivation of $\Pi_{m,n}$ is based on assumption that flux and material properties are uniform in each sub-region with neutron distribution being isotropic at each sub-region interface boundaries, i.e., a “white” or directionally homogenous boundary condition applies at each interface.

Also, reciprocity relationship can be used to determine $\Pi_{n,m}$ as follows.

$$\Pi_{m,n} V_m \Sigma_m = \Pi_{n,m} V_n \Sigma_n \qquad \text{(Eqn: 3.1-117)}$$

We modify the transport equations as shown in equations 3.1-8 and 3.1-9 to generalize the collision probability theory in a unit cell with multi sub-regions. Generalization of these two neutron transport equations based on the terminology as used in Figure 3.1-3 provides the following general neutron transport equation.

$$[\Sigma_m(\mathrm{E}) + \mathrm{D_m(E)B_m}^2]\phi_m(\mathrm{E}) =$$
$$(1 - \sum_{n}^{1,2,..,N,C(n\neq m)} \Pi_{m,n}(\mathrm{E}))[\int_0^{\infty} d\mathrm{E}'\phi_m(\mathrm{E}')[\ \Sigma_{s,m}(\mathrm{E}'\rightarrow \mathrm{E}) + \Sigma_{f,m}(E')\chi_m(E'\rightarrow E)\nu_m(E')] +$$
$$\sum_{n}^{1,2,..,N,C(n\neq m)} \frac{V_n}{V_m}\Pi_{n,m}(\mathrm{E})\left[\int_0^{\infty} d\mathrm{E}'\phi_n(\mathrm{E}')[\ \Sigma_{s,n}(\mathrm{E}'\rightarrow \mathrm{E}) + \Sigma_{f,n}(E')\chi_n(E'\rightarrow E)\nu_n(E')]\right]$$

(Eqn: 3.1-118)

where definition of the terms are similar to those as used in equations 3.1-8 and 3.1-9. This general equation is applicable for each sub-region; therefore, we have N+1 equations and N+1 unknowns as follows;

$$\phi_1(E), \phi_2(E), \phi_3(E), ..., \phi_N(E), \phi_{N+1}(E) \qquad \text{(Eqn: 3.1-119)}$$

where $\phi_m(E)$ represents the uniform flux for neutrons of energy E within sub-region m. Then we can obtain the total flux within a given sub-region by integrating or by summing $\phi_m(E)$ over all energy groups.

$$\phi_m = \int_0^{\infty} \phi_m(E)dE \approx \sum_{E_{\min}}^{E_{\max}} \phi_m(E) \qquad \text{(Eqn: 3.1-120)}$$

where m represents the sub-region of interest, i.e., m= 1, 2, …, N, N+1.

The developed methodology in this section will allow for the determination of even more detailed flux distribution for a future work. At this point, we will plot the region to region escape probabilities for two cases of m>n and m<n for $T_{\mathrm{mod}\,erator}$ value of 0.5 in order to gain some intuition in this process for a four sub-region fuel.

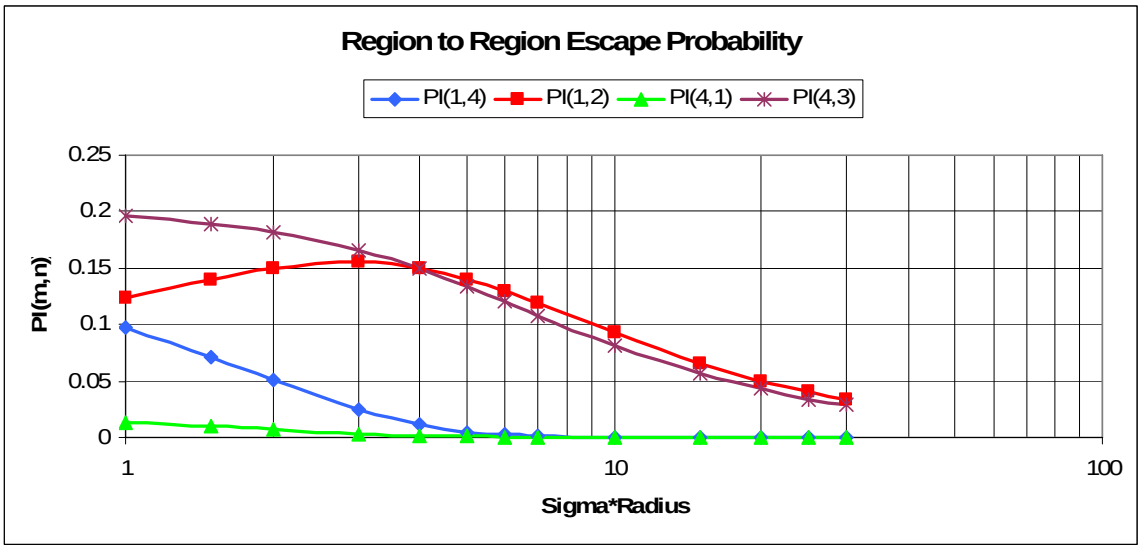

Figure 3.1- 15: Region to Region Escape Probability for $\Pi_{1,4}, \Pi_{1,2}, \Pi_{4,1}, and \Pi_{4,3}$

Figure 3.1-15 indicates that for large interaction coefficient, all of these escape probabilities approach zero. Also, as the distance between the two sub-regions increase, the escape probability between the two region decreases for a given interaction coefficient. These observations are consistent with our expectations and provide intuition in these region to region escape probabilities.

We will also show the values of region to region escape probabilities from the fuel region where the transmission and escape probabilities are derived in the previous sections for $T_{\mathrm{mod}\,eratorr}$ value of 0.5 with fuel divided to four sub-regions in accordance with Figure 3.1-3. Sub-region 5 is the moderator/coolant area. This will help us to observe the escape probability from each fuel sub-region to another fuel sub-region.

Table 3.1- 3: Region to Region Escape Probabilities for a Fuel with 4 sub-regions

Fuel Region to Region Escape Probability	$\Sigma R = 1$	$\Sigma R = 10$
Π_{11}	0.625	0.903
Π_{12}	0.123	0.092
Π_{13}	0.104	0.004
Π_{14}	0.09	1.533E-04
Π_{15}	0.063	2.995E-06
Π_{21}	0.040	0.031
Π_{22}	0.330	0.838
Π_{23}	0.350	0.125
Π_{24}	0.234	0.005
Π_{25}	0.155	9.417E-05
Π_{31}	0.020	7.891E-04
Π_{32}	0.150	0.076
Π_{33}	0.355	0.807
Π_{34}	0.290	0.114
Π_{35}	0.190	0.002
Π_{41}	0.014	2.231E-05
Π_{42}	0.100	0.002
Π_{43}	0.198	0.082
Π_{44}	0.433	0.861
Π_{45}	0.253	0.055

Observations from Table 3.1-3 are similar to those as described for Figure 3.1-15 and they are in accordance with our expectations.

3.1.13 Selection of Benchmark Problems

The following benchmark problems from OECD/NEA Burnup Credit Criticality Benchmark, Phases IV-A and IV-B [28 and 29] are selected to verify the accuracy of the developed methodology. OECD/NEA phase IV-A provides data on reactivity effects observed with fresh and irradiated MOX fuels. OECD/NEA phase IV-B includes benchmarking results on the inventories of nuclides of interest in MOX fuel following a specified burnup period. We will use the phase IV-A results for evaluating the fidelity of our model in calculating multiplication factors within the fuel cell and phase IV-B results for evaluation of our model's capabilities in determination of radionuclide inventories following a specified fuel burnup. A second benchmark problem from Reference [30] is also selected to further evaluate the capabilities of our model in the context of plutonium burnup. These test cases are of interest because plutonium-bearing fuel exhibits shorter neutron mean free paths at most energies than does uranium fuel, so the homogenization approach of the original model would be expected to lead to larger errors. The unit cell from Reference [28] is shown below.

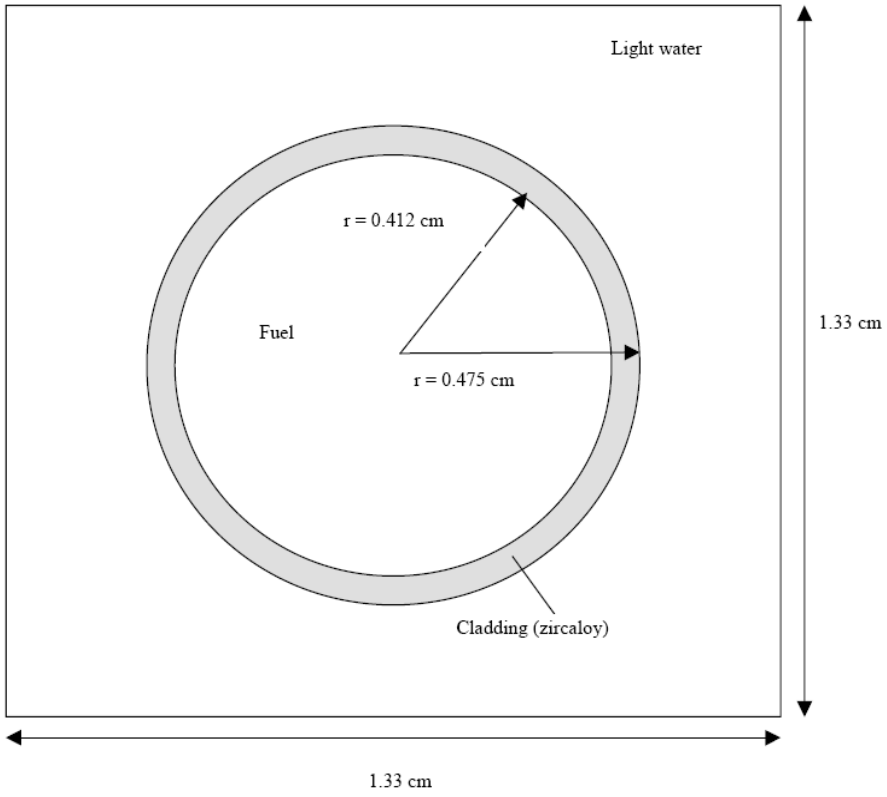

Figure 3.1- 16: Selected OECD/NEA Phase IV-A Unit Cell for Multiplication Factor Benchmarking

The initial fuel number densities for the multiplication factor benchmarking are given as follows [28]:

Table 3.1- 4: Number Densities of Actinides in Fresh MOX Fuel used for Multiplication Factor Benchmarking

Nuclide	Number Density [atm/barn.cm] for Fresh Fuel
^{234}U	2.7999E-7
^{235}U	5.8570E-5
^{236}U	—
^{238}U	2.3074E-2
^{238}Pu	2.4700E-5
^{239}Pu	8.0623E-4
^{240}Pu	3.1298E-4
^{241}Pu	1.6533E-4
^{242}Pu	5.3981E-5
^{237}Np	—
^{241}Am	—
^{243}Am	—

Table 3.1- 5: Number Densities of Actinides in Irradiated MOX Fuel used for Multiplication Factor Benchmarking

Nuclide	Number Density [atm/barn.cm] for Irradiated Fuel		
	20 MWd/kg	40 MWd/kg	60 MWd/kg
^{234}U	6.3600E-7	7.7718E-7	9.1664E-7
^{235}U	4.2219E-5	2.9018E-5	1.9181E-5
^{236}U	3.7252E-6	6.1753E-6	7.5360E-6
^{238}U	2.2732E-2	2.2365E-2	2.1986E-2
^{238}Pu	2.2785E-5	2.5504E-5	2.9509E-5
^{239}Pu	5.9182E-4	4.5028E-4	3.6327E-4
^{240}Pu	3.1445E-4	2.9067E-4	2.5605E-4
^{241}Pu	1.8251E-4	1.8125E-4	1.6525E-4
^{242}Pu	7.0592E-5	9.1733E-5	1.211E-4
^{237}Np	1.6134E-6	3.0746E-6	4.1997E-6
^{241}Am	1.8432E-5	2.2303E-5	2.1568E-5
^{243}Am	1.3528E-5	2.4023E-5	3.2566E-5

The benchmark problem from OECD/NEA phase IV-A [28] provides a mean multiplication factor and the standard deviation based on thirty seven reported values using different computer codes and techniques. These reported results are included in Table 3.1-6.

Table 3.1- 6: Benchmark Multiplication Factors for Problem # 1

Case	Mean K_{eff}	Standard Deviation
Fresh Fuel	1.3002	0.0045
Irradiated Fuel 20 MWd/kg	1.2428	0.0042
Irradiated Fuel 40 MWd/kg	1.2050	0.0041
Irradiated Fuel 60 MWd/kg	1.1754	0.0039

For isotope inventory benchmarking purposes, reference [29] is used. The MOX fuel unit cell for this case is a follows.

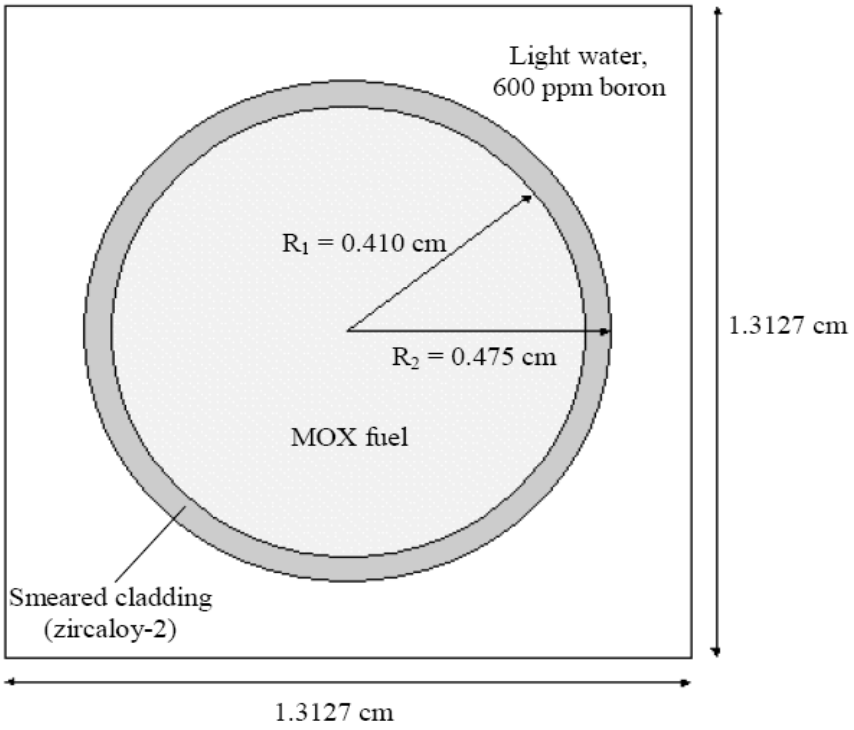

Figure 3.1- 17: Selected OECD/NEA Phase IV-B Unit Cell for Isotope Inventory Benchmarking

The initial fuel number densities for isotope inventory benchmarking as given within Reference [29] are included in Table 3.1-7.

Table 3.1- 7: Number Densities of Actinides in Initial MOX Fuel Pin used for Isotope Inventory Benchmarking from Reference [29]

Nuclide	Initial Number Density [atm/barn.cm] for the fuel pin
^{234}U	2.5952E-7
^{235}U	5.4287E-5
^{236}U	—
^{238}U	2.1387E-2
^{238}Pu	4.6610E-5
^{239}Pu	1.0156E-3
^{240}Pu	4.8255E-4
^{241}Pu	1.7491E-4
^{242}Pu	1.3201E-4
^{237}Np	—
^{241}Am	—
^{243}Am	—

Material temperature for the above benchmark are given as Fuel temperature = 900°K [29], and Coolant/Moderator temperature = 575°K [29]. The benchmark values from Reference [29] are provided in Table 3.1-8.

Table 3.1- 8: Isotope Inventory Benchmark Calculation Results for Pin Cell Model at End of Cycle 1 for MOX fuel from Reference [29]

Nuclide	Number Density at EOC1 [atm/barn.cm] for the fuel pin
^{234}U	5.3603E-7
^{235}U	4.3896E-5
^{236}U	2.5160E-6
^{238}U	2.1157E-2
^{238}Pu	4.1350E-5
^{239}Pu	8.0727E-4
^{240}Pu	4.7367E-4
^{241}Pu	2.1899E-4
^{242}Pu	1.3465E-4
^{237}Np	1.1947E-6
^{241}Am	8.7782E-6
^{243}Am	1.7080E-5

Additional literature search identified another benchmark problem pertinent to our work on problem 1 [30]. In this reference, consumption of plutonium within thorium and uranium based mixed oxide fuels within reactors are studied through the use of MOCUP, MCNP, and ORIGEN computer codes [43], [44] and [45]. We will use one of the studied

fuel pins of this reference for further validation of our developed methodology.

Specifications of the studied fuel pin in Reference [30] are included in Table 3.1-9.

Table 3.1- 9: Fuel Pin Parameters for Isotope Inventory Benchmarking from Reference [30]

Parameter	Values
Fuel temperature	900° K
Fuel radius	0.41274 cm
Clad inner radius	0.41896 cm
Clad outer radius	0.47609 cm
Fuel density	94% of theoretical
Pin pitch	1.2626 cm
Plutonium loading of the fuel	4.4 wt% (Reactor Grade)
Beginning of Cycle Plutonium Isotope Fractions	
^{238}PU	2.0%
^{239}Pu	58.0%
^{240}Pu	26.0%
^{241}Pu	10.0%
^{242}Pu	4.0%

Plutonium isotopic fractions and the total plutonium fraction in the fuel with a discharge burnup of 37 MWd/kg are given in Reference [30] and included Table 3.1-10. Reference [30] uses a discharge burnup (BU) based on a three-batch fuel cycle that is calculated from the Linear Reactivity Model as described in Reference [31].

Table 3.1- 10: Mass Percentage of Pu Isotopes to Total Pu Mass with BU=37 MWd/kg [30]

^{238}Pu	^{239}Pu	^{240}Pu	^{241}Pu	^{242}Pu	Total Pu mass fraction
2.37%	41.92%	28.73%	18.73%	8.26%	3.54 wt%

Results of our analyses based on the developed methodology will be compared against the above selected benchmark problems and conclusions will be drawn on the fidelity of our model in the following sections.

3.1.14 Calculation of the Multiplication Factors and the Isotope Inventory Using the Developed Methodology and Modified V:BUDS

V:BUDS computer code was modified to incorporate the theoretical results of sections 3.1.5 through 3.1.11. Then calculations were performed for several fuel sub-region values. The right Riemann sums numerical scheme was used to calculate the integral

values associated with the escape and transmission probabilities. The subject probabilities were calculated based on several small angular step sizes before the final selection of the angular step size in order to ensure the maximum optimal desired accuracy. For multiplication factor calculations, the modified V:BUDS input parameters for geometry and material properties are shown in Table 3.1-11. The initial isotopic contents for this case are shown in Tables 3.1-4 and 3.1-5 for fresh and irradiated fuel respectively.

Table 3.1- 11: Modified V:BUDS Input Parameters for the Multiplication Factor Benchmark Problem [28]

Parameter	Input Value
Fuel Temperature	300° K. The fuel is assumed to be uniform in temperature.
Moderator/Coolant Temperature	300° K. The moderator/coolant is assumed to be uniform in temperature.
Boron Concentration in Moderator/Coolant	600 ppm.
Fuel Density	10.4 g/cm^3.
Fuel Radius	0.412 cm.
Cladding Thickness	0.063 cm.
Fuel Center to Center Pitch	1.33 cm.

As discussed in section 3.1-11, the mean free path for thermal neutrons for typical light water reactor fuel similar to that for the benchmark problems is smaller than 1cm [3] which corresponds to about two fuel sub-regions. Therefore, selection of two fuel sub-regions would render the best comparative results, however, the results for four sub-regions were shown in this analysis for the demonstration purposes. The calculated multiplication factor values were documented in Tables 3.1-12 through 3.1-15. In addition, we calculated the multiplication factors based on the same input parameters as above using the single fuel region model from the original V:BUDS code and included the results in Table 3.1-16 for comparison purposes against the modified V:BUDS and benchmark problem. The multiplication factor for the fresh fuel was calculated for up to 12 fuel sub-regions based on the developed methodology in order to demonstrate the increased inaccuracy with increased number of fuel sub-regions as discussed within section 3.1-11.

Table 3.1- 12: Modified V:BUDS and Benchmark Multiplication factor Results for Fresh Fuel

Number of Fuel Sub-Regions (NRING)	k_{eff} From V:BUDS Developed Methodology	Mean k_{eff} From Benchmark (with σ =0.0045)
2	1.31562	1.3002
3	1.34082	1.3002
4	1.31168	1.3002
5	1.30988	1.3002
6	1.23085	1.3002
8	1.17544	1.3002
10	1.14475	1.3002
12	1.12843	1.3002

Table 3.1- 13: Modified V:BUDS Multiplication Factor and Benchmark Results for 20 MWd/kg Irradiated Fuel

Number of Fuel Sub-Regions (NRING)	k_{eff} From V:BUDS Developed Methodology	Mean k_{eff} From Benchmark (with σ =0.0042)
2	1.24852	1.24280
3	1.26571	1.24280
4	1.2316	1.24280

Table 3.1- 14: Modified V:BUDS Multiplication Factor and Benchmark Results for 40 MWd/kg Irradiated Fuel

Number of Fuel Sub-Regions (NRING)	k_{eff} From V:BUDS Developed Methodology	Mean k_{eff} From Benchmark (with σ =0.0041)
2	1.19635	1.20500
3	1.20449	1.20500
4	1.16986	1.20500

Table 3.1- 15: Modified V:BUDS Multiplication Factor and Benchmark Results for 60 MWd/kg Irradiated Fuel

Number of Fuel Sub-Regions (NRING)	K_{eff} From V:BUDS Developed Methodology	Mean K_{eff} From Benchmark (with σ =0.0039)
2	1.15043	1.17540
3	1.15462	1.17540
4	1.12082	1.17540

Table 3.1- 16: Comparison of Single Fuel Region Model (Original V:BUDS) Results versus the Benchmark

Fuel	Mean k_{eff} From Benchmark (with σ =0.0045)	k_{eff} From Single Fuel Region Model	% Difference when compared to Benchmark
Fresh Fuel	1.3002	1.26655	-2.59%
Irradiated Fuel BU=20 MWd/kg	1.24280	1.20607	-2.96%
Irradiated Fuel BU=40 MWd/kg	1.20500	1.16491	-3.33%
Irradiated Fuel BU=60 MWd/kg	1.17540	1.13192	-3.70%

The input parameters for the isotope inventory benchmark problem from OECD/NEA Phase IV-B [29] as shown in Table 3.1-17 were inserted in the multi-region fuel model. The sample results for fuel with two sub-regions are shown in Table 3.1-18. The remaining results for 3 and 4 fuel sub-regions are included in Appendix A as Tables A.3.1-1 and A.3.1-2. Also, the isotope inventories for this benchmark problem using the original V:BUDS (single fuel region) are determined and included in Table 3.1-19 for comparison purposes.

Table 3.1- 17: V:BUDS Input Parameters for the OECD/NEA Phase IV-B Isotope Inventory Benchmark Problem [29]

Parameter	Input Value
Fuel Temperature	900° K. The fuel is assumed to be uniform in temperature.
Moderator/Coolant Temperature	575° K. The moderator/coolant is assumed to be uniform in temperature.
Boron Concentration in Moderator/Coolant	600 ppm.
Fuel Density	10.4 g/cm^3.
Fuel Radius	0.410 cm.
Cladding Thickness	0.065 cm.
Fuel Center to Center Pitch	1.3127cm.

Table 3.1- 18: Modified V:BUDS Isotope Inventory and OECD/NEA Phase IV-B Benchmark Results for Irradiated MOX fuel (Number of Fuel Sub-regions = 2)

Number of Fuel Sub-Regions (NRING)	Nuclide	Number Density [atm/barn.cm] Benchmark	Number Density [atm/barn.cm] Developed Methodology
2	^{234}U	5.3603E-7	5.764E-7
	^{235}U	4.3896E-5	4.327E-5
	^{236}U	2.5160E-6	2.445E-6
	^{238}U	2.1157E-2	2.117E-2
	^{238}Pu	4.1350E-5	4.052E-5
	^{239}Pu	8.0727E-4	7.855E-4
	^{240}Pu	4.7367E-4	4.81E-4
	^{241}Pu	2.1899E-4	2.058E-4
	^{242}Pu	1.3465E-4	1.362E-4
	^{237}Np	1.1947E-6	1.192E-6
	^{241}Am	8.7782E-6	8.556E-6
	^{243}Am	1.7080E-5	1.517E-5

Table 3.1- 19: Comparison of the Isotope Inventory OECD/NEA Phase IV-B Benchmark Calculation Results to Single Fuel Region Model for Irradiated MOX fuel (Original V:BUDS Model)

Nuclide	Number Density [atm/barn.cm] Benchmark	Number Density [atm/barn.cm] Single Region Fuel Model
^{234}U	5.3603E-7	5.503E-7
^{235}U	4.3896E-5	4.239E-5
^{236}U	2.5160E-6	2.836E-6
^{238}U	2.1157E-2	2.114E-2
^{238}Pu	4.1350E-5	4.054E-5
^{239}Pu	8.0727E-4	8.144E-4
^{240}Pu	4.7367E-4	4.717E-4
^{241}Pu	2.1899E-4	2.132E-4
^{242}Pu	1.3465E-4	1.347E-4
^{237}Np	1.1947E-6	1.419E-6
^{241}Am	8.7782E-6	8.45E-6
^{243}Am	1.7080E-5	1.699E-5

In order to gain additional data to judge the fidelity of the developed model for the determination of the fuel isotope inventory for fresh and irradiated fuel, we located Reference [30] which could provide us another benchmark problem. Different isotope inventories were then calculated using the modified V:BUDS code based on the input parameters of Reference [30] benchmark problem. The results of these calculations are included in Table 3.1-20. The same calculations were performed using the original V:BUDS code (single fuel region) and the results are summarized in Table 3.1-21. The benchmark values for the isotope inventories following a 37 MWd/kg of burnup from Reference [30] are included in Table 3.1-10 of section 3.1.13.

Table 3.1- 20: Plutonium Isotopic Mass Fractions after 37 MWd/kg Burnup within the Fuel Using the Developed Methodology

No. of fuel sub-regions	^{238}Pu / Total Pu	^{239}Pu / Total Pu	^{240}Pu / Total Pu	^{241}Pu / Total Pu	^{242}Pu / Total Pu	Total Pu / Total fuel mass
2	2.14%	43.63%	31.57%	15.30%	7.35%	3.582%
3	2.04%	43.60%	33.43%	13.59%	7.34%	3.568%
4	1.97%	43.96%	34.17%	12.59%	7.30%	3.587%

Table 3.1- 21: Plutonium Isotopic Mass Fractions after 37 MWd/kg Burnup within Single Region Fuel (Original V:BUDS)

^{238}Pu / Total Pu	^{239}Pu / Total Pu	^{240}Pu / Total Pu	^{241}Pu / Total Pu	^{242}Pu / Total Pu	Total Pu / Total fuel mass
2.13%	46.60%	28.85%	15.71%	6.70%	3.771%

3.1-15 Analysis of the Results from the Developed Methodology and Discussions

In this section, we will compare the calculated multiplication factor and the isotope inventory for fresh and irradiated fuel based on the modified V:BUDS computer code to those from the benchmark problems. A comparison will also be provided against the single fuel region model using the original V:BUDS computer code. A discussion will be provided for each of the comparisons on the effectiveness of the proposed methodology.

Multiplication factor for the fresh fuel is depicted in Figure 3.1-18 using the results from Table 3.1-12 and compared to benchmark value from Reference [28] and the results from the original V:BUDS as included in Table 3.1-16.

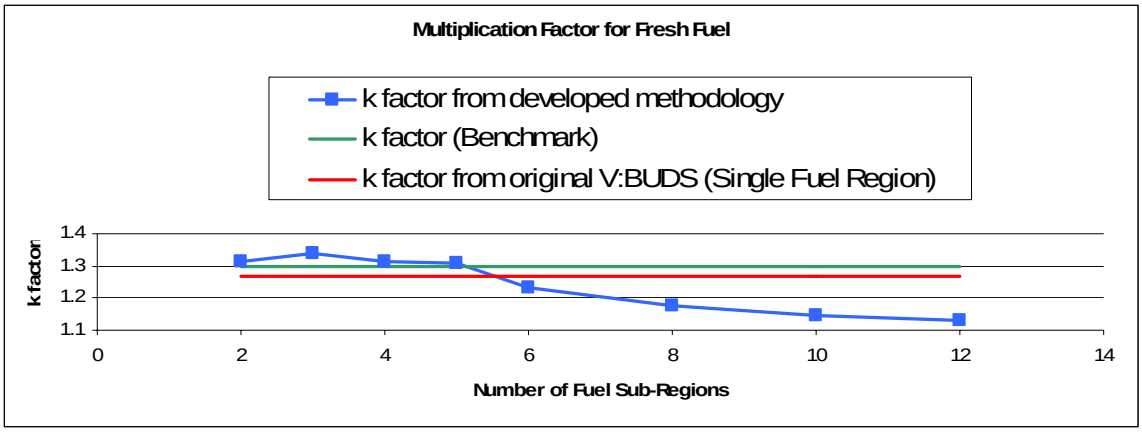

Figure 3.1- 18: Multiplication Factor for Fresh Fuel

Examination of the results from Figure 3.1-18 indicates an excellent agreement between the developed model and the benchmark problem for the two fuel sub-regions. In this model, the predicted multiplication factor deviates the benchmark value by about 1% for the 2 fuel sub-regions. By increasing the number of fuel sub-regions especially beyond four, the deviation increases and reaches 13.2% for 12 fuel sub-regions. This illustrates the issue of increased inaccuracies as the fuel sub-region characteristic length decreases when compared to the mean free path of the neutrons in the fuel as discussed in section 3.1-11. The single fuel model using the original V:BUDS computer code results in a multiplication factor that deviates the benchmark value by 2.59% which is also in good agreement with the benchmark value. These comparison results are shown in Table 3.1-22.

Table 3.1- 22: Comparison of Multiplication Factor from the Developed Methodology vs. the Benchmark Value for the Fresh Fuel

Number of Fuel Sub-Regions	% difference between Developed Model and the Benchmark	% difference between Single Fuel Region and the Benchmark
2	1.19	-2.59
3	3.12	-2.59
4	0.88	-2.59
5	0.74	-2.59
6	-5.33	-2.59
8	-9.60	-2.59
10	-11.95	-2.59
12	-13.21	-2.59

Multiplication factor for the several irradiated fuels are also depicted in Figures 3.1-19, 3.1-20, and 3.1-21 based on the results from Tables 3.1-13, 3.1.14, and 3.1-15. The results are compared to benchmark value and the calculated multiplication factors from the original V:BUDS which were included in Table 3.1-16 in order to analyze the accuracy of the developed model for irradiated fuels as well.

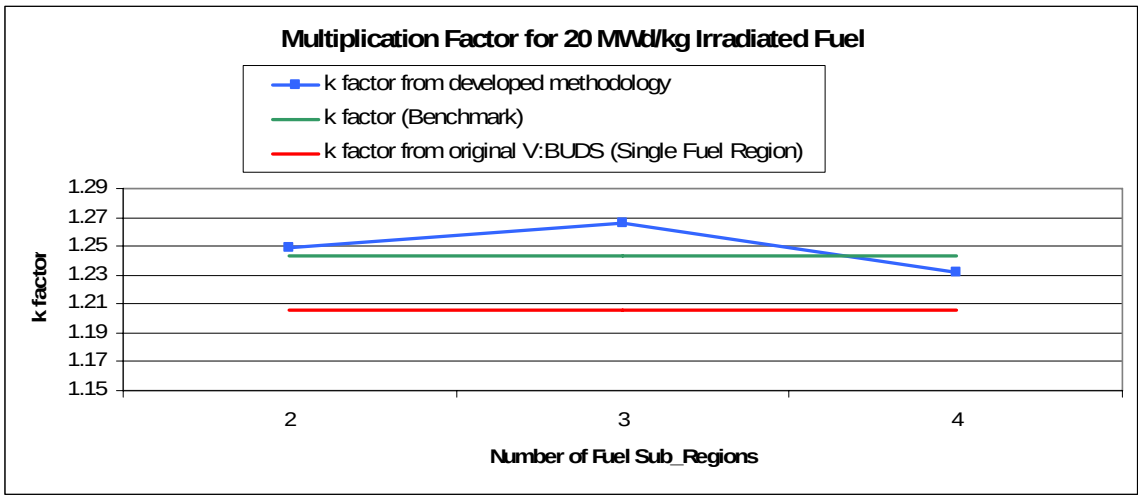

Figure 3.1- 19: Multiplication Factor for 20 MWd/kg Irradiated Fuel

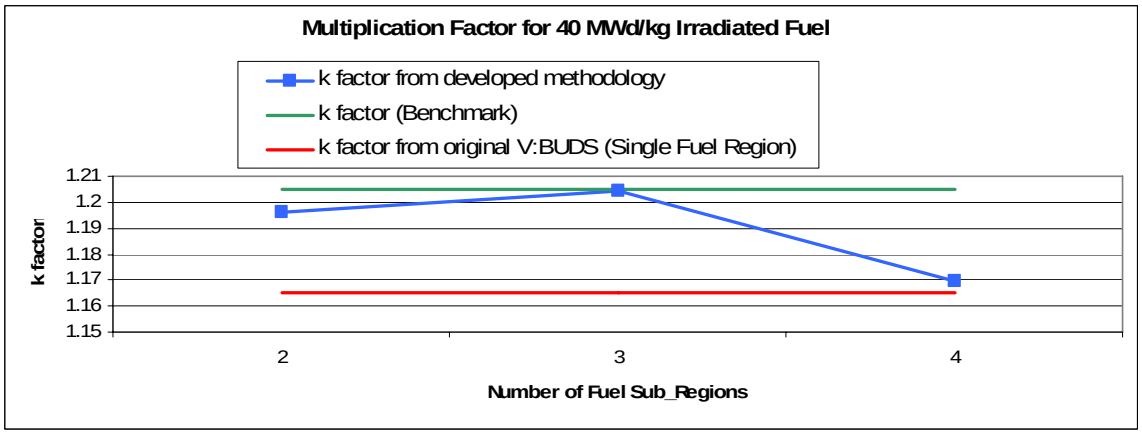

Figure 3.1- 20: Multiplication Factor for 40 MWd/kg Irradiated Fuel

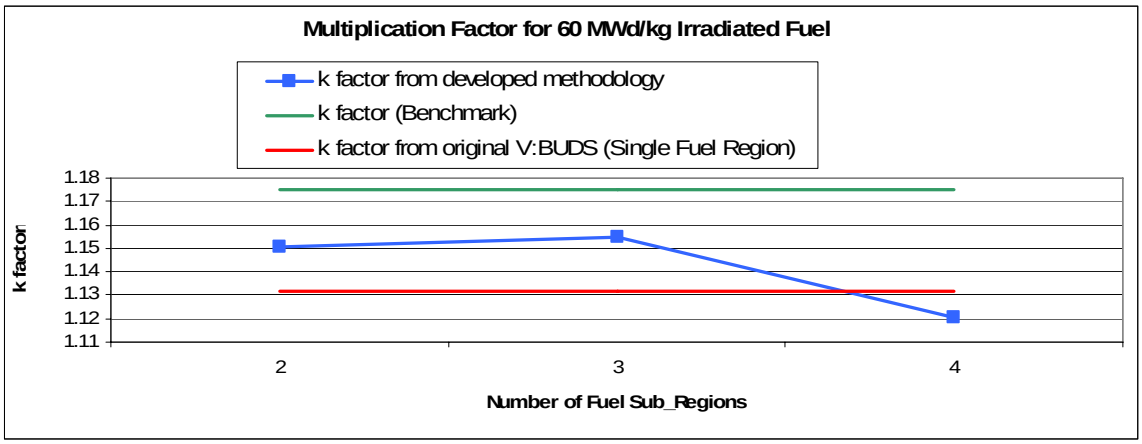

Figure 3.1- 21: Multiplication Factor for 60 MWd/kg Irradiated Fuel

Again, based on examination of the results from Figure 3.1-19 through 3.1-21 we observe an excellent agreement between the developed model and the benchmark problem for the discussed 2 fuel sub-regions. The predicted multiplication factor based on the developed model is about 1% of the value from the benchmark problem for all levels of irradiation for 2 fuel sub-regions. The single fuel region area based on the original V:BUDS model renders deviations of 2.96%, 3.33% and 3.70% for 20 MWd/kg, 40 MWd/kg and 60 MWd/kg fuel irradiations respectively. Therefore, the developed methodology provides an enhanced accuracy when compared to the single fuel region model as can be seen from Figures 3.1-18 through 3.1-21. The comparison results are included in the Table 3.1-23.

Table 3.1- 23: Comparison of Multiplication Factor from the Proposed Methodology vs. the Benchmark Value for Irradiated Fuel

Number of Fuel Sub-Regions	Fuel Irradiation (MWd/kg)	% difference between Developed Model and the Benchmark	% difference between the Single Fuel Region and the Benchmark
2	20	0.46	-2.96
	40	-0.72	-3.33
	60	-2.12	-3.70
3	20	1.84	-2.96
	40	-0.04	-3.33
	60	-1.77	-3.70
4	20	-0.90	-2.96
	40	-2.92	-3.33
	60	-4.64	-3.70

Now, we will turn our attention to evaluation of the adequacy of our proposed model in regards to determination of isotope inventory calculations and their comparisons with the identified benchmark problems. To accomplish this purpose, we will plot the isotopic inventory of several calculated isotopes from the proposed methodology. We will use a single plot for each isotope in order to perform the desired comparisons and also for the benefit of understanding the adequacy of the original and the modified V:BUDS

computer code in regards to calculation of each isotope inventory versus the total actinide calculations for a given fuel and burnup.

A typical plot for the isotope inventory calculations for ^{235}U is depicted in Figure 3.1-22. This figure also shows the results of the benchmark problem and one region fuel model from the original V:BUDS. The results for other isotopes are included in Appendix C.

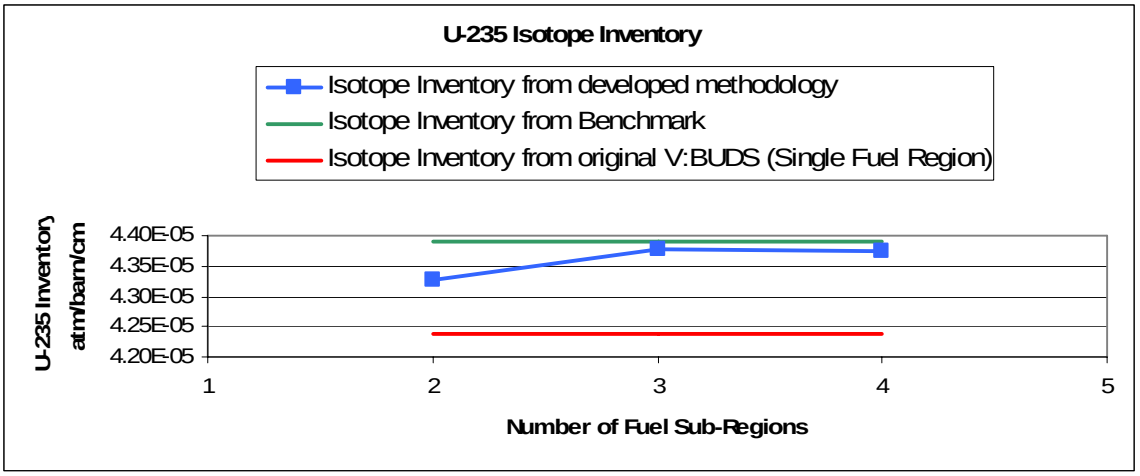

Figure 3.1- 22: ^{235}U Isotope Inventory Using OECD/NEA Phase IV-B Benchmark

The percentage of differences between the developed model and the single region fuel model versus the benchmark problem values are calculated. The results for ^{235}U are depicted in Tables 3.1-24 Similar results for isotopes ^{234}U, ^{236}U, ^{238}U, ^{238}Pu, ^{239}Pu, ^{240}Pu, ^{241}Pu, ^{242}Pu , ^{237}Np, ^{241}Am, and ^{243}Am are calculated included in Appendix B as Tables B.3.1-1 through B.3.1-11.

Table 3.1- 24: Comparison of ^{235}U Isotope Inventory from the Proposed Methodology vs. the OECD/NEA Phase IV-B Benchmark

Number of Fuel Sub-Regions	% difference between the developed model and the Benchmark	% difference between the Single Fuel Region and the Benchmark
2	-1.43	-3.43
3	-0.26	-3.43
4	-0.31	-3.43

Examination of Figures 3.1-22 and C.3.1-1 through C.3.1-11, Tables 3.1-24, and Tables B.3.1-1 through B.3.1-11 reveal that our developed model provides very good results for the subject isotopes for the discussed two fuel sub-regions.

Since the isotope inventory calculations are very methodology sensitive and largely dependant upon the codes used for the purpose, we perform additional benchmarking to ensure that our model predicts the overall actinide inventory within an irradiated fuel with a high degree of fidelity. We use Reference [30] since it has a well defined pin cell and the overall percentage of important actinides is provided for an irradiated fuel. We will refer to this benchmark problem as Weaver-Herring benchmark. The results of the comparisons with the Weaver-Herring benchmark problem are depicted for the mass percentage of total plutonium isotopes within the fuel and the mass percentage of ^{239}Pu to

the total plutonium contents within the fuel in Figures 3.1-23 and 3.1-24. Additional results from benchmarking against the Weaver-Herring are shown in Appendix C. The Weaver-Herring benchmark problem and its fuel pin parameters are defined within Tables 3.1-9 and 3.1-10 of section 3.1.13.

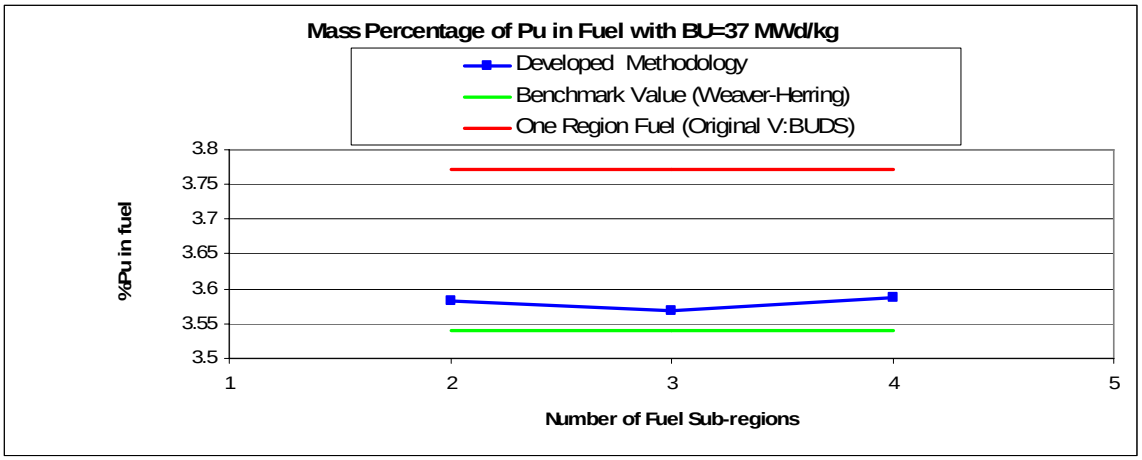

Figure 3.1- 23: Mass Percentage of Plutonium Isotopes to Total Fuel Mass in Fuel with BU=37 MWd/kg Using Weaver-Herring Benchmark

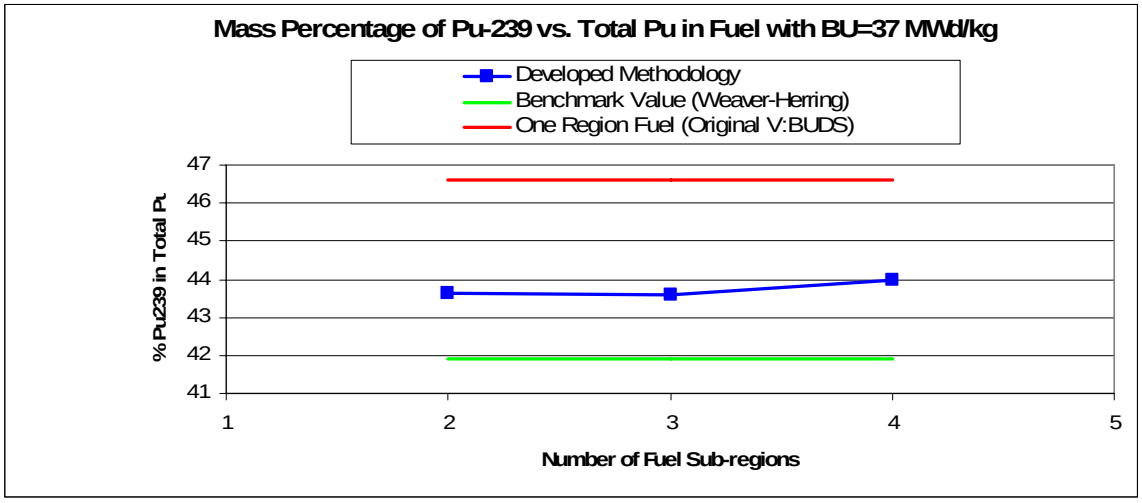

Figure 3.1- 24: Mass Percentage of ^{239}Pu to total Pu Isotopes in Fuel with BU=37 MWd/kg Using Weaver-Herring Benchmark

Table 3.1- 25: Comparison of Mass Percentage of Total Plutonium Isotopes to Total Fuel Mass Using Weaver-Herring Benchmark

Number of Fuel Sub-Regions	% difference between the Developed Model and Weaver-Herring Benchmark	% difference between the Single Fuel Region and Weaver-Herring Benchmark
2	1.19	6.53
3	0.79	6.53
4	1.33	6.53

In addition to Figure 3.1-23 and 3.1-24, Table 3.1-25 is prepared to provide the deviations for the percentage mass of total plutonium isotopes to the fuel mass between the developed methodology and a single fuel region model and Weaver-Herring [30] benchmark values. Table 3.1-25 shows that there is an excellent agreement between our proposed model and the benchmark value. The deviation is calculated to be about 1% vs. 6.5% provided by the single region fuel model. Therefore, our model represents a very good capability in calculating the total mass of plutonium isotopes in the irradiated fuel.

Also, review of Figure 3.1-24 and C.3.1-12 through C.3.1-15 show that the proposed model provides reasonable values for individual plutonium isotopes especially for ^{239}Pu. The provided values from two sub-region fuel model are generally similar or better than those provided by single region fuel model.

3.1-16 Conclusions for the Proposed Methodology

Results of our calculations indicate that the proposed methodology using the modified V:BUDS computer code yields an excellent agreement with the OECD/NEA benchmark problem in regards to the multiplication factor for fresh and irradiated fuels for small number of fuel sub-regions. The number of fuel sub-regions should be selected such that the characteristic length or mean chord length of the fuel sub-region is similar to or larger than the mean free path for the neutrons within the fuel, otherwise, inaccuracies will be introduced into the calculations due to the imposed boundary conditions at each fuel sub-

region. The error associated with the developed model is 1.19% for the multiplication factor of a fresh fuel versus 2.59% error resulted from the original model. The errors associated with the irradiated fuel are 0.46%, 1.84%, and 0.90% for 20 MWd/kg, 40 MWd/kg and 60 MWd/kg burnup respectively. These errors compare favorably against the errors from the original model that are computed to be 2.96%, 3.33% and 3.70% respectively.

Also, the proposed methodology provides an excellent prediction of the percentage of total mass of plutonium isotopes to the total mass of the fuel for a given irradiation level. This is an indication of how well our model can identify the burning of plutonium in the MOX fuels in the existing reactors. The level of agreement between the calculated ^{239}Pu between the proposed model and the benchmark problems is also very good. This fact can be used to conclude that our model is a good tool for study of any fuel form in which neutron mean free path's are short such as thermal reactor transmuter fuel.

The error analysis from our developed methodology provides values of 1.43% and 1.19% for the ^{235}U content and ratio of ^{239}Pu to the total value of plutonium within the irradiated fuel. These errors compare favorably to those from the original model that are computed at 3.43% and 6.53% respectively. As discussed earlier, the calculated values from the developed methodology approaches the benchmark values to within about 1%. It is noted that the model value will not approach the exact benchmark value due to the errors introduced by the imposed boundary conditions at each of the sub-regions.

3.2 Complex Problem # 2

3.2.1 Scope/Statement of Problem

In current reactor calculations, similar reactor fuel elements are arranged in a periodic manner so that the core system is regarded as being made up of a number of identical unit cells. A unit cell in the current literature is depicted in Figure 3.2-1.

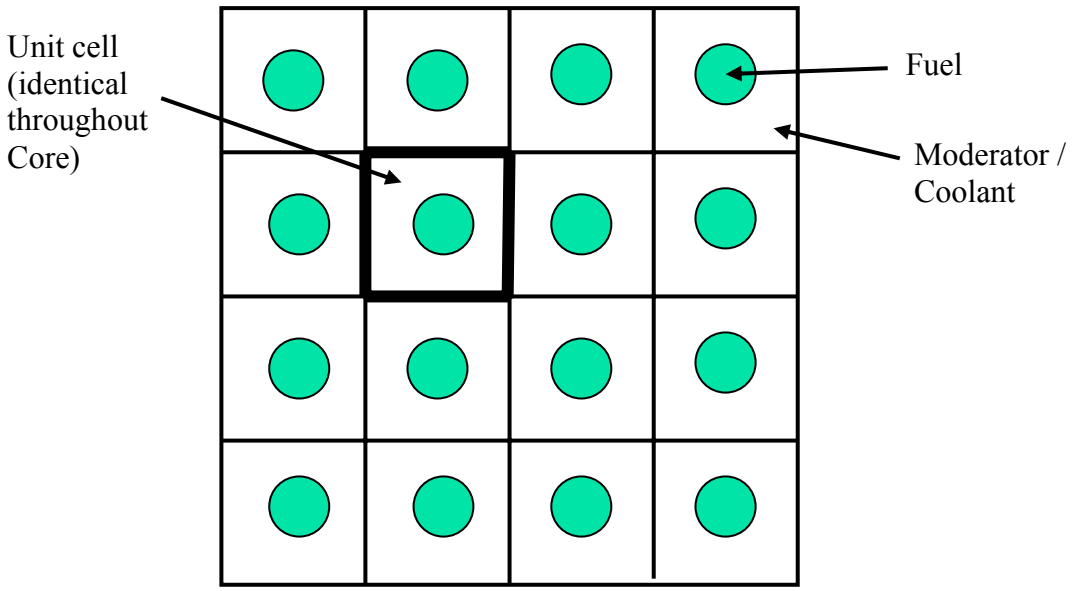

Figure 3.2- 1: Current Reactor Unit Cell Model

In the above current case, the spatial distribution of the neutron flux in the reactor has a periodic structure which can be found by computing the flux within a unit cell. Currently, collision probability theory is used to solve neutron transport equation to obtain fluxes in a unit cell for a moderator/coolant and fuel regions by decoupling the spatial and energy effects using the region to region transmission probabilities Π_0 and Π_1. Similar to

problem 1, fluxes are taken to be uniform in each of the two regions in the cell. In this case, it is noted that all unit cells within the reactor core are similar and hence the net neutron leakage across the outer boundary of each unit cell is zero. These methods are sometimes synthesized with relatively simple whole-core calculations where the lattice structure is homogenized. Such calculations can provide the flux profile throughout the reactor; the flux in each unit cell that comprises the reactor is assumed to follow the profile determined by the collision probability calculations but with magnitude set by the whole-core calculation.

This approach suffers when the composition of individual unit cells is sufficiently diverse that a homogenized whole-core calculation would be in significant error. For instance, there are several Department of Energy proposals to use weapons grade plutonium in the form of Mixed Oxide Fuel (MOX) within power reactors where the fuel is generally Uranium Oxide (UOX). The burning of MOX fuel has already been a reality in Europe for decades, as described in Reference [11]; MOX fabricated from weapons-grade plutonium is an extreme case, though, since very sharp local gradients in the neutron flux are possible with fuel of such high fissile content. Collision probability theory as developed for the identical unit cells will not be adequate for the cases such fuel is burned inside the reactor in addition to UOX fuel. This is due to the fact that zero neutron leakage assumption across the unit cell's outer boundary will not hold true any longer. This dissertation develops a methodology to solve the flux equations as derived in equations 3.1-8 and 3.1-9 by developing equivalent Π_0 and Π_1 for each of the cells

containing UOX and MOX fuels within the supercell as depicted in Figure 3.2-2. The fidelity of this modeling will then be evaluated by comparing the results to benchmark problem as identified in Reference [18]. Since the main interest of this problem is the study of the plutonium burning within a reactor core, the isotope inventory calculations for the transmuter pin will be of main interest in our benchmarking process.

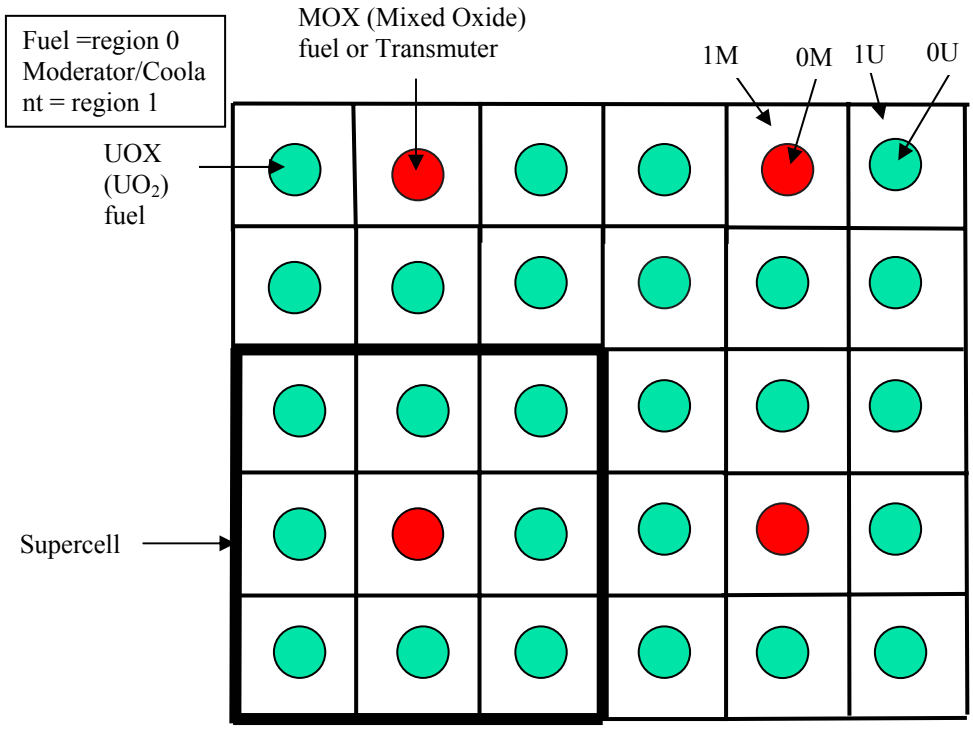

Figure 3.2- 2: Reactor Supercell Model Containing UOX and MOX Cells

3.2.2 Background/Introduction

Currently, collision probability theory is used to solve the decoupled energy and spatial fluxes in the fuel and moderator/coolant regions for the unit cell within a heterogeneous reactor core with one type of fuel. Each unit cell is assumed to consist of a lumped fuel region and moderator/coolant region that surrounds the fuel. The unit cells are all identical such that neutron leakage across the outer boundary of the unit cell is zero. This assumption is a valid one especially for large cores and the unit cells away from core boundaries.

There are a number of cases arising in advanced reactor and fuel cycle studies where strongly dissimilar unit cells exist in close proximity. In this case, substantial net leakage exists between the unit cells. Hence, the assumption of zero net neutron leakage across outer boundaries of the unit cells will not deliver reasonably accurate fluxes in the fuel and moderator/coolant regions. Therefore we can not get accurate flux distributions by solving the energy and spatially decoupled transport equations independently for each unit cell with different fuel regions. The solution presented here is designed to address the issue of net neutron leakage across the unit cell boundaries and provide a means where collision probability theory can be used to solve for the fluxes in different regions.

This approach has many practical applications that include: (1) study of burning PuO_2 fuel in power reactors that use UO_2 as their main fuel source in an attempt to dispose

weapon grade plutonium, (2) the use of uranium-free 'inert matrix' fuel consisting of recycled transuranics embedded in a (typically ZrO_2 based) matrix. and (3) study of using future reactors, especially fast-spectrum systems in which target or breeding fuel pins may be mixed with the driver lattice, in further processing of spent fuel for the purpose of burning the long half life actinides and heat generating fission products. The increased fidelity obtained from burnup calculations performed using the proposed methodology benefits (1) studies for increasing the storage capacity of spent fuel per cask for the purpose of long term storage in storage facilities such as Yucca Mountain and (2) nuclear non-proliferation studies on spent reactor fuel.

3.2.3 Developed Definitions for Solving Complex Problem Number 2

The methodology uses a collision probability theory with modified transmission and escape probabilities for each uniform region of a UOX and a MOX cell. The UOX and MOX notation is retained for convenience, but of course the approach applies to any two unit cell types within a reactor. The cells include four uniform flux regions: moderator/coolant for the two fuel types (UOX and MOX) and the two fuel regions. In the subject problem, the reactor core is taken to consist of a uniform cluster of 9 cells (supercell) as shown in Figure 3.2-2 (infinite cylindrical fuel pins) although the method generalizes to any periodic supercell configuration.

First, we define the following transmission and escape probabilities and then we identify and/or develop mathematical expressions for the defined terms.

Transmission probabilities in the four regions as depicted in Figure 3.2-2 are notated $T_{0M}, T_{1M}, T_{0U},$ and T_{1U}. Escape probabilities in the four regions are shown as $P_{0M}, P_{1M}, P_{0U},$ and P_{1U}.

We define each of the above parameters as follows;

T_{0M} = Probability that a neutron entering MOX fuel region is transmitted without interaction.

T_{1M} = Probability that a neutron entering moderator/coolant in a cell with MOX fuel is transmitted without interaction.

T_{0U} and T_{1U} are defined similarly for UOX type fuel.

P_{0M} = Probability that a neutron having had its last interaction in the MOX fuel, will escape the fuel without further interaction.

P_{1M} = Probability that a neutron, having had its last interaction in moderator/coolant of a cell with MOX fuel, will escape the moderator/coolant without further interaction.

P_{0U} and P_{1U} are defined similarly for UOX type fuel.

At any given neutron energy, P_{1M} and P_{1U} (the probabilities that neutrons born in the moderator surrounding the MOX and UOX, respectively, will escape the moderator region without interaction) are equal, and also T_{1M} and T_{1U} are equal. This is because the moderator surrounding the MOX and UOX is composed of the same material, typically the reactor coolant fluid.

$P_{1M} = P_{1U}$ (from now on called $P_1 = P_{1M} = P_{1U}$) (Eqn: 3.2-1)

$T_{1M} = T_{1U}$ (from now on called $T_1 = T_{1M} = T_{1U}$) (Eqn: 3.2-2)

Second, we introduce the following probabilities;

Π_{0i} = probability that a neutron appearing in fuel region of fuel type i (i=UOX or i=MOX) at energy E undergoes its next interaction in moderator/coolant region of that cell.

Π_{1i} = probability that a neutron appearing in moderator/coolant region of a cell with fuel type of i (i=UOX or i=MOX) at energy E undergoes its next interaction in fuel region of that cell.

Based on these definitions, we develop expressions for Π_{0i} and Π_{1i} in the following sections.

3.2.4 Methodology for Derivation of Π_{0U}

Figure 3.2-2 is used to derive the escape probabilities Π_{0U}, Π_{1U}, Π_{0M}, and Π_{1M} in accordance with the definitions as described in section 3.2.3. We will derive the subject escape probabilities within a supercell in a general manner by assuming that each supercell consists of N_U UOX fuel pins and N_M MOX fuel pins. In this case, the supercell will contain a total of $N_T = N_U + N_M$ sub-cells. The following derivations will be based on two assumptions that there is zero net neutron leakage across the boundaries of the supercell and that a neutron leaving a cell with UOX fuel pin has a $\frac{N_U}{N_T}$ chance to arrive at a UOX cell and a $\frac{N_M}{N_T}$ chance to arrive at a MOX cell. The second assumption in regards to the probability distribution is consistent with the first assumption since $\frac{N_U}{N_T} + \frac{N_M}{N_T} = 1$. It is noted that the probability distribution assumption varies from the strict definitions since a neutron that leaves a UOX fuel pin has $\frac{N_U - 1}{N_T - 1}$ chance to arrive to another UOX cell and $\frac{N_M}{N_T - 1}$ chance to arrive at the MOX cell within the supercell.

However, our simplifying assumption for neutron distribution probabilities does not factor in the exact location of the UOX and MOX cells within the supercell and assigns equal weighing to all of the UOX and MOX cells. Therefore the probability distributions are not geometry sensitive and the consideration that any neutron entering the supercell has a chance to enter a UOX or MOX cell based on the number of UOX or MOX cells within the supercell, we choose to use the $\frac{N_U}{N_T}$ and $\frac{N_M}{N_T}$ distribution but we note that this is not the only valid choice for the escape probabilities. The adequacy of this assumption and overall methodology will be assessed through the benchmarking process.

The definition and notation for transmission and escape probabilities are the same as those as defined in the statement of the problem.

$$\begin{aligned}\Pi_{0U} = {} & P_{0U}\left(1-T_{1U}\right)+P_{0U}T_{1U}\frac{N_U}{N_T}T_{0U}\left(1-T_{1U}\right)+P_{0U}T_{1U}\frac{N_M}{N_T}T_{0M}T_{0U}\left(1-T_{1U}\right)\\ & +P_{0U}T_{1U}\frac{N_U}{N_T}T_{0U}T_{1U}\frac{N_U}{N_T}T_{0U}\left(1-T_{1U}\right)+P_{0U}T_{1U}\frac{N_U}{N_T}T_{0U}T_{1U}\frac{N_M}{N_T}T_{0M}T_{0U}\left(1-T_{1U}\right)\\ & +P_{0U}T_{1U}\frac{N_M}{N_T}T_{0M}T_{0U}T_{1U}\frac{N_U}{N_T}T_{0U}\left(1-T_{1U}\right)\\ & +P_{0U}T_{1U}\frac{N_M}{N_T}T_{0M}T_{0U}T_{1U}\frac{N_M}{N_T}T_{0M}T_{0U}\left(1-T_{1U}\right)+\ldots\end{aligned}$$

(Eqn: 3.2-3)

Equation 3.2-3 can be rearranged in order to visualize the patterns of similar terms for any further simplification.

$$\Pi_{0U} = P_{0U}\left(1-T_{1U}\right)\left\{\begin{array}{l}\left[1+\left(T_{1U}\frac{N_U}{N_T}T_{0U}\right)+\left(T_{1U}\frac{N_U}{N_T}T_{0U}\right)^2+\left(T_{1U}\frac{N_U}{N_T}T_{0U}\right)^3+\ldots\right]+\\ \left[\left(T_{1U}T_{0U}\right)\left(\frac{N_M}{N_T}T_{0M}\right)+\left(T_{1U}T_{0U}\right)^2\left(\frac{N_M}{N_T}T_{0M}\right)^2+\left(T_{1U}T_{0U}\right)^3\left(\frac{N_M}{N_T}T_{0M}\right)^3+\ldots\right]+\\ \left[\begin{array}{l}2\left(T_{1U}\frac{N_U}{N_T}T_{0U}\right)\left(T_{1U}T_{0U}\right)\left(\frac{N_M}{N_T}T_{0M}\right)+\\ 3\left(T_{1U}\frac{N_U}{N_T}T_{0U}\right)\left(T_{1U}T_{0U}\right)^2\left(\frac{N_M}{N_T}T_{0M}\right)^2+\\ 4\left(T_{1U}\frac{N_U}{N_T}T_{0U}\right)\left(T_{1U}T_{0U}\right)^3\left(\frac{N_M}{N_T}T_{0M}\right)^3+\ldots\end{array}\right]+\\ \left[\begin{array}{l}3\left(T_{1U}\frac{N_U}{N_T}T_{0U}\right)^2\left(T_{1U}T_{0U}\right)\left(\frac{N_M}{N_T}T_{0M}\right)+\\ 6\left(T_{1U}\frac{N_U}{N_T}T_{0U}\right)^2\left(T_{1U}T_{0U}\right)^2\left(\frac{N_M}{N_T}T_{0M}\right)^2+\\ 10\left(T_{1U}\frac{N_U}{N_T}T_{0U}\right)^2\left(T_{1U}T_{0U}\right)^3\left(\frac{N_M}{N_T}T_{0M}\right)^3+\ldots\end{array}\right]+\\ \left[\begin{array}{l}4\left(T_{1U}\frac{N_U}{N_T}T_{0U}\right)^3\left(T_{1U}T_{0U}\right)\left(\frac{N_M}{N_T}T_{0M}\right)+\\ 10\left(T_{1U}\frac{N_U}{N_T}T_{0U}\right)^3\left(T_{1U}T_{0U}\right)^2\left(\frac{N_M}{N_T}T_{0M}\right)^2+\ldots\end{array}\right]\end{array}\right\}$$

(Eqn: 3.2-4)

Equation 3.2-4 reveals similar term patterns that helps us to depict the subject equation in a much more compact form.

$$\Pi_{0U} = P_{0U}\left(1-T_{1U}\right)\left\{\begin{array}{l}\left[\sum_{i=0}^{\infty}\left(T_{1U}\frac{N_U}{N_T}T_{0U}\right)^i\right]+\\ \left[\left(T_{1U}T_{0U}\right)\left(\frac{N_M}{N_T}T_{0M}\right)\sum_{i=0}^{\infty}\left(T_{1U}T_{0U}\right)^i\left(\frac{N_M}{N_T}T_{0M}\right)^i\right]+\\ \left[\left(T_{1U}\frac{N_U}{N_T}T_{0U}\right)\sum_{i=1}^{\infty}(i+1)\left(T_{1U}T_{0U}\right)^i\left(\frac{N_M}{N_T}T_{0M}\right)^i\right]+\\ \left[\sum_{i=2}^{\infty}\left(T_{1U}\frac{N_U}{N_T}T_{0U}\right)^i\sum_{j=1}^{\infty}\left(ij+2^{(j-1)}\right)\left(T_{1U}T_{0U}\right)^j\left(\frac{N_M}{N_T}T_{0M}\right)^j\right]\end{array}\right\}$$

(Eqn: 3.2-5)

The first two terms inside the brackets of Equation 3.2-5 can be further simplified.

$$\Pi_{0U} = P_{0U}\left(1-T_{1U}\right)\left\{\begin{array}{l}\left[\frac{1}{1-T_{1U}\frac{N_U}{N_T}T_{0U}}\right]+\left[\frac{\left(T_{1U}T_{0U}\right)\left(\frac{N_M}{N_T}T_{0M}\right)}{1-\left(T_{1U}T_{0U}\right)\left(\frac{N_M}{N_T}T_{0M}\right)}\right]+\\ \left[\left(T_{1U}\frac{N_U}{N_T}T_{0U}\right)\sum_{i=1}^{\infty}(i+1)\left(T_{1U}T_{0U}\right)^i\left(\frac{N_M}{N_T}T_{0M}\right)^i\right]+\\ \left[\sum_{i=2}^{\infty}\left(T_{1U}\frac{N_U}{N_T}T_{0U}\right)^i\sum_{j=1}^{\infty}\left(ij+2^{(j-1)}\right)\left(T_{1U}T_{0U}\right)^j\left(\frac{N_M}{N_T}T_{0M}\right)^j\right]\end{array}\right\}$$

(Eqn: 3.2-6)

Equation 3.2-6 is the desired escape probability from UOX fuel. However, it can be noted that the contributions from the third, fourth and subsequent terms inside the brackets of Equation 3.2-6 are of higher order in the probabilities when compared to the first two terms of the subject bracket. For example, the first term inside the brackets of equation 3.2-6 is in the order of magnitude of 1. The second term is in the order of magnitude of third power of a representative transmission probability. The third term is in the order of fifth power of a representative transmission probability. Given a typical transmission probability, it can be easily deduced that the third term is considerably smaller than the second term. This will also be true for the fourth term inside the brackets of equation 3.2-6 which is in the order of seventh power of a representative transmission probability. Hence, the third, fourth and subsequent terms inside the brackets of equation 3.2-6 can be neglected at the cost of ignoring particle tracks that traverse multiple cells before colliding once again. This simplification is similar to the Wigner approximation [3, 5] as used in lattices with uniform unit cells with single fuel type. The simplification basically translates to considering the interactions of a neutron escaping from a given unit cell with immediate neighboring unit cells. After replacing T_{1U} with T_1, equation 3.2-6 is therefore reduced to:

$$\Pi_{0U} = P_{0U}\left(1-T_1\right)\left\{\left[\frac{1}{1-T_1\dfrac{N_U}{N_T}T_{0U}}\right]+\left[\frac{\left(T_1T_{0U}\right)\left(\dfrac{N_M}{N_T}T_{0M}\right)}{1-\left(T_1T_{0U}\right)\left(\dfrac{N_M}{N_T}T_{0M}\right)}\right]\right\} \qquad \text{(Eqn: 3.2-7)}$$

For demonstration purposes, we will compare the values of Π_{0U} calculated from equation 3.2-7 for several given values of Σ for MOX fuel (Σ_{MOX}) and T_1 value of 0.5 with Π_0 calculated from the original model as shown in equation 3.1-3. Π_{0U} and Π_0 are plotted versus $(\Sigma_{UOX} R_{UOX})$ values. The results are depicted in Figure 3.2-3.

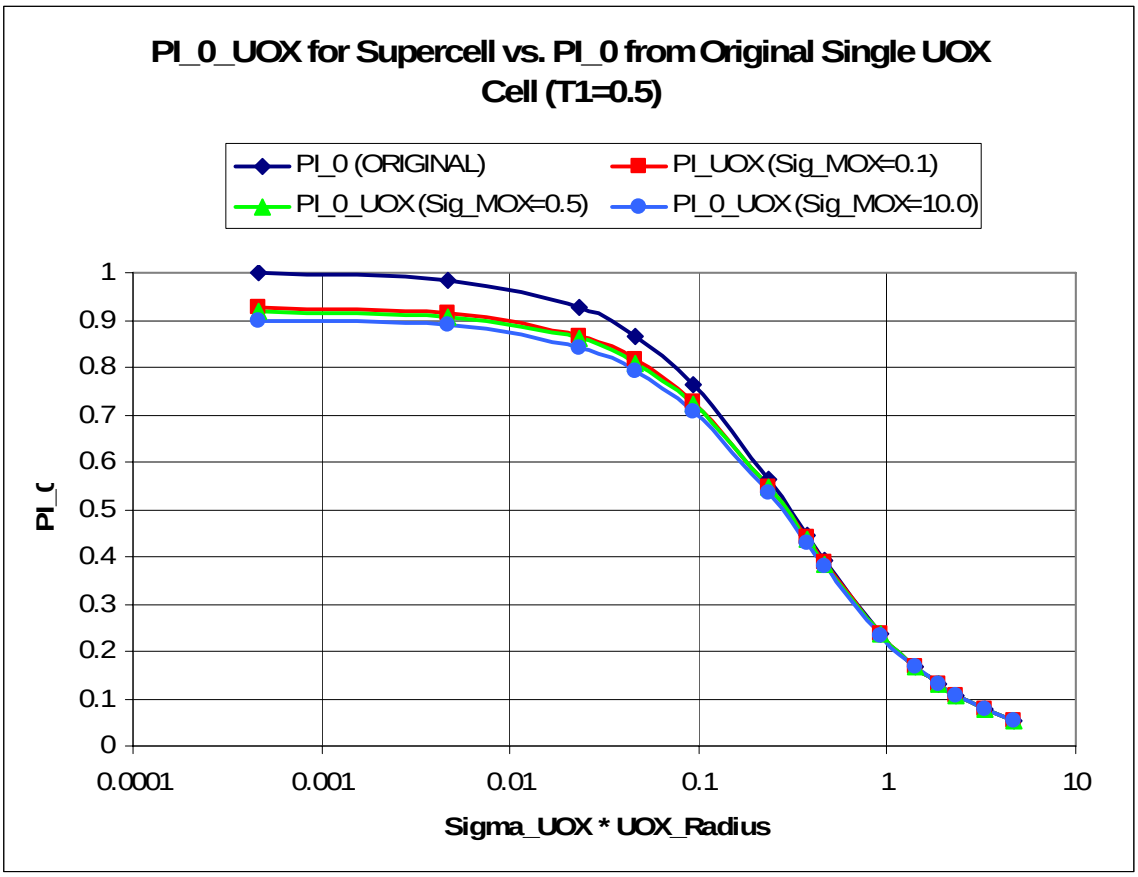

Figure 3.2- 3: Comparison of Escape Probabilities from UOX fuel within the Supercell based on Developed Methodology and the UOX fuel in a Single Cell from the Original Methodology for T_1=0.5

Examination of Figure 3.2-3 indicates that Π_{0U} is not very sensitive to (Σ_{MOX}) especially for values of above 0.1; the MOX pin becomes essentially black to neutrons as its cross section becomes large. Also, Π_{0U} values are always less than Π_0 from the single cell. This is a correct result since some of the neutrons that escape the UOX fuel have their next interaction in the MOX fuel within the supercell and hence there are less neutrons to interact with the moderator. For large values of $(\Sigma_{UOX} R_{UOX})$, the values of Π_{0U} and Π_0 approach each other which is another indication for the validity of the derived equation 3.2-7. This is due to the fact that at large $(\Sigma_{UOX} R_{UOX})$ values, fewer neutrons escape the UOX fuel and hence there are smaller numbers of neutrons available to interact with the moderator or the MOX fuel. Therefore, Figure 3.2-3 indicates the reasonableness of the derived equation 3.2-7.

Π_{0U} and Π_0 are also plotted based on similar parameters as those for Figure 3.2-3 except for T_1 value of 0.1 in order to observe the effects of T_1 on the escape probabilities. As can be seen from Figures 3.2-3 and 3.2-4, a decrease in transmission probability in the coolant/moderator results in an increase in the escape probabilities. This is in accordance with our expectation since with decrease in moderator/coolant transmission probability a higher number of neutrons will collide with the coolant/moderator.

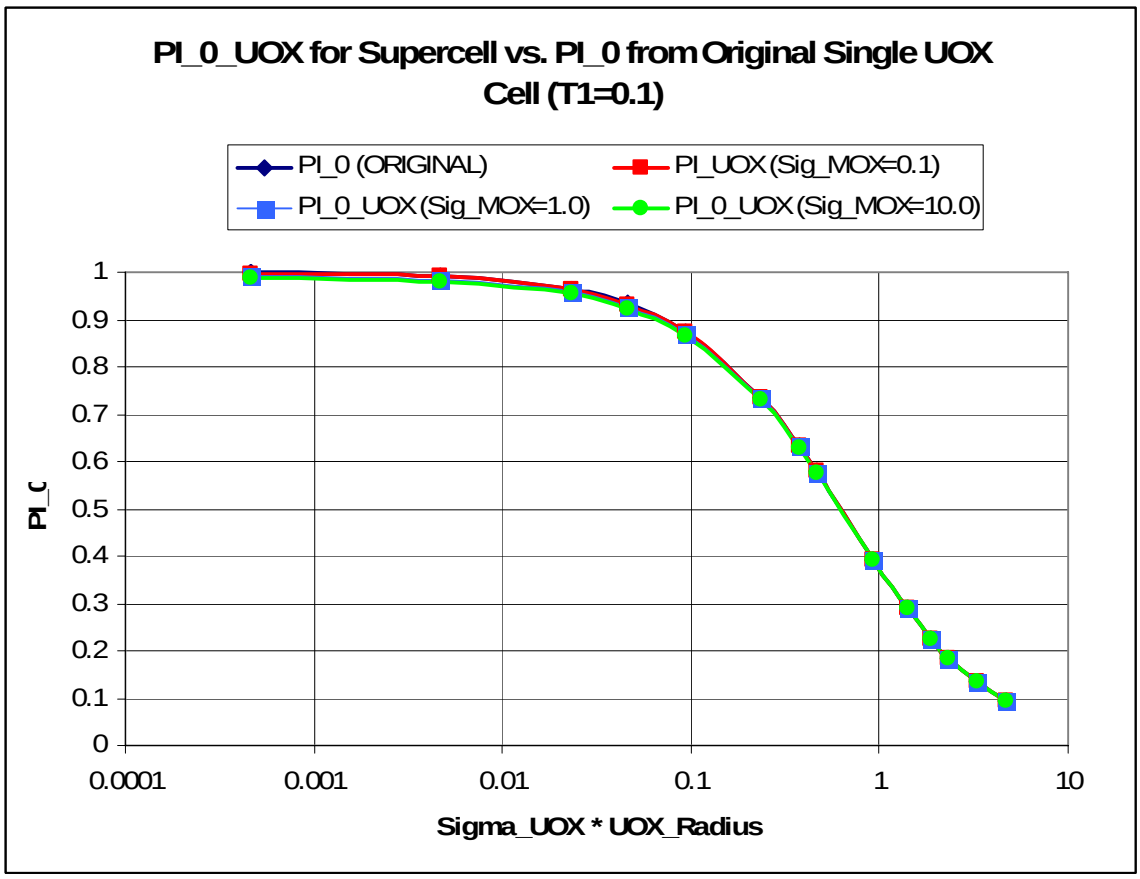

Figure 3.2- 4: Comparison of Escape Probabilities from UOX fuel within the Supercell based on Developed Methodology and the UOX fuel in a Single Cell from the Original Methodology for T_1=0.1

3.2.5 Methodology for Derivation of Π_{0M}

The methodology for derivation of Π_{0M} is the same as that for Π_{0U} and is not repeated here. The form of Π_{0M} is similar to Equation 3.2-7 and is depicted in Equation 3.2-8.

$$\Pi_{0M} = P_{0M}\left(1-T_1\right)\left\{\left[\frac{1}{1-T_1\frac{N_M}{N_T}T_{0M}}\right]+\left[\frac{\left(T_1T_{0M}\right)\left(\frac{N_U}{N_T}T_{0U}\right)}{1-\left(T_1T_{0M}\right)\left(\frac{N_U}{N_T}T_{0U}\right)}\right]\right\} \qquad \text{(Eqn: 3.2-8)}$$

Again, for demonstration purposes, we will compare the values of Π_{0M} calculated from equation 3.2-8 for several given values of Σ for UOX fuel $\left(\Sigma_{UOX}\right)$ and T_1 value of 0.5 with Π_0 calculated from the original model as shown in equation 3.1-3. Π_{0M} and Π_0 are plotted versus $\left(\Sigma_{MOX}R_{MOX}\right)$values. The results are depicted in Figure 3.2-5.

Comparison of Figures 3.2-3 and 3.2-5 reveals the differences between the escape probabilities from UOX and MOX fuels due to the difference in the number of these fuels within the supercell. This difference is more pronounced for the larger $\left(\Sigma_{UOX}R_{UOX}\right)$ values and smaller $\left(\Sigma_{MOX}R_{MOX}\right)$ values.

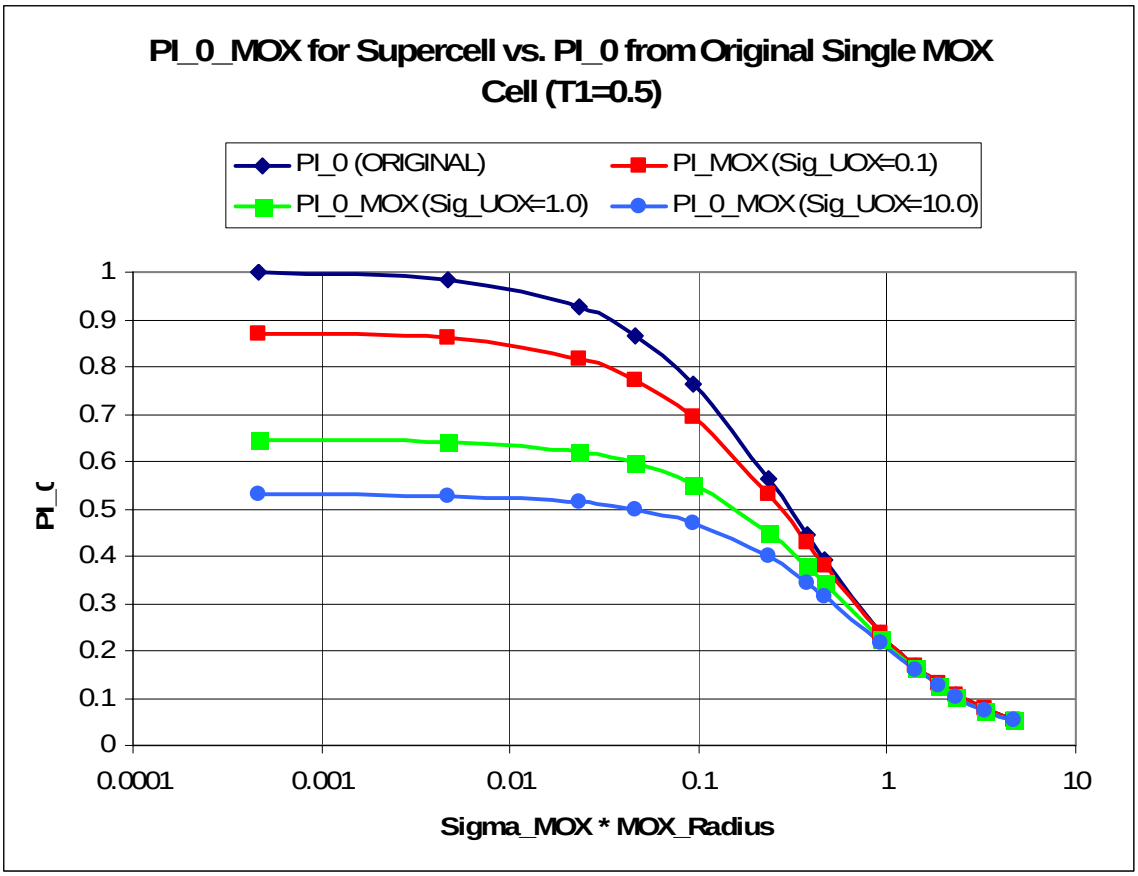

Figure 3.2- 5: Comparison of Escape Probabilities from MOX fuel within the Supercell based on Developed Methodology and the MOX fuel in a Single Cell from the Original Methodology for T_1=0.5

3.2.6 Derivation of P_{0U}, T_{0U}, P_{0M} and T_{0M}

The subject escape and transmission probabilities for infinite cylinders have been derived in several references such as [9], [10] and [36] and are discussed within the statement of

Problem 1 of this dissertation. Hence we will just present the results for these terms from reference [10].

$$P_{0U} \approx \frac{1+\left(c+\frac{2}{3}\right)\left(\Sigma_U R_U\right)+\frac{8}{3}c\left(\Sigma_U R_U\right)^2}{1+\left(c+2\right)\left(\Sigma_U R_U\right)+\left(2c+\frac{4}{3}\right)\left(\Sigma_U R_U\right)^2+\frac{16}{3}c\left(\Sigma_U R_U\right)^3} \qquad \text{(Eqn: 3.2-9)}$$

$$T_{0U} = 1-\left(\Sigma_U R_U\right)P_{0U} \qquad \text{(Eqn: 3.2-10)}$$

In Equations 3.2-9 and 3.2-10, Σ_U is the UOX fuel total macroscopic interaction cross section, and R_U is the radius of UOX fuel. Equations 3.2-9 and 3.2-10 are also valid for the MOX fuel when the properties and dimensions of MOX fuel are used. Value of c is taken to be 0.3567 from reference [10]. Note that Equation 3.2-9 constitutes a rational approximation to the true escape probability. The rational approximation preserves the limiting behavior as $\left(\Sigma_{UOX} R_{UOX}\right)$ approaches zero and infinity, but it requires many fewer floating point operations to compute than do the modified Bessel functions in the analytic expression for P_{0U} .

Examination of equation 3.2-9 indicates that transmission probability through a fuel rod is a function of $\left(\Sigma R\right)$ for that fuel. The term Σ is then a function of the fuel burnup and the energy of the neutron traversing the fuel. Consequently, $T_{0U}, T_{0M}, P_{0U}, P_{0M}$ and hence

Π_{0U} and Π_{0M} are functions of the fuel burnup and neutron energy level. The V:BUDS algorithm calculates the escape probability Π_0 for an energy group at a given burnup for a given fuel type. In order to code equation 3.2-7 into V:BUDS in order to get the desired fuel isotopic content for UOX fuel, we need to supply V:BUDS with values of T_{0M} for all the energy groups at a given burnup value so the proper values of Π_{0U} can be calculated at energy group and burnup value. To accomplish this purpose, the MOX cell is modeled in the V:BUDS and it is run for a given burnup value. The escape probability T_{0M} for each energy group and burnup value is written into a text file. Then the UOX cell is modeled in V:BUDS with the above text file included and the code is run. The result of the run determines the isotopic content of the UOX fuel as well as the T_{0U} needed for a second iteration of the MOX fuel simulation. This T_{0U} is written to a text file and the same procedure is used to obtain the isotopic contents for the MOX fuel.

The accuracy and validity of our modeling can be judged based on the comparison with benchmark values as included in section 3.2-7.

3.2.7 Selection of Benchmarking Problem

Our literature survey indicated that Reference [18] included results from neutronic analysis of several supercell configurations that are directly applicable to the scope of our problem. Reference [18] provided the results on the isotopic inventory of a transmuter

(MOX) pin that is located in the center of a nine pin supercell as well as the isotopic inventory of the UOX pins in terms of the fuel burnup. The supercell and its parameters from Reference [18] are included in Figure 3.2-3 and Tables 3.2-1 and 3.2-2. We will use these specifications for benchmarking purposes and compare the results from our work against the results from Reference [18] in order to verify the adequacy of our model.

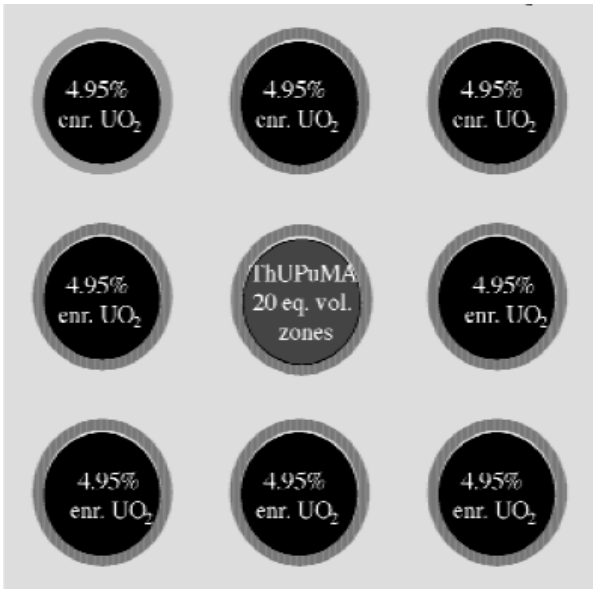

Figure 3.2- 6: Nine Pin Supercell Model For Benchmarking [Ref. 18]

Table 3.2- 1: Benchmark Problem Fuel Parameters [18]

Fuel Parameter
Fuel pin radius = 0.4096 cm
Pellet height = 1.5 cm (not relevant)
Pin pitch = 1.27 cm
Densities: ThO_2 : 10.0 g/cm^3 UO_2 : 11.0 g/cm^3 [Pu-MA]O_2 : 12.0 g/cm^3 ZrO_2 : 5.39 g/cm^3 The overall density for transmuter pin is a linear combination of the atomic fractions of the constituents.

Table 3.2- 2: Contents of UO_2 and Th-U-Pu-MA pins in the Benchmark Problem [18]

Pin in the Supercell	Initial Isotopic Inventory
UO_2 fuel pin	^{235}U 4.95 % ^{238}U 95.05 %
Th-U-Pu-MA transmuter pin	Th = 82 wt%, U = 12 wt%, Pu-MA = 6 wt% Isotopic contents of U are; ^{234}U 0.027% ^{235}U 0.908% ^{236}U 0.578% ^{238}U 98.487% Isotopic contents of Pu-MA are; ^{237}Np 6.03% ^{238}Pu 1.77% ^{239}Pu 49.0% ^{240}Pu 21.71% ^{241}Pu 3.29% ^{242}Pu 5.90% ^{241}Am 10.79% ^{243}Am 1.32%

3.2.8 Results of the Developed Methodology and Comparison to the Benchmark

Now, we can obtain the isotopic inventory of the UOX and MOX fuels for a given burnup using the developed methodology. The results are plotted in Figures 3.2-7 through 3.2-15.

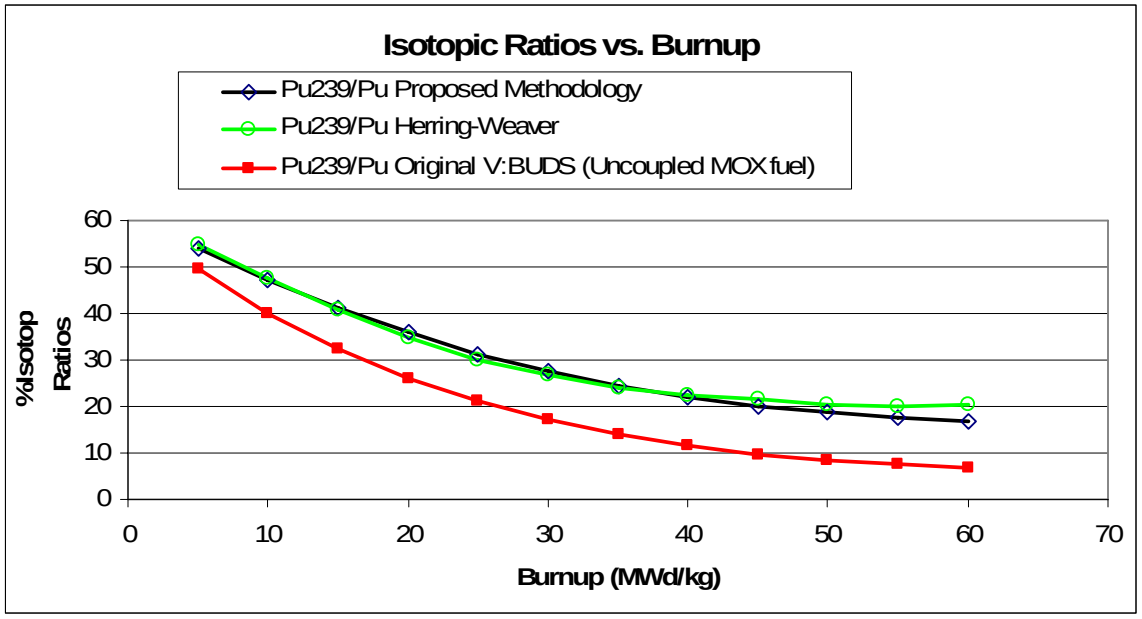

Figure 3.2- 7: Ratio of ^{239}Pu masses to the total plutonium mass versus burnup in the transmuter pin

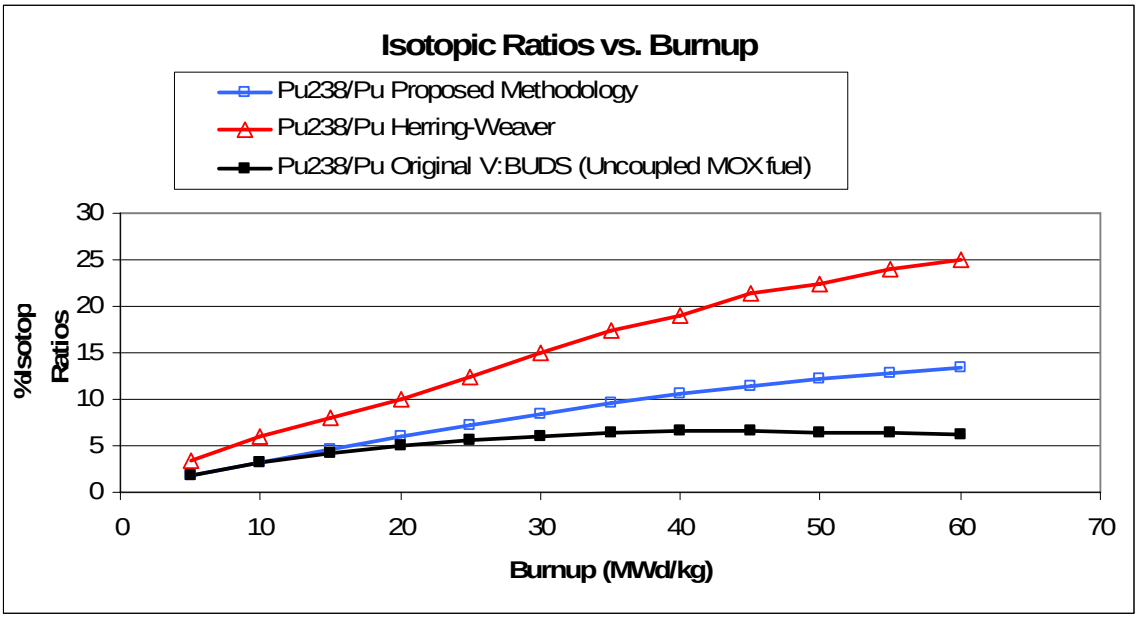

Figure 3.2- 8: Ratio of ^{238}Pu masses to the total plutonium mass versus burnup in the transmuter pin

Figures 3.2-7 and 3.2-8 show the ratio of the mass of ^{239}Pu and ^{238}Pu to the total mass of the plutonium in the transmuter pin verses the fuel burnup. The same ratios from the benchmark problem [18] are also depicted. Evaluation of these results indicates an excellent agreement between our methodology and the benchmark for ^{239}Pu isotope ratio. The agreement is also good for ^{238}Pu for low burnup values. The deviation for ^{238}Pu ratio from the benchmark value gradually increases with increased fuel burnup. Studies of other references such as [16] indicate that V:BUDS provides good agreements for generation of ^{238}Pu and ^{243}Am for the MOX fuel burnup when compared to other sophisticated and validated codes such as Monteburn. Hence we deduce that our model can also produce good results for ^{238}Pu and ^{243}Am when compared to other benchmark computer codes. As can be deduced from the theory of burning the transmuter pin, the

^{239}Pu is destroyed during the process and ^{238}Pu is generated which are both beneficial from the non-proliferation stand point. Both ^{239}Pu and ^{238}Pu ratios as shown in Figures 3.2-7 and 3.2-8 depict this behavior which validates the theory of our modeling concept. In addition, Figures 3.2-7 and 3.2-8 depict the ^{239}Pu and ^{238}Pu isotopic ratio to the total plutonium content of the fuel for the same MOX fuel and parameters using the original V:BUDS code. In this case, the subject MOX fuel is not neutronically coupled to the other fuel type within the supercell. We performed this exercise in order to get an insight to the effects of neutronic coupling between the MOX and UOX fuels on the amount of plutonium contents of the fuel. Figures 3.2-7 and 3.2-8 indicate that the results from neutronically uncoupled MOX fuel deviates drastically from the benchmark values and hence it does not accurately calculate the plutonium content ratios. We also show the results from the neutronically uncoupled MOX fuel using the original V:BUDS code in the following Figures in order to gain further understanding of isotopic inventory within a transmuter pin for several burnup conditions.

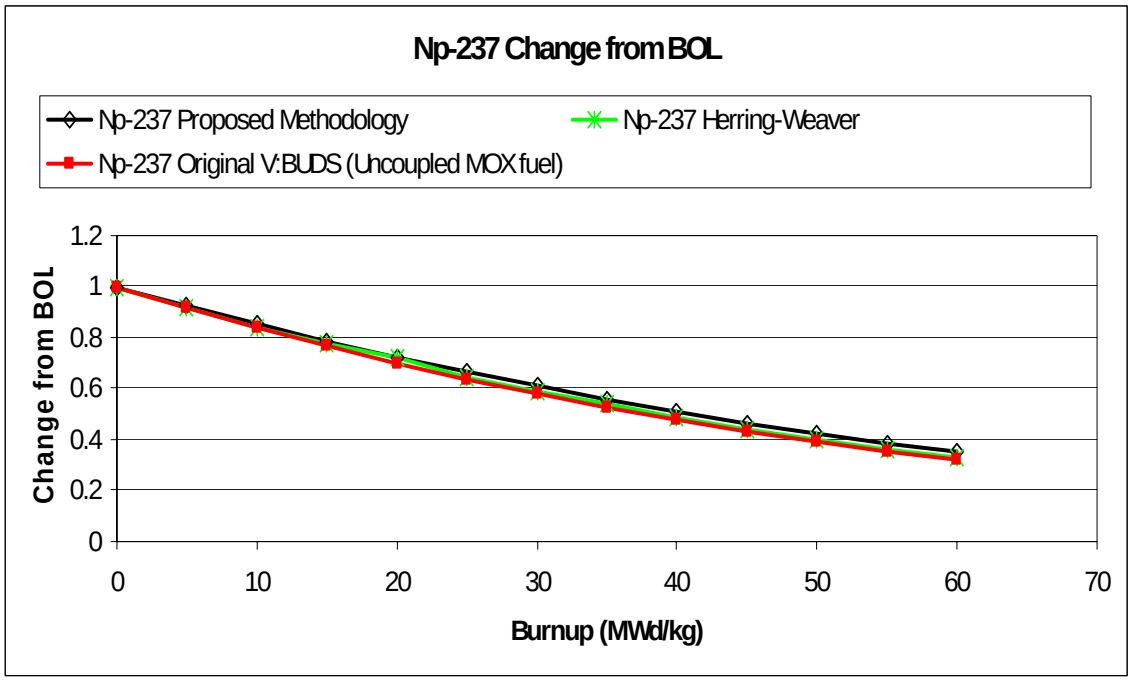

Figure 3.2- 9: Ratio of mass of ^{237}Np to its initial mass in the transmuter pin versus fuel burnup

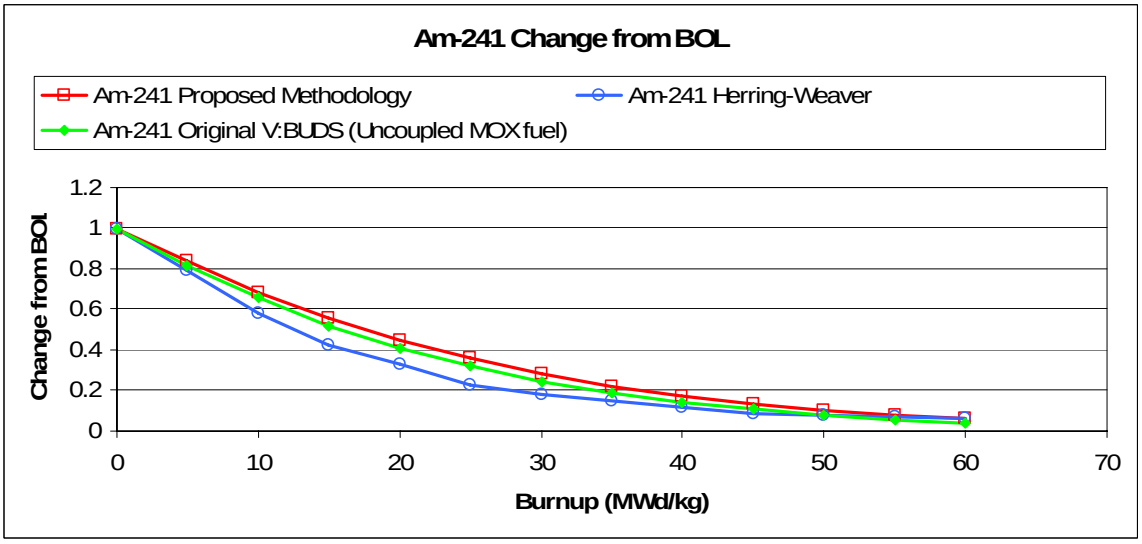

Figure 3.2- 10: Ratio of mass of ^{241}Am to its initial mass in the transmuter pin versus fuel burnup

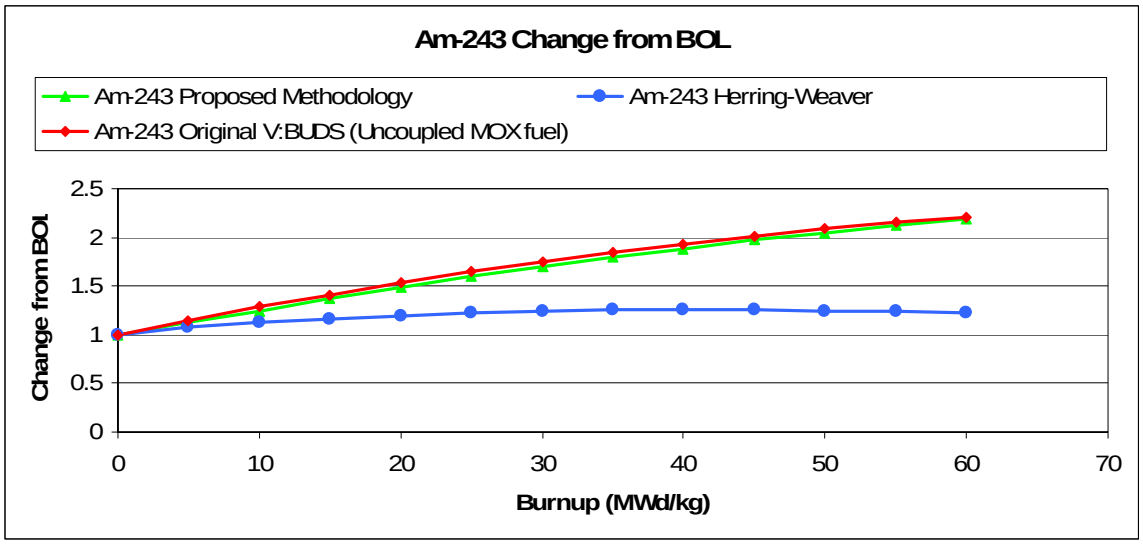

Figure 3.2- 11: Ratio of mass of ^{243}Am to its initial mass in the transmuter pin versus fuel burnup

Figures 3.2-9 and 3.2-10 show the ratio of mass of ^{237}Np and ^{241}Am to their values prior to initiation of the burnup versus the burnup. These plots represent the mass inventory of the subject isotopes in the transmuter pin versus burnup. Again, there is a good agreement between our model and the benchmark values. This agreement is especially very good for ^{237}Np and ^{241}Am. Again, the behavior of the subject isotope ratios indicates the validity of our supercell modeling concept. It is noted that the subject isotopic ratios derived from our work and the ratios derived from the neutronically uncoupled MOX fuel are very close due to the fact that these are not absolute masses of the isotopes but are the ratios of the isotopes at a given burnup and its original mass and hence the neutronic coupling is not a factor in determination of these ratios. As discussed previously, the results for ^{243}Am as shown in Figure 3.2-11 deviates from the benchmark problem at higher burnup

values, however, our model provides a good agreement when compared to other benchmark problem for ^{243}Am [16].

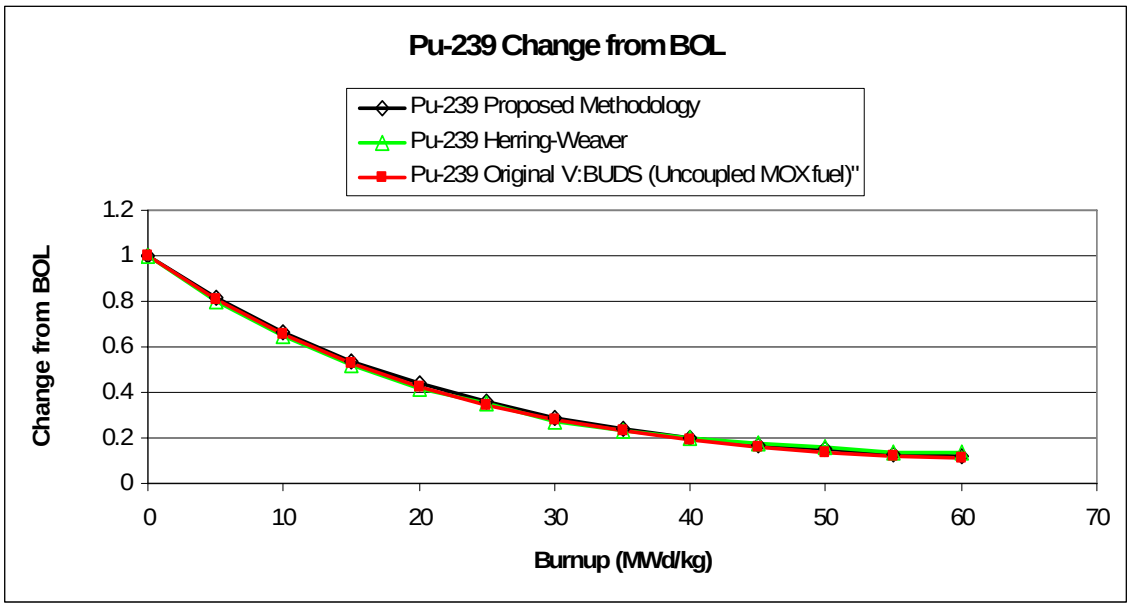

Figure 3.2- 12: Ratio of mass of ^{239}Pu to its initial mass in the transmuter pin versus fuel burnup

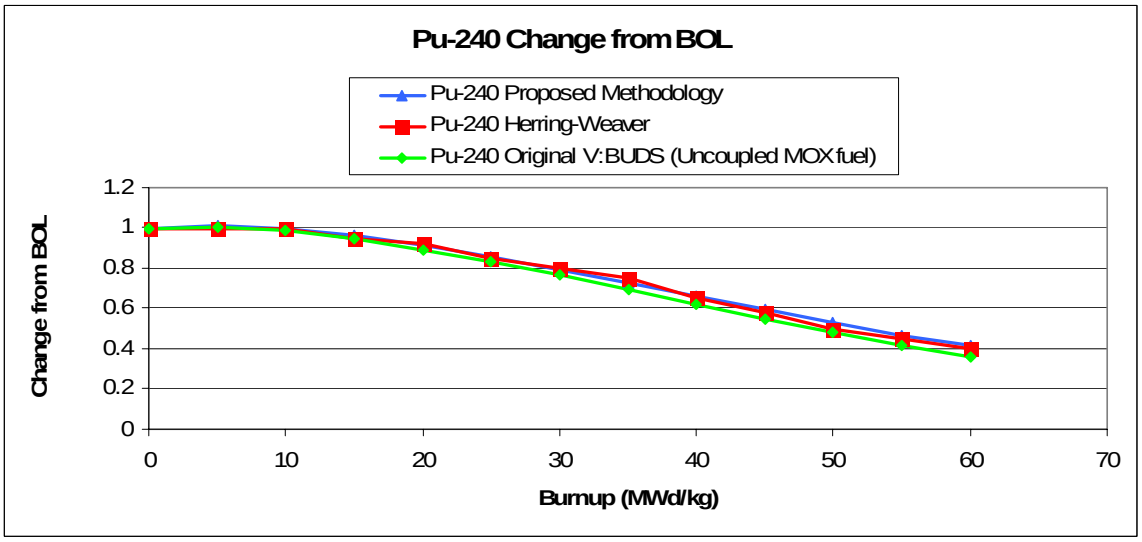

Figure 3.2- 13: Ratio of mass of ^{240}Pu to its initial mass in the transmuter pin versus fuel burnup

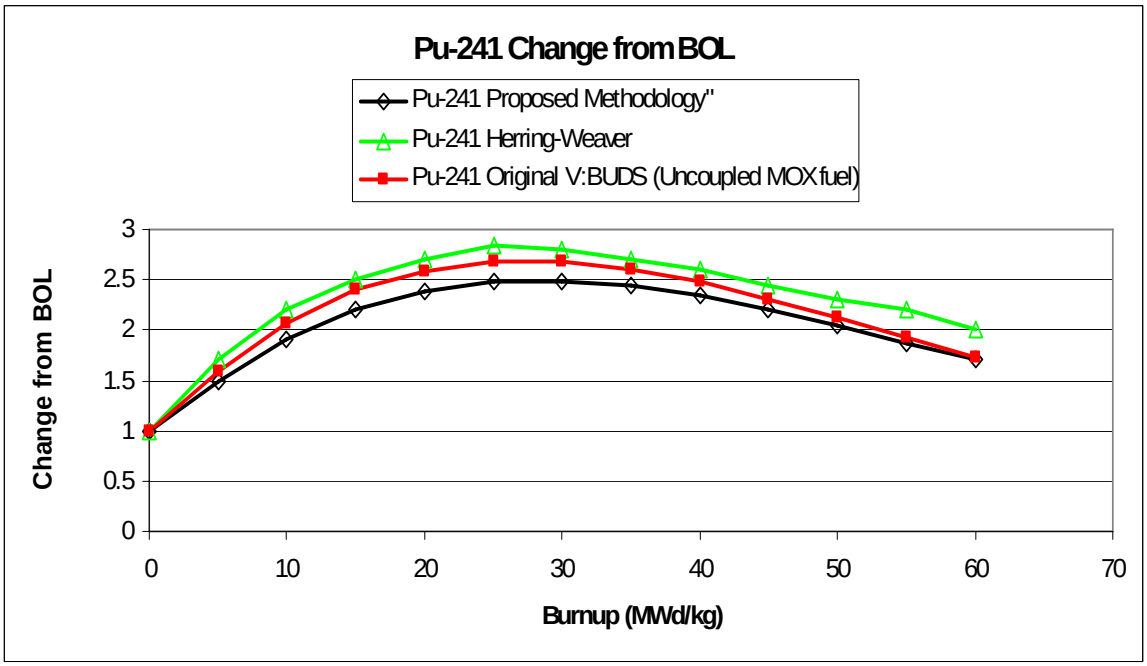

Figure 3.2- 14: Ratio of mass of ^{241}Pu to its initial mass in the transmuter pin versus fuel burnup

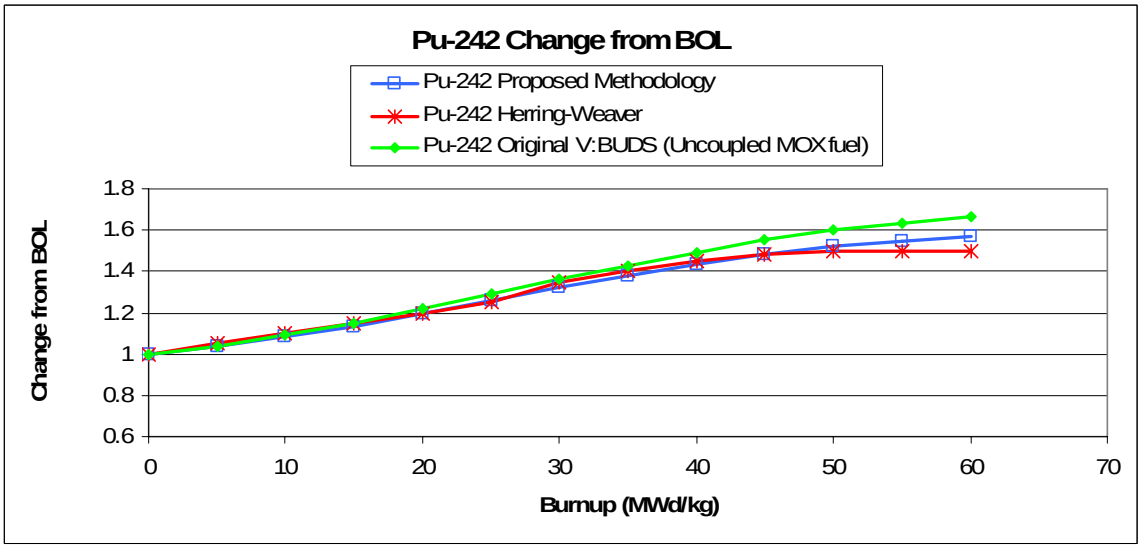

Figure 3.2- 15: Ratio of mass of ^{242}Pu to its initial mass in the transmuter pin versus fuel burnup

Figures 3.2-12 through 3.2-15 also show the ratio of mass of ^{239}Pu, ^{240}Pu, ^{241}Pu, and ^{242}Pu to their values prior to initiation of the burnup versus the burnup. These plots represent the mass inventory of the subject isotopes in the transmuter pin versus burnup. Our model represents an excellent agreement with the benchmark values for the subject isotopes.

Now we will turn our attention to the UO_2 fuel cells and compare the results to the benchmark problem.

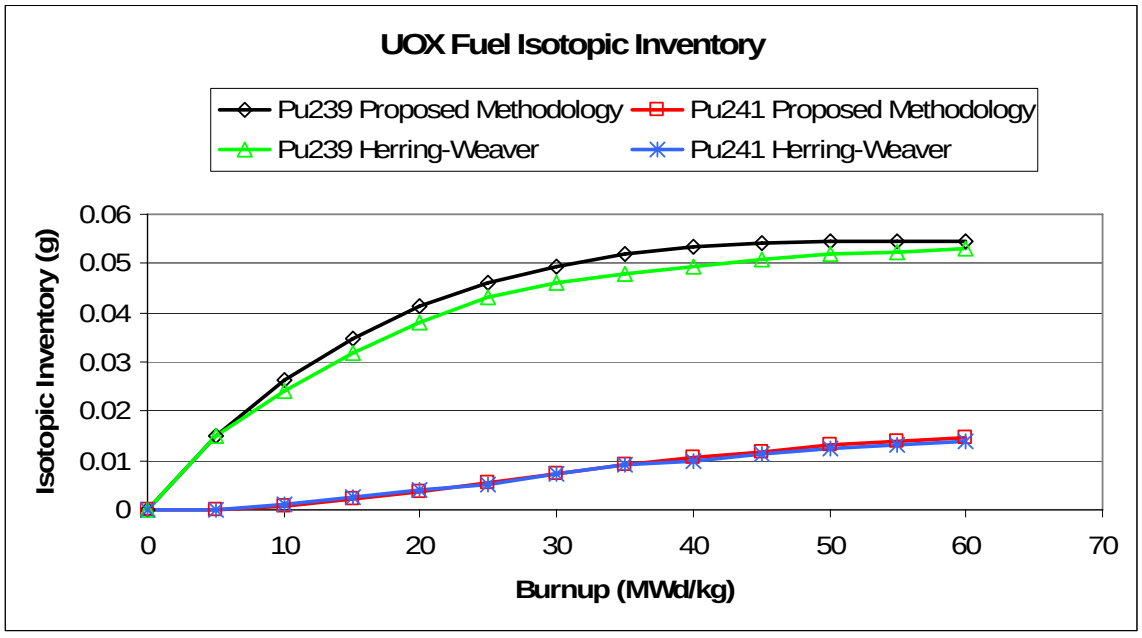

Figure 3.2- 16: Mass of ^{239}Pu and ^{241}Pu in the UO_2 fuel versus fuel burnup

Figure 3.2-16 depicts the mass of ^{239}Pu and ^{241}Pu in the UO_2 fuel pins versus the burnup. The calculated values using our methodology and model closely corresponds with the benchmark problem values.

As a last step for this problem, we will attempt to observe any differences in neutron energy spectra for a fuel pin between a case when it is neutronically coupled with fuel pin of a different type and a case when the fuel pin has no net neutronic coupling with any other fuel pin, i.e., all of the unit cells contain the same fuel type. The parameters of the benchmark problem [30] with fresh fuel conditions will be used for this demonstration. For this purpose, we will obtain the neutron energy spectra for the MOX and UOX using the original V:BUDS code and a single unit cell parameters. These will represent the uncoupled neutron energy spectra. Then, we will use the developed methodology with problem two and plot the neutron energy spectra for the MOX and UOX fuel pins using the unit cell parameters from the benchmark. This will represent the coupled neutron energy spectra for each of the fuel types. The coupled and uncoupled neutron energy spectra for each fuel type are then superimposed in order to reveal the differences in the spectra due to the neutronic coupling effects. The results are depicted in Figures 3.2-17 and 3.2-18.

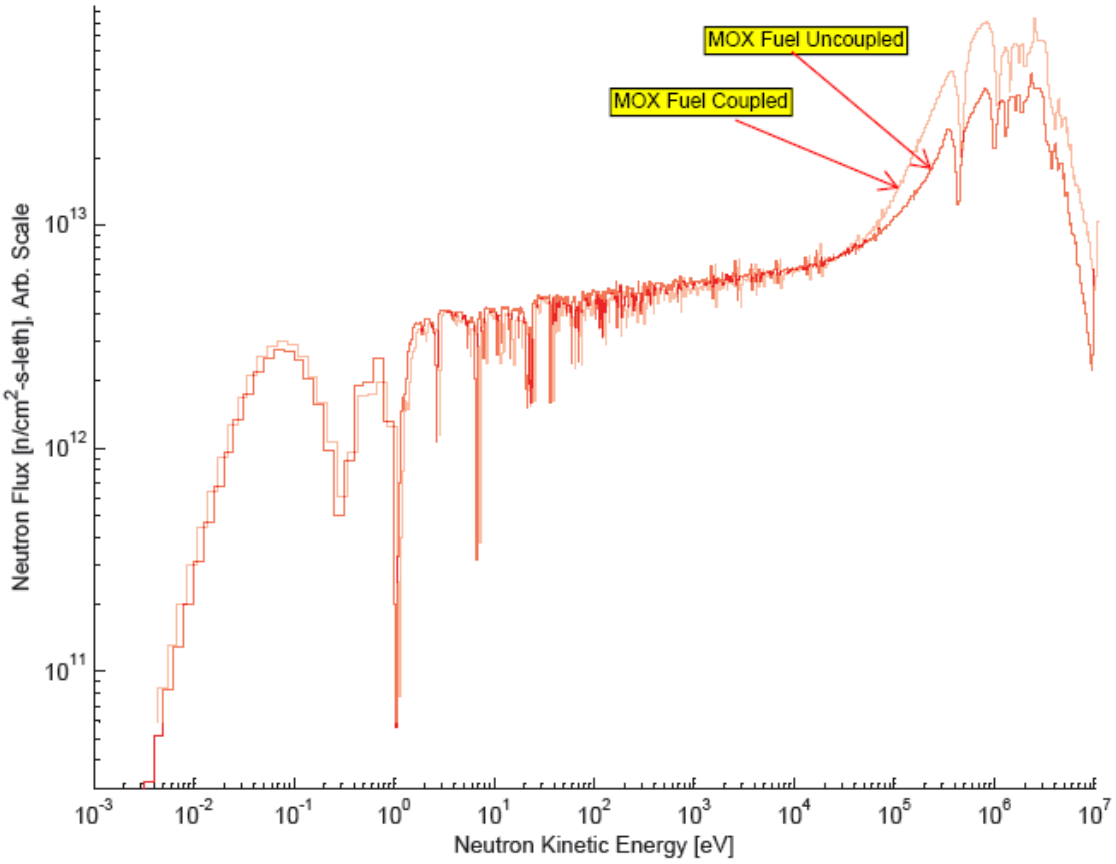

Figure 3.2- 17: Comparison of Neutron Energy Spectra for Neutronically Coupled and Uncoupled MOX Fuel

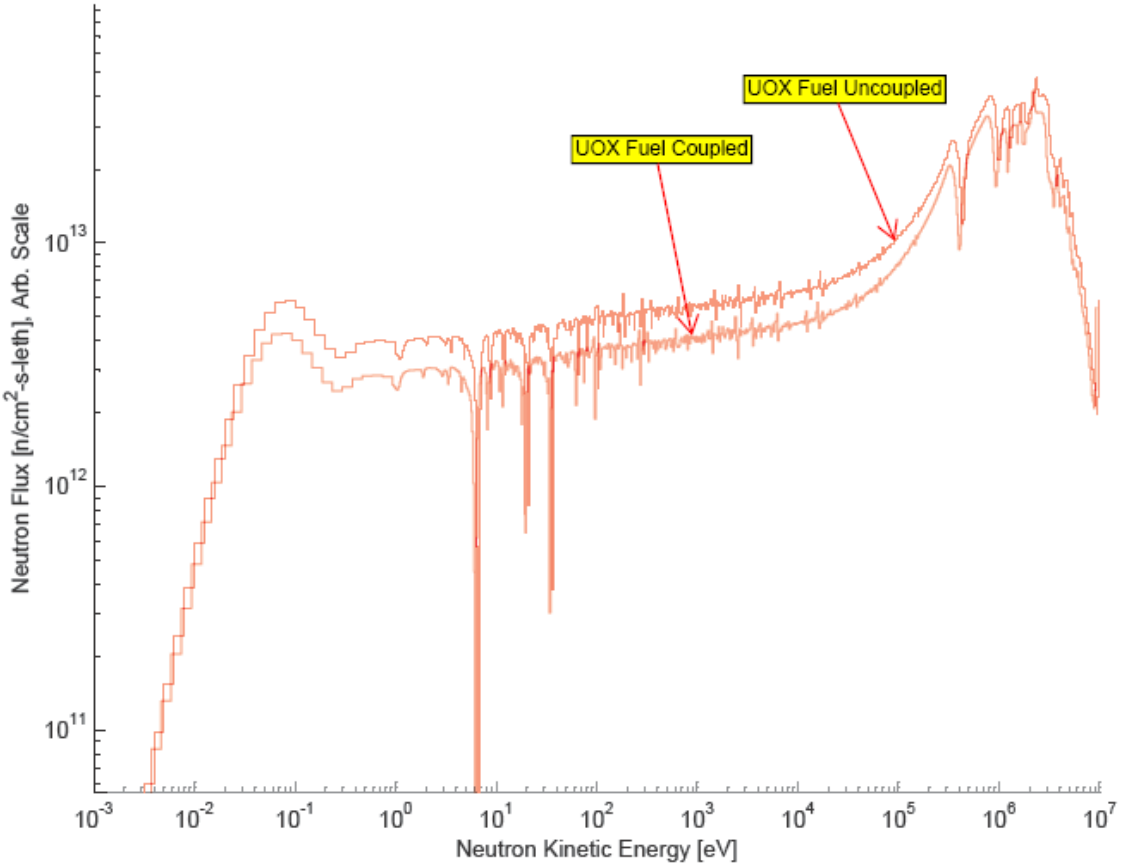

Figure 3.2- 18: Comparison of Neutron Energy Spectra for Neutronically Coupled and Uncoupled UOX Fuel

Figure 3.2-17 indicates that the coupling effects for the MOX fuel is increase in neutron flux in the fast neutron region of the spectrum. However, for the UOX fuel type, the coupling slightly decreases the neutron flux in the fast and epithermal regions. This is due to the fact that the fresh UOX fuels for this problem are the driver pins and hence the fast and epithermal neutrons are decreased in number in order to drive the MOX fuel pin and keep the supercell cell at its reactivity level.

3.2.9 Discussion of Results

Our developed methodology provides excellent results in regards to calculation of the isotopic inventories of the UOX and MOX or transmuter fuel pins as a function of the fuel burnup. Generally, the results of calculated isotope inventories are within 5% or less of values from the benchmark problems. Based on these results, we conclude that the model is a reliable tool for the study of burning plutonium-bearing and other strongly heterogeneous fuel loadings in typical power reactors and the fuel cycle studies. This model provides answers to desired isotopic constituents of UOX and MOX fuel pins with minimal amount of inputs to the V:BUDS computer code and the results are obtained with only few seconds of computer run time.

4. Conclusions

The work contained in this dissertation expands the collision probability theory and its applications in the study of fuels exhibiting sharp flux and power gradients as well as heterogeneous reactor cores. These scenarios are common in many of the advanced reactor and fuel cycle concepts proposed under the Global Nuclear Energy Partnership and other efforts to develop next-generation nuclear technologies capable of deep fuel burn and actinide transmutation. The work has been presented within the structure of two analyzed problems.

In the first problem, the current neutron transport equations for a unit cell configuration has been expanded to consider the fuel region as a multi-region area in order to address the shortcomings of the current theory where the entire fuel region is considered as a single lump and treated as one uniform medium. The single fuel region simplification results in assumptions that the neutron flux and material properties are uniform throughout the fuel region which in turn disregards the effects of spatial fuel self shielding. Spatial self shielding becomes an important driver of reactor physical behavior when the neutron mean free path in the fuel pins becomes small. This situation most typically arises in mixed-oxide or inert matrix fuels in water reactors, where plutonium and other constituents interact very strongly with low-energy neutrons.

In this work, the fuel region is divided into a series of annular sub-regions and mathematical expressions are derived for the transmission and escape probabilities for each of these sub-regions. Then these sub-regional probabilities are combined in a manner that accounts for the neutron flux variation across the fuel sub-regions in order to derive a single escape probability from the entire fuel region in a given fuel cell. Therefore an effective flux profile is obtained that accounts for the effects of the self shielding within the fuel. The developed methodology enables us to use the V:BUDS computer code as a base and it is enhanced to include the above stated procedure.

The results of this work are compared to two benchmark problems. The results indicate the existence of good agreement between our work and the benchmark problems for the multiplication factors and inventories of radionuclides as a function of fuel burnup when the number of fuel calculation of multiplication sub-regions is relatively small. In these cases, it also provides improvements for multiplication factors and inventories of isotopes of importance in the fuel cycle and nuclear non-proliferation studies such as ^{235}U, ^{239}Pu, ^{241}Pu and ^{242}Pu over the original single fuel region model results. The variance between the results and the benchmark problems increases with increasing number of fuel sub-regions. Hence the developed work offers improvements over the existing methodology provided that representative distances within a fuel sub-region is in the same order of magnitude as the average mean free path of neutrons.

The error associated with the developed methodology is 1.19% for the multiplication factor of a fresh fuel versus 2.59% error that is resulted from the original model. The errors associated with the irradiated fuel are 0.46%, 1.84%, and 0.90% for 20 MWd/kg, 40 MWd/kg and 60 MWd/kg burnup respectively. These errors compare favorably against the errors from the original model that are computed to be 2.96%, 3.33% and 3.70% respectively.

In regards to the capabilities of the developed methodology for the estimation of the isotopic content of fuel, the error analysis provides values of 1.43% and 1.19% for the ^{235}U content and ratio of ^{239}Pu to the total value of plutonium within the irradiated fuel. These errors compare favorably to those from the original model that are computed at 3.43% and 6.53% respectively.

The above methodology addresses the main shortcoming of the existing theory and provides improvements in regards to calculation of isotopic inventory as a function of fuel burnup. These improvements in the isotopic inventory result in higher-fidelity results suitable for fuel cycle and nuclear non-proliferation studies with essentially no additional execution time. The methodology will also help in better optimization of the spent fuel storage casks, temporary and permanent storage facilities via providing more accurate estimation of heat generating radionuclides.

Therefore, the developed methodology improves the capabilities of the current collision probability theory in predicting the multiplication factors and fuel isotopic contents by a factor of approximately 2 which corresponds to a minimum of 50% reduction in the calculated subject values.

In the second problem, collision probability theory has been extended to lift the zero net neutron leakage across the fuel cell boundaries assumption that was present in the initial methodology. The existing theory assumed that the reactor core is loaded with a single type of nuclear fuel and hence is not adequate for inclusion of multiple types of fuel where strong heterogeneity is introduced within a fuel lattice. The zero net neutron leakage assumption operates on a premise that the neutronic coupling between the fuel elements within the fuel lattice is so weak that local flux profiles can be accurately treated using a single unit cell with reflecting boundary conditions. The developed methodology derives escape probabilities that account for this neutronic coupling between the elements. The results of this methodology was compared to benchmark problems and found to be in excellent agreement. The most important application of the developed methodology is to determine the isotopic content of different fuel materials when they are included within a reactor such as those for the purpose of burning reactor / weapon grade plutonium within civilian power reactors. Again this improvement in fidelity comes at minimal expense in model execution time. The developed methodology will allow us to easily evaluate the design of different MOX or inert matrix fuel (IMF)

types for the purpose of depleting its plutonium contents and render radionuclides that are consistent with the nuclear non-proliferation criteria.

The developed methodology improves the results of isotopic inventory calculations within a strongly heterogeneous fuel lattice by almost an order of magnitude in some cases. This improvement is the result of incorporations of the neutronic coupling effects between the fuel elements with the fuel lattice. For example, the errors associated with the ratio of the ^{239}Pu to the overall fuel plutonium content is decreased from 25.5% at a typical burnup of 20 MWd/kg when calculated by the original theory to 2.5% when the developed methodology is used.

In summary, we have developed a new methodology that allows collision probability theory to operate at higher fidelity for diverse reactor core and fuel content configurations.

APPENDIX A

Results for Isotope Inventories Using Modified V:BUDS Based on Reference [29]

Benchmark Input Parameters

Table A.3.1- 1: Modified V:BUDS Isotope Inventory and OECD/NEA Phase IV-B Benchmark Results for Irradiated MOX fuel (Number of Fuel Sub-regions = 3)

Number of Fuel Sub-Regions (NRING)	Nuclide	Number Density [atm/barn.cm] Benchmark	Number Density [atm/barn.cm] Developed Methodology
3	^{234}U	5.3603E-7	5.899E-7
	^{235}U	4.3896E-5	4.378E-5
	^{236}U	2.5160E-6	2.145E-6
	^{238}U	2.1157E-2	2.117E-2
	^{238}Pu	4.1350E-5	4.019E-5
	^{239}Pu	8.0727E-4	7.897E-4
	^{240}Pu	4.7367E-4	4.898E-4
	^{241}Pu	2.1899E-4	1.906E-4
	^{242}Pu	1.3465E-4	1.375E-4
	^{237}Np	1.1947E-6	1.07E-6
	^{241}Am	8.7782E-6	8.433E-6
	^{243}Am	1.7080E-5	1.173E-5

Table A.3.1- 2: Modified V:BUDS Isotope Inventory and OECD/NEA Phase IV-B Benchmark Results for Irradiated MOX fuel (Number of Fuel Sub-regions = 4)

Number of Fuel Sub-Regions (NRING)	Nuclide	Number Density [atm/barn.cm] Benchmark	Number Density [atm/barn.cm] Developed Methodology
4	^{234}U	5.3603E-7	5.938E-7
	^{235}U	4.3896E-5	4.376E-5
	^{236}U	2.5160E-6	2.069E-6
	^{238}U	2.1157E-2	2.117E-2
	^{238}Pu	4.1350E-5	3.994E-5
	^{239}Pu	8.0727E-4	7.939E-4
	^{240}Pu	4.7367E-4	4.951E-4
	^{241}Pu	2.1899E-4	1.821E-4
	^{242}Pu	1.3465E-4	1.387E-4
	^{237}Np	1.1947E-6	1.052E-6
	^{241}Am	8.7782E-6	8.307E-6
	^{243}Am	1.7080E-5	9.864E-6

APPENDIX B

Comparison for Isotope Inventory from the Proposed Methodology vs. the OECD/NEA Phase IV-B Benchmark

Table B.3.1- 1: Comparison of ^{234}U Isotope Inventory from the Proposed Methodology vs. the OECD/NEA Phase IV-B Benchmark

Number of Fuel Sub-Regions	% difference between the developed model and the Benchmark	% difference between the Single Fuel Region and the Benchmark
2	7.53	2.66
3	10.05	2.66
4	10.78	2.66

Table B.3.1- 2: Comparison of ^{236}U Isotope Inventory from the Proposed Methodology vs. the OECD/NEA Phase IV-B Benchmark

Number of Fuel Sub-Regions	% difference between the developed model and the Benchmark	% difference between the Single Fuel Region and the Benchmark
2	-2.82	12.72
3	-14.75	12.72
4	-17.77	12.72

Table B.3.1- 3: Comparison of ^{238}U Isotope Inventory from the Proposed Methodology vs. the OECD/NEA Phase IV-B Benchmark

Number of Fuel Sub-Regions	% difference between the developed model and the Benchmark	% difference between the Single Fuel Region and the Benchmark
2	0.06	-0.08
3	0.06	-0.08
4	0.06	-0.08

Table B.3.1- 4: Comparison of ^{238}Pu Isotope Inventory from the Proposed Methodology vs. the OECD/NEA Phase IV-B Benchmark

Number of Fuel Sub-Regions	% difference between the developed model and the Benchmark	% difference between the Single Fuel Region and the Benchmark
2	-2.01	-1.96
3	-2.81	-1.96
4	-3.41	-1.96

Table B.3.1- 5: Comparison of ^{239}Pu Isotope Inventory from the Proposed Methodology vs. the OECD/NEA Phase IV-B Benchmark

Number of Fuel Sub-Regions	% difference between the developed model and the Benchmark	% difference between the Single Fuel Region and the Benchmark
2	-2.70	0.88
3	-2.18	0.88
4	-1.66	0.88

Table B.3.1- 6: Comparison of ^{240}Pu Isotope Inventory from the Proposed Methodology vs. the OECD/NEA Phase IV-B Benchmark

Number of Fuel Sub-Regions	% difference between the developed model and the Benchmark	% difference between the Single Fuel Region and the Benchmark
2	1.55	-0.42
3	3.41	-0.42
4	4.52	-0.42

Table B.3.1- 7: Comparison of ^{241}Pu Isotope Inventory from the Proposed Methodology vs. the OECD/NEA Phase IV-B Benchmark

Number of Fuel Sub-Regions	% difference between the developed model and the Benchmark	% difference between the Single Fuel Region and the Benchmark
2	-6.02	-2.64
3	-12.96	-2.64
4	-16.85	-2.64

Table B.3.1- 8: Comparison of ^{242}Pu Isotope Inventory from the Proposed Methodology vs. the OECD/NEA Phase IV-B Benchmark

Number of Fuel Sub-Regions	% difference between the developed model and the Benchmark	% difference between the Single Fuel Region and the Benchmark
2	1.15	0.40
3	2.12	0.40
4	3.01	0.40

Table B.3.1- 9: Comparison of ^{237}Np Isotope Inventory from the Proposed Methodology vs. the OECD/NEA Phase IV-B Benchmark

Number of Fuel Sub-Regions	% difference between the developed model and the Benchmark	% difference between the Single Fuel Region and the Benchmark
2	-0.23	18.77
3	-10.44	18.77
4	-11.94	18.77

Table B.3.1- 10: Comparison of ^{241}Am Isotope Inventory from the Proposed Methodology vs. the OECD/NEA Phase IV-B Benchmark

Number of Fuel Sub-Regions	% difference between the developed model and the Benchmark	% difference between the Single Fuel Region and the Benchmark
2	-2.53	-3.74
3	-3.93	-3.74
4	-5.37	-3.74

Table B.3.1- 11: Comparison of ^{243}Am Isotope Inventory from the Proposed Methodology vs. the OECD/NEA Phase IV-B Benchmark

Number of Fuel Sub-Regions	% difference between the developed model and the Benchmark	% difference between the Single Fuel Region and the Benchmark
2	-11.18	-0.53
3	-31.32	-0.53
4	-42.25	-0.53

APPENDIX C

Isotope Inventory Plots from the Proposed Methodology vs. the OECD/NEA Phase IV-B Benchmark

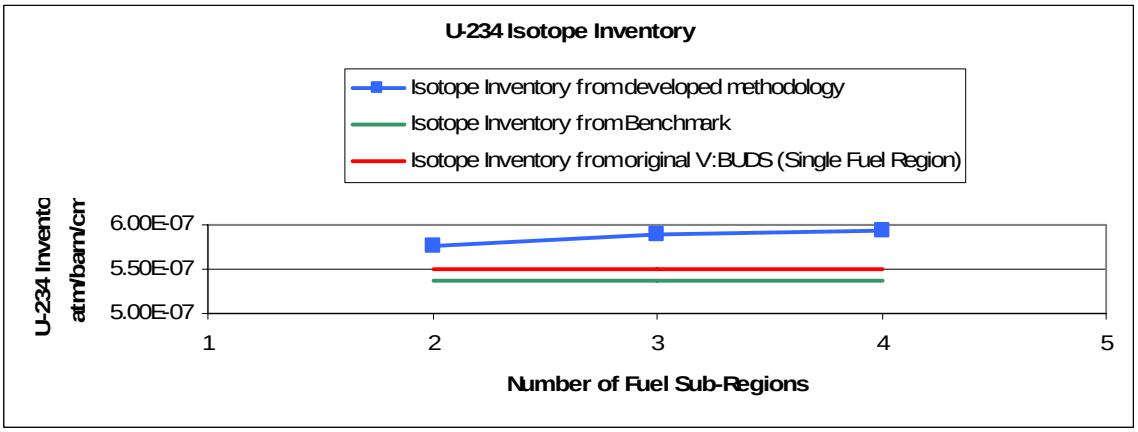

Figure C.3.1- 1: ^{234}U Isotope Inventory Using OECD/NEA Phase IV-B Benchmark

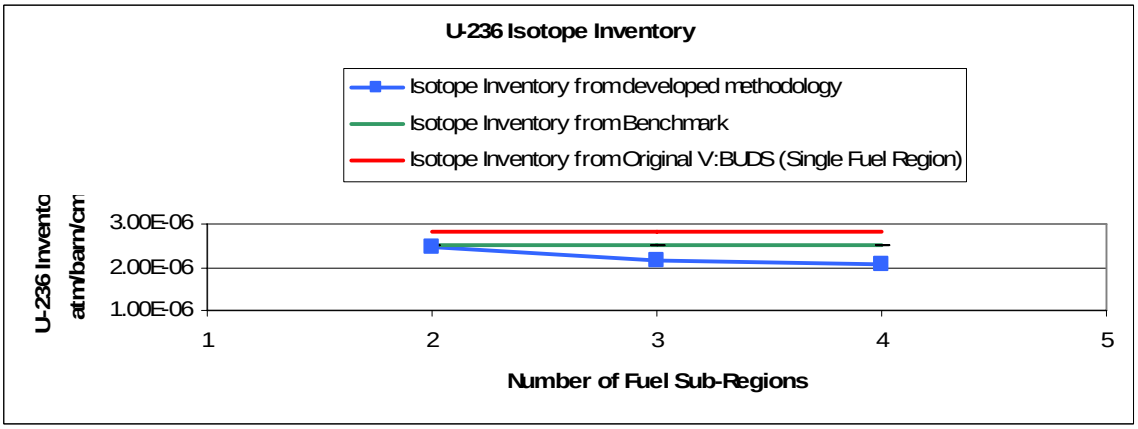

Figure C.3.1- 2: ^{236}U Isotope Inventory Using OECD/NEA Phase IV-B Benchmark

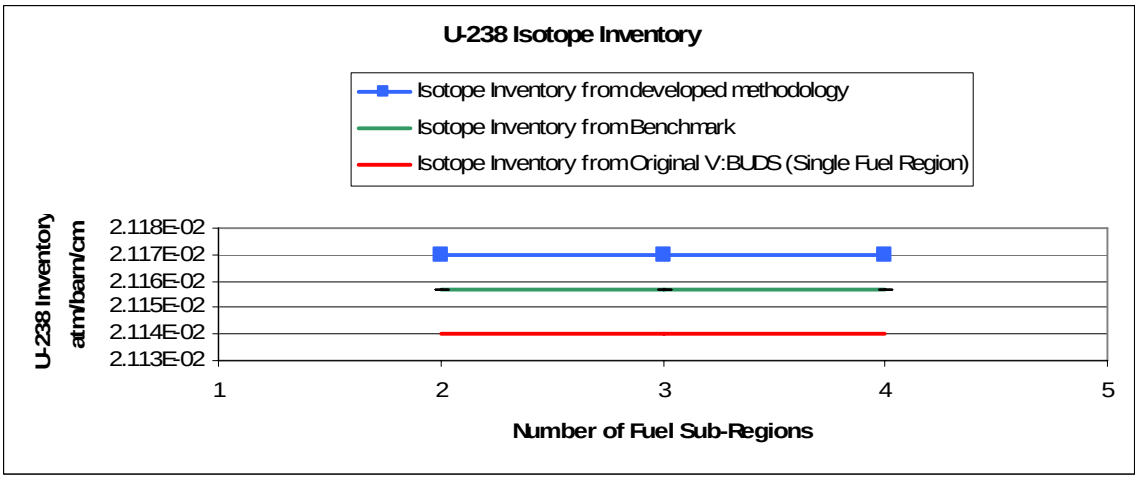

Figure C.3.1- 3: ^{238}U Isotope Inventory Using OECD/NEA Phase IV-B Benchmark

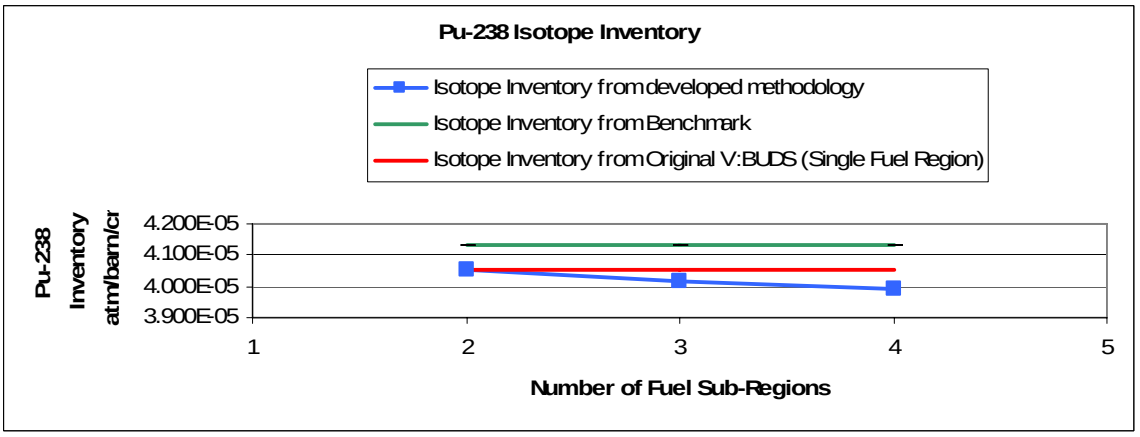

Figure C.3.1- 4: ^{238}Pu Isotope Inventory Using OECD/NEA Phase IV-B Benchmark

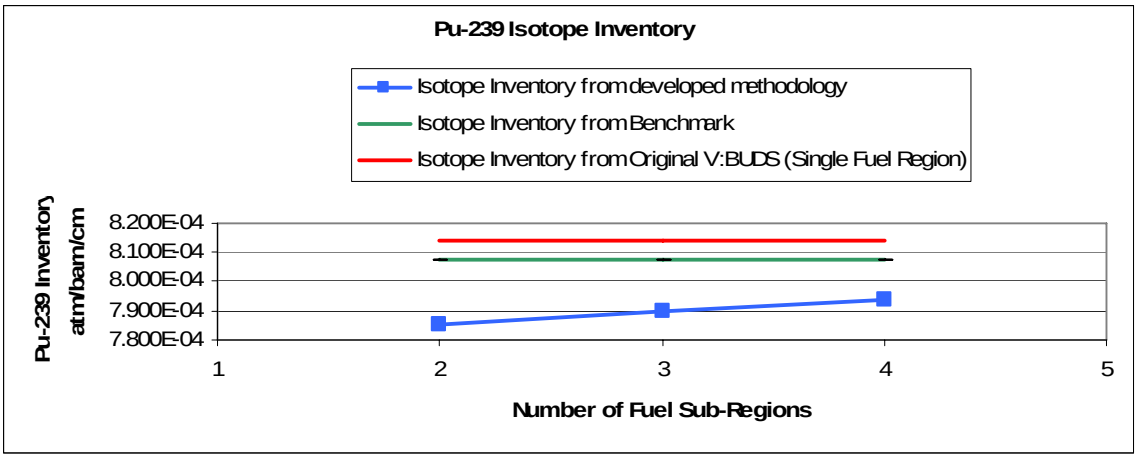

Figure C.3.1- 5: ^{239}Pu Isotope Inventory Using OECD/NEA Phase IV-B Benchmark

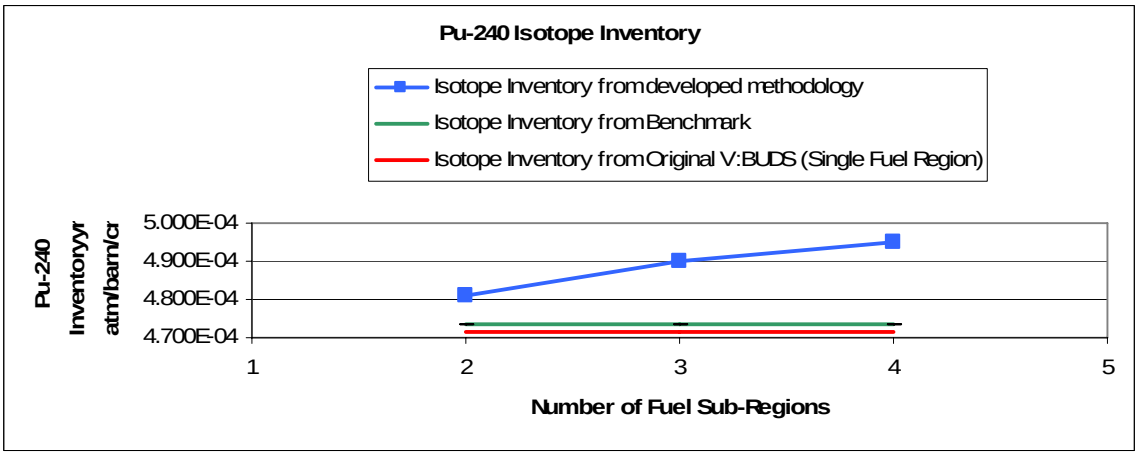

Figure C.3.1- 6: ^{240}Pu Isotope Inventory Using OECD/NEA Phase IV-B Benchmark

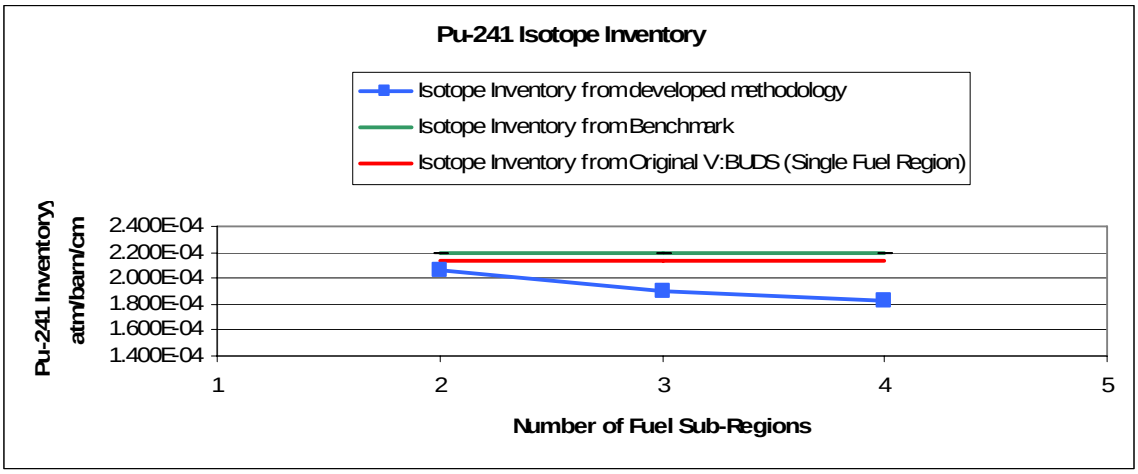

Figure C.3.1- 7: ^{241}Pu Isotope Inventory Using OECD/NEA Phase IV-B Benchmark

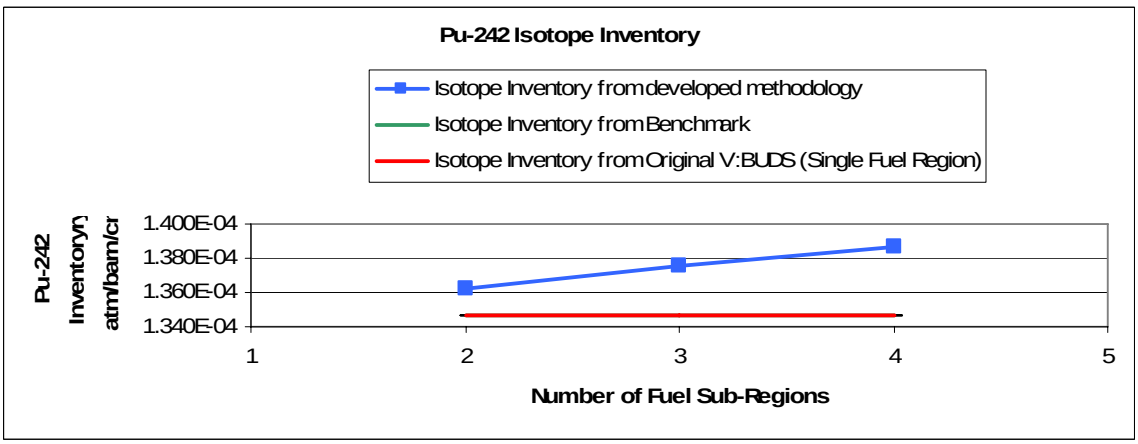

Figure C.3.1- 8: ^{242}Pu Isotope Inventory Using OECD/NEA Phase IV-B Benchmark

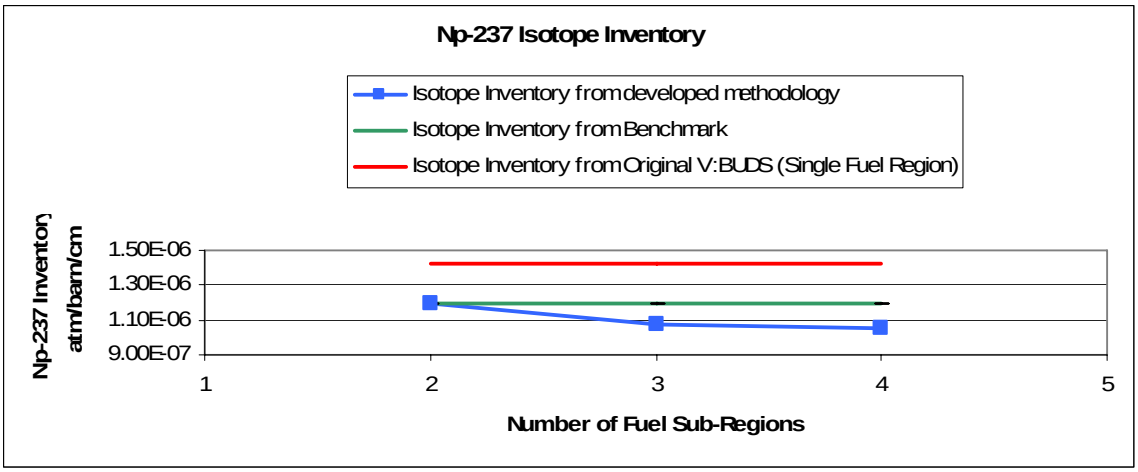

Figure C.3.1- 9: ^{237}Np Isotope Inventory Using OECD/NEA Phase IV-B Benchmark

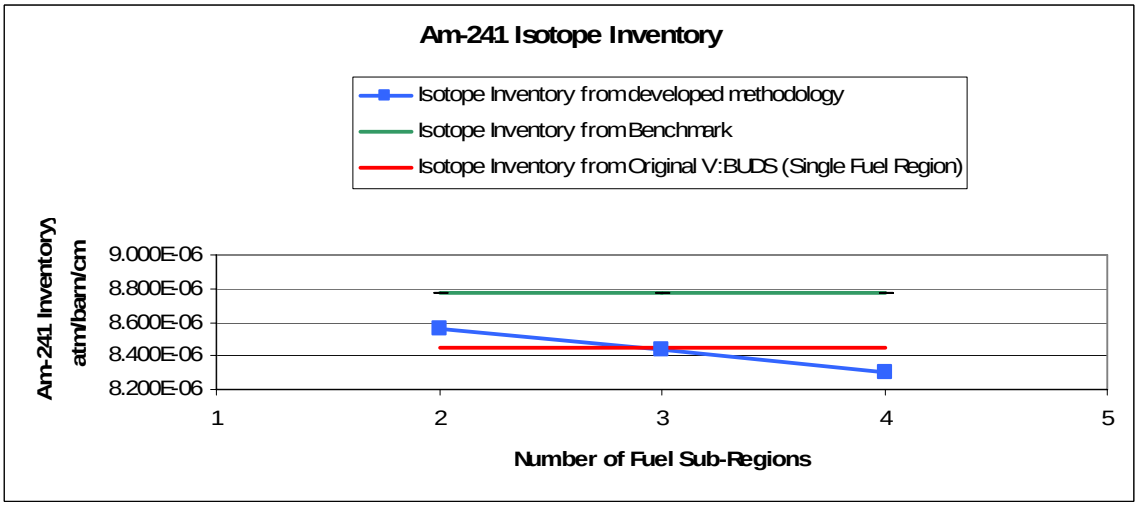

Figure C.3.1- 10: ^{241}Am Isotope Inventory Using OECD/NEA Phase IV-B Benchmark

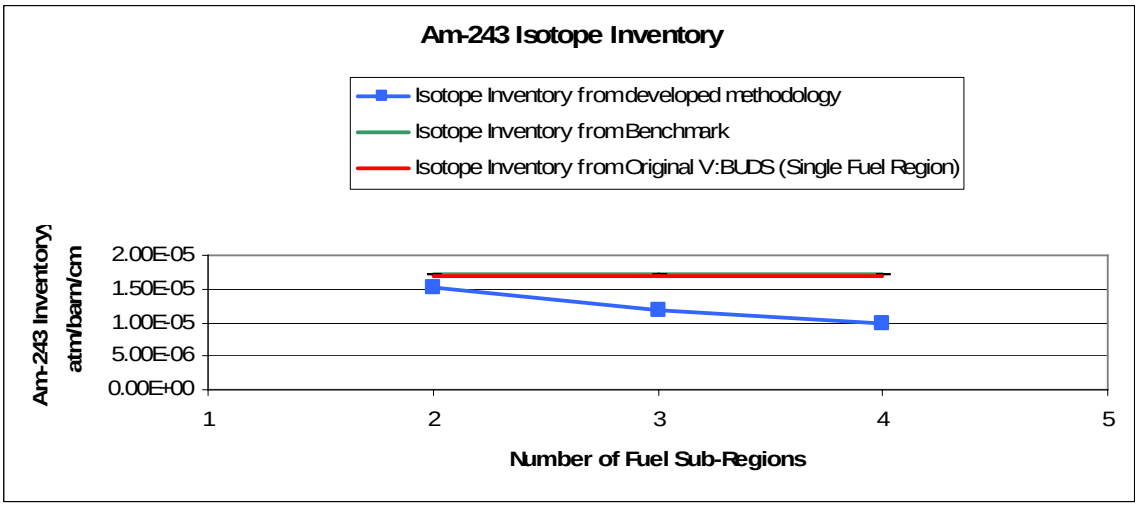

Figure C.3.1- 11: ^{243}Am Isotope Inventory Using OECD/NEA Phase IV-B Benchmark

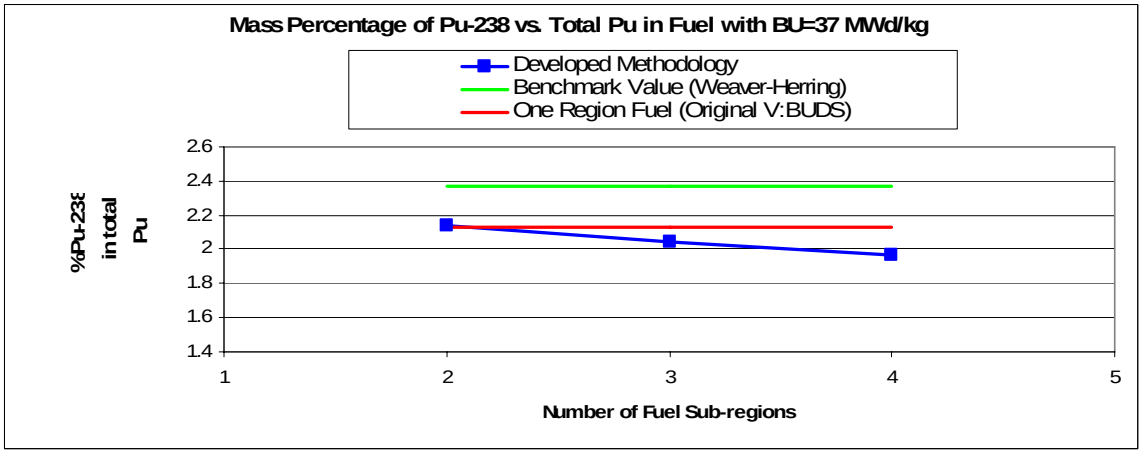

Figure C.3.1- 12: Mass Percentage of ^{238}Pu to total Pu Isotopes in Fuel with BU=37 MWd/kg Using Weaver-Herring Benchmark

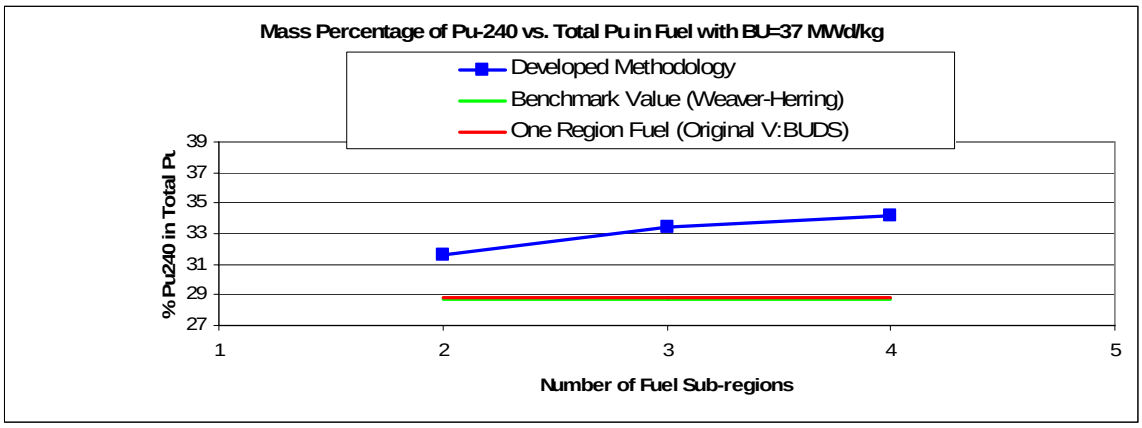

Figure C.3.1- 13: Mass Percentage of ^{240}Pu to total Pu Isotopes in Fuel with BU=37 MWd/kg Using Weaver-Herring Benchmark

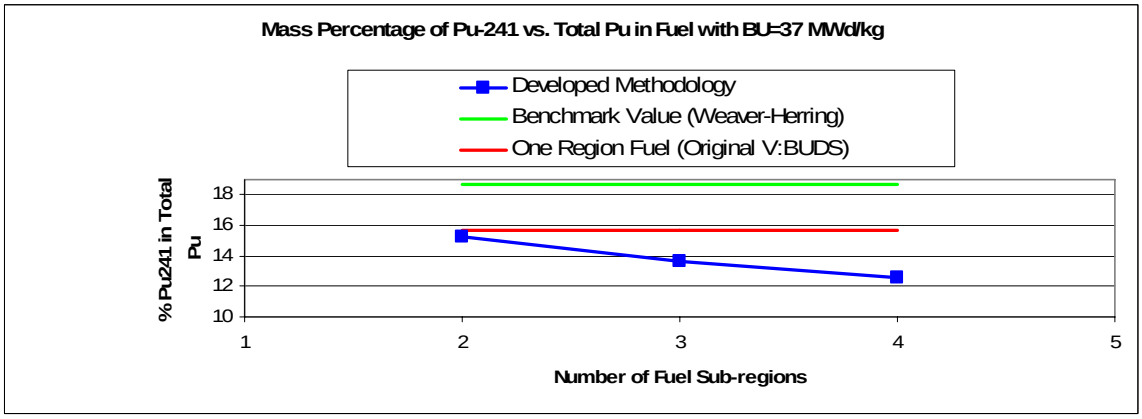

Figure C.3.1- 14: Mass Percentage of ^{241}Pu to total Pu Isotopes in Fuel with BU=37 MWd/kg Using Weaver-Herring Benchmark

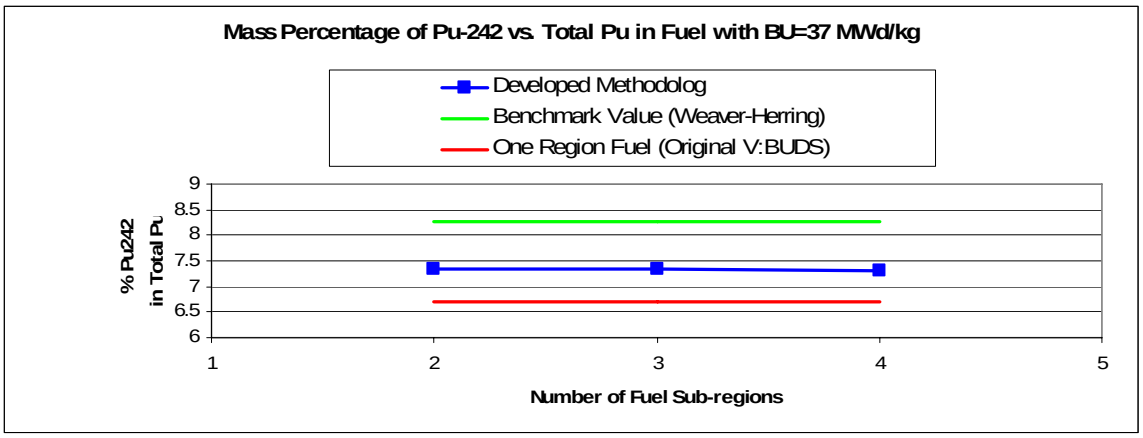

Figure C.3.1- 15: Mass Percentage of ^{242}Pu to total Pu Isotopes in Fuel with BU=37 MWd/kg Using Weaver-Herring Benchmark

Bibliography

[1] Report of the National Energy Policy Development Group, 2001, www.whitehouse.gov/energy

[2] A.F. HENRY, *Nuclear-Reactor Analysis*, The MIT Press, Cambridge, Massachusetts, Fourth Printing, 1986.

[3] J.J. DUDERSTADT and L.J. HAMILTON, *Nuclear Reactor Analysis*, John Wiley & Sons, 1976.

[4] G.I. BELL and S. GLASSTONE, *Nuclear Reactor Theory*, Van Nostrand Reinhold Company, 1970.

[5] W.M. STACEY, *Nuclear Reactor Physics*, John Wiley & Sons, 2001.

[6] R.V. MEGHREBLIAN and D.K. Holmes, *Reactor Analysis*, McGraw Hill Book Company, 1960.

[7] K.M. CASE and P.F. ZWEIFEL, *Linear Transport Theory*, Addison-Wesley Publishing Company, 1967.

[8] E.E. LEWIS and W.F. MILLER, JR., *Computational Methods of Neutron Transport*, American Nuclear Society, Inc, La Grange Park, Ill, 1993.

[9] K.M.CASE, G. PLACZEK, and F. deHOFFMANN, *Introduction to the Theory of Neutron Diffusion*,

[10] E.A. SCHNEIDER, *A Comprehensive Physical and Economic Model of the Nuclear Fuel Cycle*, Ph.D. Dissertation, Cornell University, 2002.

[11] Proceedings of the Workshop on the Physics and Fuel Performance of Reactor-Based Plutonium Disposition, 28-30 September 1998, OECD Development Centre, Paris, France.

[12] W. JI, J.L. COLIN, W.R. MARTIN, and J.C. LEE, *Reactor Physics Analysis of the VHTGR Core*, Presentation to Oak Ridge National Laboratory, December 2-3, 2004.

[13] H.S. ISBIN, *Introductory Reactor Theory, Reinhold Publishing Corporation*, New York, 1963.

[14] J.R. LAMARSH, *Introduction to Nuclear Reactor Theory*, Addison-Wesley Publishing Company, Reading, MA, 1966.

[15] A.M. WEINBERG and E.P. WIGNER, *The Physical Theory of Neutron Chain Reactors*, The University of Chicago Press, 1958.

[16] E.A. SCHNEIDER, M.R.DEINERT, S.T. HERRING, and K.B. CADY, *Burnup Simulations and Spent Fuel Characteristics of ZrO_2 Based Inert Matrix Fuels*, Journal of Nuclear Materials 361 (2007) 41-51.

[17] E.A. SCHNEIDER, M.R. DEINERT and K.B. CADY, *A computationally simple model for determining the time dependent spectral neutron flux in a nuclear reactor core*, Journal of Nuclear Materials. (2006).

[18] J.S. HERRING, P.E. MACDONALD and K.D.WEAVER, *Thorium Based Transmuter Fuels for Light Water Reactors*, Nuclear Technology, Vol.147, July 2004.

[19] W.F. MILLER and W.H. REED, *Ray-Effect Mitigation Methods for Two Dimensional Neutron Transport Theory*, Nuclear Science and Engineering, Vol. 62, p.391, 1977.

[20] P.N. BROWN and U.R. HANEBUTTE, *Spherical Harmonics Solutions to the 3D Kobayashi Benchmark Suite*, in PHYSOR 2000, ANS International Topical Meeting on the Advances in Reactor Physics and Mathematics and Computation into the Next Millennium, American Nuclear Society, May 2000.

[21] ORIGEN-ARP website: http://www.ornl.gov/sci/origen-arp/index.htm.

[22] S.M. BOWMAN, D.F. HOLLENBACH, M.D. DeHART, B.T. REARDEN, I.C. GAULD and S. GOLUOGLU, *SCALE 5: Powerful New Criticality Safety Analysis Tools*, The 7th International Conference on Nuclear Criticality Safety (ICNC2003), October 20–24, 2003, Tokai Research Establishment Japan Atomic Energy Research Institute, Tokai-mura, Japan.

[23] D. F. HOLLENBACH and M. E. Dunn, *Status and Preliminary Testing of Continuous-Energy KENO V.a and KENO-VI*.

[24] I. GERMINA, I.C. GAULD and V. JODOIN, *LWR Cross Section Libraries for ORIGEN-ARP in SCALE 5.1*, published in ORNL SCALE website.

[25] M.D. DeHART, *Lattice Physics Capabilities of the SCALE Code System Using TRITON*, Submitted to the American Nuclear Society for a session at the PHYSOR-2006 Topical Meeting on Reactor Physics: Advances in Nuclear Analysis and Simulation, Vancouver, British Columbia, Canada September 10–14, 2006.

[26] S.M. BOWMAN and D.F.GILL, *Validation of Standardized Computer Analyses for Licensing Evaluation/TRITON Two-Dimensional and Three-Dimensional Models for Light Water Reactor Fuel*, Submitted to the American Nuclear Society for a session at the PHYSOR-2006 Topical Meeting on Reactor Physics: Advances in Nuclear Analysis and Simulation, Vancouver, British Columbia, Canada September 10–14, 2006.

[27] E.A.SCHNEIDER, J.G. BARRATT, K.B. Cady and M.R. DEINERT, *Visualization of Coupled Spectral and Burnup Calculations: an Intuition-Building Tool*, Proceedings of the 2005 American Society for Engineering Education Annual Conference & Exposition.

[28] OECD Nuclear Energy Agency, "*Burnup Credit Criticality Benchmark Phase IV-A: Reactivity Prediction Calculations for Infinite Arrays of PWR MOX Fuel Pin Cells*", NEA Technical Report NEA/NSC/DOC (2003)3, 2003.

[29] OECD Nuclear Energy Agency, "*Burnup Credit Criticality Benchmark Phase IV-B: Results and Analysis of MOX Fuel Depletion Calculations*", NEA Technical Report NEA/NSC/DOC (2003)4, 2003.

[30] KEVAN D. WEAVER and J. STEPHEN HERRING, *Performance of Thorium-Based Mixed-Oxide Fuels for the Consumption of Plutonium in Current and Advanced Reactors,* Nuclear Technology, Vol. 143, July 2003.

[31] M.J. DRISCOLL, T.J. DOWNAR, and E.E. PILAT, *The Linear Reactivity Model for Nuclear Fuel Management,* American Nuclear Society, La Grange Park, Illinois, 1990.

[32] R. SANCHEZ and N.J. McCORMICK, *A Review of Neutron Transport Approximations,* Nuclear Science and Engineering, Vol. 80, 481-535 (1982).

[33] R.G. COCHRAN and N. TSOULFANIDIS, *The Nuclear Fuel Cycle: Analysis and Management*, American Nuclear Society, LA Grange Park, IL, 2nd Edition.

[34] T. TAKEDA and T. SEKIYA, *Space and Angle Dependent Collision Probability in Cell Problems,* Journal of Nuclear Energy, Vol-27, pp. 15 to 24.

[35] E.E. LEWIS and F.T. ADLER, *A Boltzmann Integral Equation Treatment of Neutron Resonance Absorption in Reactor Lattices*, Nuclear Science and Engineering, Vol. 37, pp 117-126, 1966.

[36] J.J. DUDERSTADT and W.R. MARTIN, *Transport Theory*, John Wiley & Sons Publishing, 1979.

[37] P.H. KIER, *A Method of Calculating Resonance Absorption in a Circularized Cell,* Nuclear Science and Engineering, 26, 230-236, 1966.

[38] E.E. LEWIS, *Progress in Multidimensional Neutron Transport Computation*, Nuclear Science and Engineering, 64, 279-293, 1977.

[39] R. SANCHEZ, *Approximate Solutions of the Two-Dimensional Integral Transport Equation by Collision Probability Methods,* Nuclear Science and Engineering, 64, 384-404, 1977.

[40] Energy Information Administration web site www.eia.doe.gov, Official energy statistics from the U.S. government.

[41] South Carolina Advisory Council Minutes, June 8, 2006, http://www.energy.sc.gov.

[42] OECD 2003 / NEA 4451, *Plutonium Management in the Medium Term, A Review by the OECD/NEA Working Party on the Physics of Plutonium Fuels and Innovative Fuel Cycles (WPPR)*, ISBN 92-64-02151-5.

[43] J. F. BRIESMEISTER, Ed., *MCNP - A General Monte Carlo N-Particle Transport Code, Version 4A*, LA-12625-M (CCC-200).

[44] A. G. CROFF, *A Users' Manual for the ORIGEN2 Computer Code*, ORNL/TM-7175 (CCC-371).

[45] R. S. BABCOCK, D. E. WESSOL, C. A. WEMPLE, and S. C. MASON, *The MOCUP Interface: A Coupled Monte Carlo/Depletion System,* 1994 Topical Meeting on Advances in Reactor Physics, Knoxville, TN, p. III-368 (April 11-14, 1994).

VITA

Robert Matavosian was born in Tehran, Iran, the son of Mr. and Mrs. Matavos Matavosian. After completing his work at Azadegan High School, Tehran, Iran, he was admitted to the Mechanical Engineering Department of Arya-Mehr University of Technology in Tehran, Iran. He received his Bachelor of Science degree in 1978 with valedictorian standing in his graduating class. He then entered the Mechanical Engineering Department at the University of California at Berkeley, California, where he received his Master of Science in June of 1979 and Master of Engineering in June of 1980. He started his professional career as a nuclear and mechanical systems engineer with a leading architect/engineering firm in the United States and then joined a leading nuclear reactor vendor where he was responsible for the design and field startup of nuclear steam supply systems for several pressurized water reactors in the United States. He is currently a senior technical advisor to the Sandia National Laboratories and Los Alamos National Laboratory. He enrolled in the Ph.D. program for the Nuclear and Radiation Engineering program within the Mechanical Engineering Department of The University of Texas in Austin in the spring semester of 2005.

Permanent Address: 1460 Buttermilk Road, Lenoir City, Tennessee 37771

This dissertation was typed by the author.